Performance Enhancement of MIMO Transmission Techniques with Limited Number of Receive Antennas

Ilmiawan Shubhi

Performance Enhancement of MIMO Transmission Techniques with Limited Number of Receive Antennas

by

Ilmiawan Shubhi

Graduate School of Informatics

Kyoto University

Kyoto, Japan

September 2017

Preface

With the ever-growing demand for higher data rates in wireless communication services, various techniques have been proposed to increase system capacity. Among these techniques, multiple-input multiple-output (MIMO) transmission, as a method of multiplying the capacity of a radio link using multiple transmit and receive antennas to exploit multipath propagation, has attracted considerable attention. In practice, however, physical constraints limit the number of antennas that can be embedded on a user terminal and may prevent the realization of MIMO transmission. Considering this limitation, three approaches can be taken, and are investigated throughout this thesis.

First, the user can be forced to handle multiple streams transmission from multiple transmit antennas even when the number of receive antennas is smaller than that of transmit antennas. In wireless communications, this scenario is called overloaded MIMO. Although signal detection in such scenario is possible, significant performance degradation cannot be avoided. In a system with channel coding, in particular, this circumstance leads to a quality degradation on the soft input of the decoder. To counter this problem, a joint decoding technique is proposed and is presented in the second chapter of this thesis. In this technique, instead of conducting the decoding process *separately* for each stream, the decoding process is conducted *jointly* between streams. Observation via computer simulation for MIMO systems with turbo codes shows that the proposed technique significantly improves the throughput and bit error rate (BER) performance of the systems.

Second, multi-user MIMO (MU-MIMO) with user collaboration approach so called collaborative interference cancellation (CIC) can also be used. In this approach, neighboring users share their received signals and equivalently increase the number of their receive antennas. The interference suppression capability of each user, therefore, can be increased. After sharing their received signals, each of the users in this approach will conduct signal detection by using conventional detection techniques such as zero forcing (ZF), minimum mean square error (MMSE), maximum likelihood detection (MLD), or QR decomposition-based MLD with M-algorithm (QRM-MLD).

To reduce the requirement of signal exchanges required by this approach, user selection scheme can be employed to select several collaborating users out of a larger number of available users. The user selection technique, however, should be tailored based on

the purpose and the detection technique used by the users. In this thesis, a user selection technique suitable to maximize the BER performance of a QRM-MLD algorithm is proposed.

In addition to the user selection technique, field experiments are also conducted to verify the effectiveness of MU-MIMO with CIC in actual environments. This is important, in particular, by the fact that in the actual environment, unideal conditions such as channel correlation and frequency offset occur. Due to the time constraint, however, the field experiments do not consider user selection in the collaboration process. Both of the user selection techniques for QRM-MLD and the field experiment results of the MU-MIMO with CIC are discussed in Chapter 3.

The last approach that can be taken in MIMO transmission with a limited number of antennas is MU-MIMO with precoding. In this approach, the interference cancellation process is initiated from the BS side, i.e. the precoding process. Using ZF precoder, for example, the BS determines the precoder matrix in such a way that it can cancel out the interuser interference on the upcoming transmission. It should be noted, however, this approach requires accurate channel state information (CSI) at the transmitter. This circumstance is hard to be obtained, especially when the user is moving in a multipath environment and experiencing Doppler spread. Having Doppler spread, the channel will fluctuate and causes a phenomenon so called channel aging. In this condition, a mismatch between the precoder and the actual channel matrix occurs. This mismatch causes the signal to be phase-shifted and interuser interference arises at each user.

To counter this problem, channel prediction can be exploited as a virtual CSI to update the precoder matrix. It should be noted, however, frequently updating the precoder matrix results in a drastic increase in the computational complexity. In this thesis, therefore, another method to exploit the channel prediction is proposed to improve the performance of MU-MIMO under time-varying channel. In particular, the predicted channel is exploited as an information source to conduct power allocation. The goal of this power allocation is to minimize the interuser interference at the receiver. Computer simulations show that the proposed technique could improve the BER performance of the users which have large Doppler spread while maintaining the performance of the users with small Doppler spread.

Besides of its stand alone implementation, all of those approaches can be used com-

plementary to exploit their optimum potential for future wireless communications. The transmitters, for example, could collect the information of the user environment to decide which users will be served either by the first, second, and third approach. A method to intelligently conduct such service, however, will not be investigated in this thesis and will be left as an interesting topic for future research.

Acknowledgments

I would like to express deep gratitude to my supervisor Professor Hiroshi Harada for his kindness and trust when I become a member of his laboratory, as well as for his helpful advice and support for my research activities. Without his patience, continuous encouragement, and careful review support, the present thesis could not have been completed.

My gratitude also goes to Associate Professor Hidekazu Murata, for his constant encouragement and guidance. He has walked me through all the stages of the writing of this thesis. Without his consistent and constructive instruction, this thesis could not have reached its present form.

I express my most sincere and heartfelt thanks to Associate Professor Takeshi Matsumura and Assistant Professor Keiichi Mizutani, for their strong support of my research by helpful suggestions, as well as careful review of this thesis.

I am grateful to Dr. Ou Zhao, a senior member graduated from this laboratory, for his valuable advice and support both for my academic and daily life during my study at Kyoto University.

I am greatly indebted to Mr. Tatsuki Chiba and Mr. Masahiro Arai, for giving me some helpful input on this work, and Ms. Maki Shibayama, the staff member of Harada laboratory, for being a dependable ally in handling my bureaucratic affairs. Likewise, I appreciate the openness and friendliness of all the Harada laboratory members and their valuable advice and suggestions for my research.

I would also like to thank the LPDP of the Ministry of Finance, Indonesia, for providing sufficient scholarship for my overseas life in Japan. Without this financial support during my Ph.D. studies, this present thesis would not have been possible.

Finally, I would like to express deep gratitude to my dear parents, for their long-term support to my study in Japan, and I wish to greatly appreciate my wife, Mrs. Rosmalini Harahap, for her continuous encouragements during my life, and my daughter, Almaira Madina Ilmi and Syakila Hikari Ilmi for giving me their best smile.

Contents

List of Figures

List of Tables

Nomenclature

Acronyms

3GPP	Third-Generation Partnership Project
5G	Fifth Generation
ADC	Analog to Digital Converter
BER	Bit Error Rate
BPSK	Binary Phase Shift Keying
BS	Base Station
CIC	Collaborative Interference Cancellation
CRC	Cyclic Redundancy Check
CSI	Channel State Information
DFT	Discrete Fourier Transform
EE	Energy Efficiency
EXIT	Extrinsic Information Transfer
FEC	Forward Error Correction
GI	Guard Interval
IDD	Iterarive Detection and Decoding
IDFT	Inverse Discrete Fourier Transform
IEEE	Institute of Electrical and Electronics Engineers
i.i.d.	independent and identically distributed
LLR	Log-Likelihood Ratio
LPDP	Lembaga Pengelola Dana Pendidikan
LTE	Long Term Evolution
MAP	Maximum A Posteriori

MI	Mutual Information
MIMO	Multiple-Input Multiple-Output
MLD	Maximum Likelihood Detection
MMED	Maximum Minimum Euclidean Distance
MMED-M	Maximum Minimum Euclidean Distance with M-algorithm
MMSE	Minimum Mean Square Error
MRT	Maximum Ratio Transmission
MS	Mobile Station
MU	Multi User
OFDM	Orthogonal Frequency Division Multiplexing
QAM	Quadrature Amplitude Modulation
QPSK	Quadrature Phase Shift Keying
QRM-MLD	QR decomposition-based MLD with M-algorithm
RM	Rate Matching
SNR	Signal to Noise Ratio
SU	Single User
TU	Typical Urban
UDP	User Datagram Protocol
USRP	Universal Software Radio Peripheral
ZF	Zero Forcing

Roman Symbols

a	Amplitude of ray arrived at the user
$\bar{a}$	Amplitude of virtual ray used for channel prediction
b	Transmitted bit
$\boldsymbol{b}$	Vector of bit combination
$\hat{b}$	Transmitted bit used to calculate mutual information
$\hat{\boldsymbol{b}}$	Vector of transmitted bit combination used to calculate mutual information
$\tilde{\boldsymbol{b}}$	Vector of bit combination which is used as a reference point at joint turbo decoding
$\mathcal{B}$	Set of all possible bit combinations in joint turbo decoding
$d^{(0)}$	Systematic part of turbo decoder outputs
$\boldsymbol{d}^{(0)}$	Bit combination of systematic part of turbo decoder outputs
$d^{(1)}$	Parity 1 part of turbo decoder outputs
$\boldsymbol{d}^{(1)}$	Bit combination of parity 1 part of turbo decoder outputs
$d^{(2)}$	Parity 2 part of turbo decoder outputs
$\boldsymbol{d}^{(2)}$	Bit combination of parity 2 part of turbo decoder outputs
$\bar{\boldsymbol{d}}$	Vector of stored accumulative Euclidean distance in MMED-M
$\tilde{\boldsymbol{d}}^{(0)}$	Bit combination of systematic part of turbo decoder outputs which is used as a refference point at joint turbo decoding
e	Symbol error of two possible transmitted symbols
$\boldsymbol{e}$	Vector of symbol error of two possible vector of transmitted symbols
$\boldsymbol{E}$	Matrix of surviving nodes from all selection stage in MMED-M
E_1	Unique symbol error from one transmit antenna
$\mathcal{E}$	Set of all possible symbol error from one transmit antenna
$\mathcal{E}_1$	Set of all unique symbol error from one transmit antenna
f	Subcarrier index
F	Total number of subcarriers in one OFDM symbol
$\boldsymbol{F}$	Matrix of Doppler shift estimator
$\bar{f}$	Doppler shift occurs at the user

$\tilde{f}$	Estimated Doppler shift used for channel prediction
$\boldsymbol{G}$	Channel-equivalent Matrix
h	Elements of channel matrix
$\boldsymbol{H}$	Channel matrix
$\tilde{h}$	Elements of predicted channel matrix
$\tilde{\boldsymbol{H}}$	Predicted channel matrix
I	Mutual information
$\boldsymbol{I}$	Identity matrix
j	Transmitted bits index
J	Total number of transmitted bits
k	User index
K	Number of users served by a BS in an MU-MIMO with precoding
$\tilde{k}$	User index having minimum interference level
l	Bit index of turbo decoder inputs
L	Number of input bits of turbo decoder
n	Random Gaussian noise
$\boldsymbol{n}$	Vector of noise
$\bar{n}$	Index of the ray arrived at the user
$\bar{N}$	Number of rays arrived at the user
$\ddot{\boldsymbol{n}}$	Vector of noise after multiplication with unitary matrix, $\boldsymbol{Q}$
$\tilde{n}$	Index of virtual ray used for channel prediction
$\tilde{N}$	Number of virtual rays used for channel prediction
p	Allocated power
$\bar{p}$	Power of each user when equal power allocation is used
$\hat{p}$	Excess power of the user after achieving minimum power to achieve target BER
$\tilde{p}$	Power required by the user to achieve its target BER
$Pr(.)$	Probability of (.)
q	Bit index in modulated symbol
Q	Total number of bits in each modulated symbol
Q	Q function

$\boldsymbol{Q}$	Unitary matrix part of QR decomposition
r	Rank index in the channel submatrix
R	Number of rank of the channel submatrix
$\boldsymbol{R}$	Upper triangular matrix part of QR decomposition
$\boldsymbol{R}_{yy}$	Correlation matrix of the received signal vector
s	Modulated symbol
$\boldsymbol{s}$	Vector of modulated symbols
S	Number of states in each turbo encoder
$\hat{\boldsymbol{s}}$	Vector of recovered version of the transmitted symbols
$\tilde{s}$	Modulated symbol after power allocation
$\mathcal{S}$	Set of all possible transmitted symbols from one transmit antenna
t	Time
u	Modulated output bit of turbo codes
U	User subset
$\hat{U}$	User subset which is selected to conduct CIC
$\mathcal{U}$	Set of all possible user subsets
$\boldsymbol{V}$	Interference level matrix
$\boldsymbol{W}$	Precoder matrix
x	Discrete time index
$\boldsymbol{x}$	Vector of precoded symbols
X	Number of training symbols
y	Received signal
$\boldsymbol{y}$	Vector of received signals
$\ddot{y}$	Received signal of the training symbols
$\ddot{\boldsymbol{y}}$	Vector of received signals of the training symbols
$\tilde{y}$	Received signal after multiplication with unitary matrix, $\boldsymbol{Q}$
$\tilde{\boldsymbol{y}}$	Vector of received signals after multiplication with unitary matrix, $\boldsymbol{Q}$

Greek Symbols

α	Value of forward recursion in turbo decoding
β	Value of backward recursion in turbo decoding
γ	Probability of transmitted bit
δ	Average number of QR decompositions and Euclidean distance calculations in one user selection loop
θ	Phase shift experiencing by user
λ	Singular value of a matrix
μ	Average number of Euclidean distance calculation processes at each stage of MMED-M
ρ	Current state at trellis encoder/decoder
P	Aggregate of all the states ρ
ρ'	Next state at trellis encoder/decoder
P'	Aggregate of all the states ρ'
ϕ	Current state at joint turbo decoder
ϕ'	Next state at joint turbo decoder
Φ	Aggregate of all the states ϕ
Φ'	Aggregate of all the states ϕ'
σ	Standard deviation of noise
τ	Aggregate of all transitions in conventional turbo decoder
T	Aggregate of all transitions in joint turbo decoding

Subscripts and or Superscript

$d_{\min}$	Square root of minimum Euclidean distance of all possible transmitted symbols
$\bar{d}_{\max}$	Maximum value of $\bar{d}_{\min}$ from all possible user subsets
$\bar{d}_{\min}$	Minimum accumulative Euclidean distance in one user subset
E_{s}	Average energy of the transmitted signals
f_{D}	Maximum Doppler frequency

G_{S} Number of candidates in MMED-M

I_{A} A priori values of mutual information

I_{E} Extrinsic values of mutual information

K_{act} Number of active users in MU-MIMO with CIC

K_{ava} Number of available users in MU-MIMO with CIC

K_{col} Number of collaborating users in MU-MIMO with CIC

K_{QRM} Number of candidates in QRM-MLD

L_{a} A priori LLR value

L_{e} Extrinsic LLR value

N_{ED} Number of Euclidean distance calculation required in the MMED user selection technique

N'_{ED} Number of Euclidean distance calculation required in the MMED-M user selection technique

n_{r} Receive antenna index

N_{r} Number of receiver antennas

n_{t} Transmit antenna index

N_{t} Number of transmit antennas

P_{e} Error probability

T_{P} Precoder update period

Chapter 1

Introduction

Wireless communication has been experiencing a drastic growth in these last two decades. Having only tenths of kilobit per second of data rate around twenty years ago, we are currently able to have more than tenths mega bit per second (Mbps) of data rate with various services and applications. In fact, researchers from both academia and industry are now at the final stage in preparing for the fifth generation (5G) wireless communications. In this new generation, it is expected that more than 100 Mbps of minimum data rate can be obtained even for users with high mobility.

Among several major breakthroughs in wireless communication technologies, multiple-input multiple-output (MIMO) has been playing a significant role in current wireless communication technologies. Exploiting multiple transmit and receive antennas, MIMO systems can yield a significant improvement in spectral efficiency [1–3]. Owing to this capability, MIMO systems have been adopted by the third-generation partnership project (3GPP) for use in the long-term evolution (LTE) standard. Furthermore, its enhanced variant so called massive MIMO is currently considered as one of the promising technique to realize high-speed and reliable data transmission for the 5G communications. Typically, a MIMO system requires the number of receive antennas to be greater than or equal to that of transmit antennas. However, despite the trend of increasing number of antennas in both transmitters and receivers, some user terminals might not be

able to meet this condition owing to limitations in their form factor. In regards of this limitations, three approaches can be considered.

First, the user can be forced to handle multiple streams transmission from multiple transmit antennas even when the number of receive antennas is smaller than that of transmit antennas. In wireless communications, this scenario is called overloaded MIMO. Second, multi-user MIMO (MU-MIMO) with user collaboration approach so called collaborative interference cancellation (CIC) can also be used. In this approach, neighboring users share their received signals and equivalently increase the number of their receive antennas. Last, MU-MIMO transmission with precoding might also be employed. Differ with previous two approaches, the interference cancellation process in this approach is initiated from the BS side, i.e. the precoding process.

Besides for its stand alone implementations, these three approaches might also be used complementary in the future wireless communication system. Considering a multi-cell system, for example, MU-MIMO with precoding can be used in each cell to serve multiple users which uniformly distributed across the cell. When several users in a cell are closely located, those users can conduct CIC to improve their detection capabilities, while the other users remain to use precoding technique. Using this joint approaches, the diversity of the users which are served by the MU-MIMO with precoding could also be improved. Last, for the user located in the cell-edge, multiple transmission from different BS can be applied. This scenario is, in general, equal to an overloaded MIMO scenario. Using an appropriate detection and decoding technique, transmission from multiple BS using a lower-order modulation technique has a better performance compared to that of single BS transmission with higher-order modulation. By properly utilizing these three approaches, therefore, a significant improvement on the overall system throughput can be obtained.

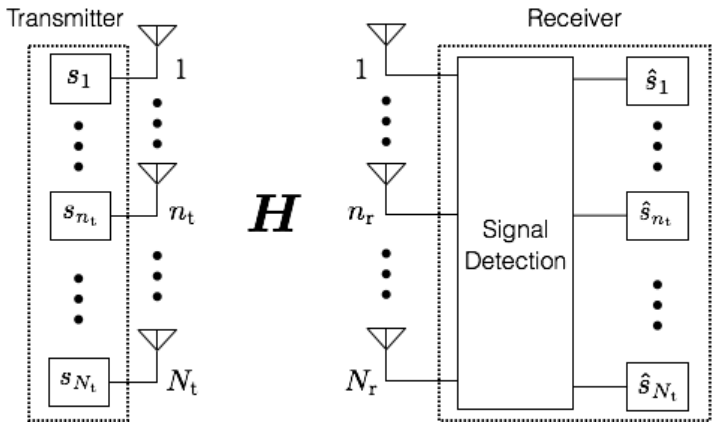

Fig. 1.1. Single user MIMO.

1.1 Approaches on MIMO Systems Under Limited Number of Receive Antennas

1.1.1 Overloaded MIMO

A point-to-point or single user (SU) MIMO, is a MIMO system, in which a transmitter equipped with more than one antenna communicates with a user which is also equipped with more than one antenna. Using this technique, the capacity of transmission to the designated user can be increased through spatial multiplexing. Figure 1.1 shows a simple block diagram of an SU-MIMO system. As can be seen in the figure, the modulated symbols from the transmitter, $\boldsymbol{s}$, are transmitted through N_t transmit antennas. In the figure, $\boldsymbol{H}$ is a $N_\mathrm{r} \times N_\mathrm{t}$ matrix of a wireless channel. Passing through this wireless channel, the signals are then received by a user equipped with N_r receive antennas and can be written as

$$\boldsymbol{y} = \boldsymbol{H}\boldsymbol{s} + \boldsymbol{n}, \tag{1.1}$$

where $\boldsymbol{y}$ is an $N_\mathrm{r} \times 1$ vector of received signals, $\boldsymbol{s}$ is an $N_\mathrm{t} \times 1$ vector of transmitted symbols, and $\boldsymbol{n}$ is an $N_\mathrm{r} \times 1$ vector of noise.

In a conventional SU-MIMO, the number of receive antennas, N_{r}, is larger than or equal to that of transmit antennas, N_{t}. This, in particular, holds due to the fact that a significant performance degradation occurs in the detection process for the case of $N_{\mathrm{r}} < N_{\mathrm{t}}$. This performance degradation applies even if maximum likelihood detection (MLD) is used. In addition, low complexity decoding techniques such as zero forcing (ZF) and minimum mean square error (MMSE) algorithm only can be implemented when $N_{\mathrm{r}} \geq N_{\mathrm{t}}$.

Owing to the form factor limitations, however, the number of antennas that can be implemented at a user is very limited. This circumstance leads to a scenario where the number of transmit antennas is larger than that of receive antennas, i.e. an overloaded MIMO system. In addition to the scenario where $N_{\mathrm{r}} < N_{\mathrm{t}}$, overloaded MIMO can also be defined as the condition when the rank of matrix $\boldsymbol{H}$ is less than N_{t}. This circumstance could occur, for example, due to channel correlation between the receive antennas.

1.1.2 Multi-user MIMO with Collaborative Interference Cancellation

In wireless communication, MU-MIMO is an advanced MIMO technology [4] where several transmit antennas at a base station (BS) serves independent radio terminals each having one or multiple antennas. This architecture is in contrast with SU-MIMO which considers a single multi-antenna transmitter communicating with a single multi-antenna receiver. To enhance the communication capabilities of all terminals, MU-MIMO applies an extended version of space-division multiple access to allow multiple transmitters to send separate signals and multiple receivers to receive separate signals simultaneously in the same band.

In MU-MIMO, one of the techniques that can be taken to conduct the interference mitigation is by using CIC [5–8]. The technique can be clearly seen in Fig. 1.2. In this thesis, a downlink MU-MIMO communications where a BS equipped with N_{t} transmit

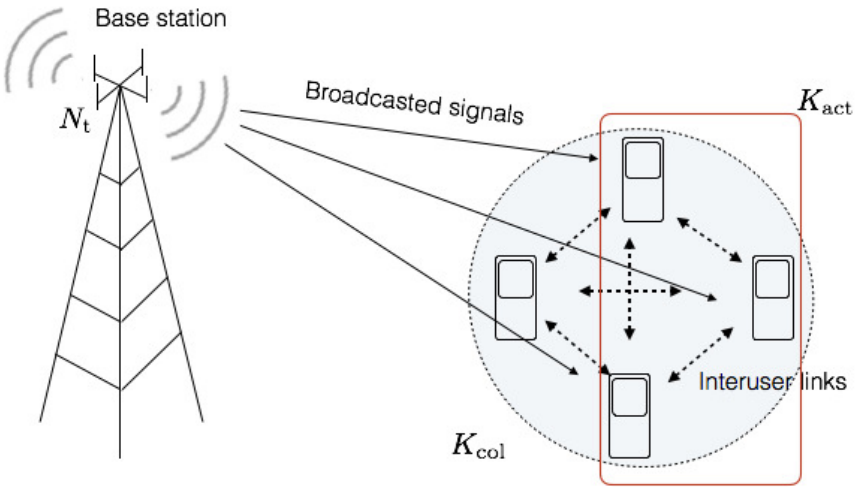

Fig. 1.2. MU-MIMO with collaborative interference cancellation.

antennas serves K_{act} users out of K_{col} users is considered. For simplicity, each user is assumed to have one receive antenna. In MU-MIMO with CIC, neighboring users share their received signals without decoding and equivalently increase the number of their receive antennas. Thus, the interference suppression capability of the users can be increased.

To conduct CIC, the K_{col} collaborating users form a cluster and exchange their CSI and their received signals. This signal-exchange can be conducted using either in-band or out-band channels. In the future wireless communication systems, however, the mobile terminals will be most likely equipped with an additional transceiver unit, namely for a small cell implementation. Therefore, the CIC process with a dedicated channel is assumed in this thesis. Thus, there is no interference between the transmitted signals from the BS to the users with the inter-user signals for CIC.

Let $\boldsymbol{y} = [y_1, y_2, \ldots, y_{K_{\text{col}}}]^{\text{T}}$, where y_k is the received signal for kth user. The received signals for K_{col} collaborating users can be written in resemblant with SU-MIMO scenario

as

$$\boldsymbol{y} = \boldsymbol{H}\boldsymbol{s} + \boldsymbol{n}, \tag{1.2}$$

where $\boldsymbol{H}$ is a $K_{\text{col}} \times N_{\text{t}}$ matrix of a wireless channel, $\boldsymbol{s}$ is an $N_{\text{t}} \times 1$ vector of transmitted symbols, and $\boldsymbol{n}$ is an $K_{\text{col}} \times 1$ vector of noise. To demodulate the transmitted symbols, users of MU-MIMO with CIC systems can conduct a similar detection technique such in SU-MIMO. By using MLD technique, for example, the vector of transmitted symbols can be recovered by

$$\hat{\boldsymbol{s}} = \underset{\boldsymbol{s} \in \mathcal{S}^{N_{\text{t}}}}{\operatorname{argmin}} \|\boldsymbol{y} - \boldsymbol{H}\boldsymbol{s}\|_{\text{F}}^2, \tag{1.3}$$

where $\mathcal{S}^{N_{\text{t}}}$ is the set of all possible vectors of transmitted symbols and $\|(.)\|_{\text{F}}^2$ is the Frobenius norm of (.). For the case of MMSE, $\hat{\boldsymbol{s}}$ can be obtained by exploiting the correlation of the received signals as

$$\hat{\boldsymbol{s}} = \boldsymbol{H}^{\text{H}} \boldsymbol{R}_{yy}^{-1} \boldsymbol{y}, \tag{1.4}$$

where $(.)^{\text{H}}$ is the Hermitian transpose of (.) and $\boldsymbol{R}_{yy}$ is the correlation matrix of the received signal vector.

1.1.3 Multi-user MIMO with Precoding

Another approach in conducting the MU-MIMO is by using the precoding technique [9–12]. Differ with the MU-MIMO with CIC, interference cancellation in MU-MIMO with precoding is initiated from the BS. In Fig. 1.3, a simple block diagram of MU-MIMO with precoding is shown. In the figure, K is the number of users served by the BS. As can be seen in the figure, the modulated symbols are firstly precoded using a precoder matrix, $\boldsymbol{W}$, to obtain a vector of precoded symbols, $\boldsymbol{x}$. Mathematically, this process can be written as

$$\boldsymbol{x} = \boldsymbol{W}\boldsymbol{s}. \tag{1.5}$$

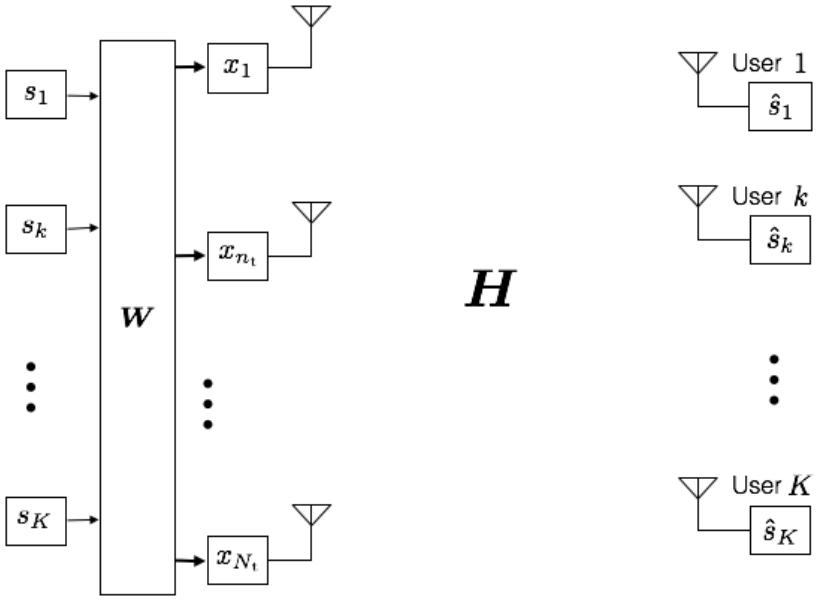

Fig. 1.3. MU-MIMO with precoding.

In this thesis, ZF precoding is used as the precoding technique. ZF precoding is a spatial signal processing by which the multiple transmit antennas can null inter-user interference signals. Using ZF precoding, the precoder matrix is calculated as

$$\boldsymbol{W} = \boldsymbol{H}^{\dagger} = \boldsymbol{H}^{\mathrm{H}} \left(\boldsymbol{H}\boldsymbol{H}^{\mathrm{H}} \right)^{-1}, \tag{1.6}$$

where $(\cdot)^{\dagger}$ represents the pseudo-inverse of $(\cdot)$. Passing through a wireless channel matrix, $\boldsymbol{H}$, the vector of the received symbols of all K users can be written as

$$\hat{\boldsymbol{s}} = \boldsymbol{H}\boldsymbol{x} + \boldsymbol{n}, \tag{1.7}$$

where $\boldsymbol{n}$ is the $K \times 1$ vector of noise. Eq. (1.7) can also be written as

$$\hat{\boldsymbol{s}} = \boldsymbol{G}\boldsymbol{s} + \boldsymbol{n}, \tag{1.8}$$

where $\boldsymbol{G} = \boldsymbol{H}\boldsymbol{W}$ denotes the $K \times K$ channel-equivalent matrix. Using ZF precoder, and assuming the channel matrix is static in one precoder-updating period, the channel-equivalent matrix is equal to an identity matrix with the size of $K \times K$. Eq. (1.8) then

can be written as

$$\hat{\boldsymbol{s}} = \boldsymbol{s} + \boldsymbol{n}. \tag{1.9}$$

As pointed out in above equation, ZF precoding process cancels the channel matrix and thus, no interference occurs at each user. Each user, therefore, can conduct a simple demodulation process.

1.2 Key Challenges

1.2.1 Challenges in Overloaded MIMO Systems

In a point-to-point communications, transmission through multiple antennas, i.e. SU-MIMO, has a significant advantage over a single-antenna transmission with higher-order modulation in terms of better spatial diversity. Transmission through multiple antennas also provides more randomness, which is an important factor for transmission with channel coding. However, a multiple-antenna transmission has a remaining difficulty in the signal detection process, in particular, when the number of receive antennas is smaller than that of transmit antennas [13]. In a transmission with channel coding, this difficulty directly affects the quality of the log-likelihood ratio (LLR) as a decoder input.

In Fig. 1.4, transmission of two signal streams with binary phase shift keying (BPSK) modulation is shown. The first and second signal streams are assumed to undergo channel fading with the same phase response. The second signal stream, however, has a channel response with a slightly lower amplitude. The LLR values for the first and second streams are calculated and plotted by assuming that the received signals spread throughout the real axis. In the figure, the LLR 1 values are obtained by calculating the log value of the ratio between the likelihood of the first stream transmits bit “1” and the likelihood of the first stream transmits bit “0”. Meanwhile, the LLR 2 values are obtained by calculating the log value of the ratio between the likelihood of the second stream transmits bit “1”

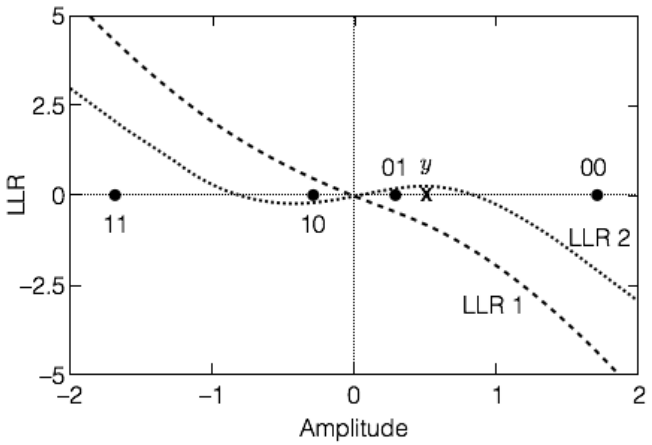

Fig. 1.4. Example of LLR values for two streams transmission using BPSK.

and the likelihood of the second stream transmits bit bit "0", respectively. In Fig. 1.4, the cross mark labeled y represents the received signal after noise contamination when the first stream transmits one bit of "1" and the second stream transmits one bit of "0".

From the figure, it can be observed that the received signal has a negative LLR value for the first stream and a positive value for the second stream. These values indicate that the first stream has a higher probability of being decoded as 0 while the second stream has a higher probability of being decoded as 1. By exploiting its channel coding gain, the decoding process is expected to be able to flip the bits to the correct bits. Considering the shorter distance, flipping back to 10 should have a higher probability than either 00 or 11.

This expectation, however, cannot be fulfilled by the conventional decoding scheme as the decoding processes for the first and second streams in the conventional decoding scheme are conducted *separately*. Therefore, it is more probable that the decoding process flips the bits to 00 or 11. This is because flipping the bit to 10 requires both LLR values to be reversed while flipping the bit to 00 or 11 only requires one LLR to be reversed. Due to this reason, a novel method to improve the performance of decoding process for

the overloaded MIMO scenario needs to be addressed.

1.2.2 Challenges in MU-MIMO with CIC

In MU-MIMO with CIC, detection capability of users is improved by sharing their received signal with the neighboring users. A larger number of collaborating users will, in general, provide better user collaboration gain. It should be noted, however, while it provides a larger diversity, a larger number of collaborating user also requires a larger number of signal exchanges between users. In such cases, a user selection is required to capture the most advantages of MIMO systems [14–16]. It should be pointed out, however, user selection should be designed based on the detection algorithms that will be used in the detection process. For the case of basic MIMO detection algorithms such as ZF, MLD, and MMSE, suitable user selection techniques can be found in [17–21].

Recent development in the detection algorithm, however, establishes several detection algorithms which have a notable potential. A detection algorithm so called QR-decomposition based MLD with M-algorithm (QRM-MLD), for example, capable to obtain a near optimum MLD performance with a significant reduction in complexity. This reduction can be benefited as rather than calculating all possible transmitted symbols, QRM-MLD only calculates several candidates on its calculation. Despite its similarity with MLD (where the detection is based on the Euclidean distance), QRM-MLD has a significant difference with the conventional MLD, that is, the detection process in QRM-MLD is conducted in a recursive manner. The user selection technique suitable for MLD, therefore, will not also be suitable for QRM-MLD. In this regards, a novel user selection technique, which accommodates the recursive manner of QRM-MLD, should be addressed.

In addition to the above problem, MU-MIMO with CIC also has an issue with the lack of performance evaluation in the real environment presented in the previous literature.

Performance evaluation of MU-MIMO with CIC is important as unlike the theoretical scenario which commonly considers identically independent distribution (i.i.d.) Rayleigh fading, actual environments experiencing channel shadowing and channel correlation between users. In the signal processing at the users, the differences at the user sampling time, frequency offset, and signal to noise ratio might also affect the CIC performance. In addition, the reliability of the interuser links in a mobile environment also needs to be confirmed. Field experiments to verify the effectiveness of MU-MIMO with CIC, therefore, needs to be conducted.

1.2.3 Challenges in MU-MIMO with Precoding

Differ with the other two approaches, MU-MIMO with precoding starts its interference cancellation processes at the BS. In each user, the detection process is held by using a simple detection algorithm. MU-MIMO with precoding, however, relies heavily on the accuracy of channel state information (CSI) owned by the BS. Meanwhile, the accurate CSI is hard to be obtained especially when the users are moving and experiencing channel fluctuation. Implementation of this technique, therefore, generally considered a low mobility scenario [22–25]. Future wireless communications, on the other hand, should be able to handle communications for the high-mobility users. In such users, the channel will fluctuate, causing a mismatch between the precoder and the actual downlink channel.

Unfortunately, this issue will be even more severe in the near future. As the sub 3 GHz bands which are commonly used in current mobile communications has been immensely crowded, higher-frequency bands will most likely be utilized in the future wireless communications. The Doppler spread as the source of the channel aging effect, on the other hand, has its value proportional to the carrier frequency. Using frequency bands at around 6 GHz suggested for early step of 5G presented in [26] (this carrier frequency will also be used as a simulation parameter in Chapter 4), for example, already tripled

the maximum Doppler frequency compared to that of current wireless communication systems. In other words, the channel will fluctuate faster, resulting in a more severe mismatch between the precoder and the actual channel.

One straight forward approach to diminish the mismatch between the precoder and the actual channel is by frequently updating the precoder matrix. To reduce the requirement of uplink transmission, channel prediction technique can be used. It should be noted, however, frequently update the precoder matrix drastically increases in computational complexity, especially when the number of transmit antennas and the number of served users is considerably large. A novel technique to intelligently exploit channel prediction, therefore, should be investigated.

1.3 Thesis Outline and Contributions

As described in the above explanation, all of the overloaded MIMO, MU-MIMO with CIC, and MU-MIMO with precoding approaches have issues that need to be tackled. In this thesis, those issues are addressed and possible solutions are proposed for each approach. Specifically, contributions of this thesis can be written as follow.

- In Chapter 2, the potential problem occurred in the implementation of overloaded MIMO is addressed. A novel decoding technique so called joint turbo decoding is then proposed. Using the proposed technique, the decoding performance of overloaded MIMO systems for the case of turbo code is used as the channel code could be significantly improved. For a better analysis, the extrinsic information transfer (EXIT) function for the proposed technique is also derived, and the comparison of the BER performance, throughput, and computational complexity between the conventional turbo decoding and the joint turbo decoding is provided.

- In Chapter 3, MU-MIMO with CIC is discussed and its potential problems are investigated. Specifically, a user selection technique which is suitable when QRM-MLD is used as detection algorithm is proposed. In addition, field experiments to verify the effectiveness of MU-MIMO with CIC in the actual environments are also conducted. It is worth to note, however, due to the time constraint, the field experiment did not consider the proposed user selection techniques.

- In Chapter 4, the problem in MU-MIMO with precoding under a time-varying channel is shown. Next, a technique to exploit Doppler shift information to create a predicted channel matrix is given. Based on the predicted channel matrix, a novel power allocation technique which could significantly reduce the interuser interference in a time-varying MU-MIMO is then presented in this chapter.

Chapter 2

Improving Decoding Capabilities on Overloaded MIMO: Joint Decoding Technique

2.1 Introduction

The problem in the implementation of overloaded MIMO lies with the significant performance degradation that occurs in the detection process [13]. In a system with channel codes, this degradation leads to a significant reduction in the quality of the decoder input. This issue can be optimally tackled by employing joint maximum a posteriori (joint-MAP) detection-decoding technique. This technique, however, has very high computational complexity. Thus, a more feasible decoding technique for the overloaded MIMO system is required.

In this thesis, an overloaded MIMO system which uses turbo codes as its forward error correction (FEC) technique is investigated. Turbo codes are selected to be used in this thesis due to their ability to achieve a performance close to the Shannon limit [27, 28]. Thus, a combination of turbo codes and MIMO systems has excellent potential for high-data-rate communications with low power consumption [29, 30]. This thesis, in particular, investigates the turbo codes which have been used in LTE standard [31], under an orthogonal frequency division multiplexing (OFDM) scenario.

The simplest approach to conduct turbo-MIMO decoding is by using separate processes for detection and decoding. In this approach, soft information from the MIMO detection block is sent to the decoding blocks. In each decoding block, turbo decoding is conducted independently to each transmitted stream [32, 33]. In this thesis, this technique is labeled as *conventional turbo decoding*. Using conventional turbo decoding, however, significant performance degradation due to the quality degradation of soft information occurs. Unfortunately, this degradation cannot be avoided by increasing the number of iterations in turbo decoding. As can be seen in [27], the relative performance enhancement of turbo decoding after a certain number of iterations is negligible.

To improve the decoding performance, information exchanges between detection blocks and the decoding blocks can be implemented. In [34], hard information is used as the decoding feedback. To increase the decoding quality even further, iterative detection and decoding (IDD) techniques, which employ soft information exchanges between those blocks can be implemented [35–47]. In these techniques, however, repetitive detection processes are required to generate updated soft information. Therefore, a low complexity detection algorithm should be used in these techniques. In [38–40], MAP-based detection algorithms with complexity reduction are employed. These algorithms, however, can only be implemented in the typical MIMO system where the number of receive antennas is not less than that of transmit antennas. In [42, 43], the IDD technique is employed for a multiuser detection. The technique in [42, 43] uses parallel minimum mean square error (MMSE) cancellers to reduce the complexity in the multiuser detector blocks. Similar methods can also be seen in [45–47]. It should be noted, however, these techniques still require the detection block to update its weighting vector in each iteration process to generate extrinsic information. In addition, the multiplications of these vectors with soft information from the decoding blocks are also needed. As these processes are conducted

in a sequential manner, the IDD techniques could have a significant signal processing delay.

In this thesis, a novel technique to improve the decoding performance of overloaded MIMO systems is presented. Similar to the conventional turbo decoding technique, the proposed technique conducts the detection process only once and removes the potential of the detection stage to become a bottleneck in the whole detection-decoding process. However, instead of conducting separate turbo decoding for each signal stream, the proposed technique conducts the decoding process *jointly* between all signal streams. In this thesis, the proposed technique is called *joint turbo decoding*.

2.2 Overloaded MIMO-OFDM with Turbo Codes

Figure 2.1 shows a block diagram of a MIMO-OFDM system with turbo codes using N_{t} transmit antennas and N_{r} receive antennas. Herein, as in the overloaded case, $N_{\mathrm{t}} > N_{\mathrm{r}}$.

2.2.1 Turbo Encoding

The turbo codes used in the LTE system are systematic parallel concatenated convolutional codes with two 8-state encoders and one internal interleaver [31]. In this thesis, a scenario with the interleaver size in each stream is equal is considered. The trellis diagram of each encoder can be seen in Fig. 2.2.

For an input block size of L bits, the outputs of the turbo encoder consist of three length-L streams $d_l^{(0)}$, $d_l^{(1)}$, and $d_l^{(2)}$, which are referred to as the "Systematic", "Parity 1", and "Parity 2" streams, respectively, as well as 12 tail bits due to trellis termination. In LTE, the tail bits are multiplexed to the ends of the three output streams, whose length thus increases to $L + 4$ bits each [31].

To support higher data rates, LTE provides a rate matching (RM) function. In the RM, each of the three output streams is rearranged with sub-block interleavers.

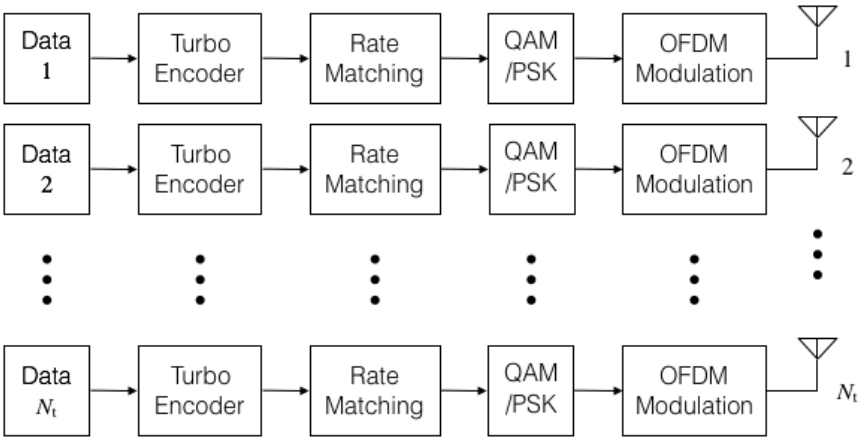

(a) Transmitter.

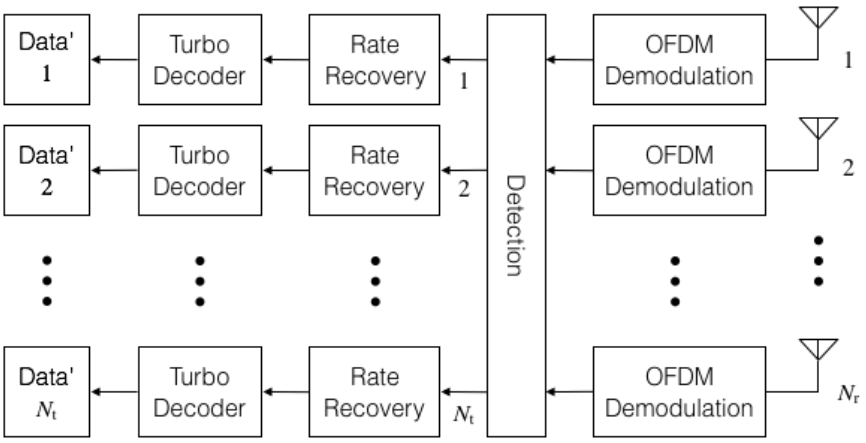

(b) Receiver.

Fig. 2.1. MIMO-OFDM system with turbo codes.

Then, a single output buffer is formed by placing the rearranged systematic bits at the beginning, followed by bit by bit interlacing of the two rearranged parity bits with a total length of $3L + 12$ bits. The outputs are then passed to a circular buffer for bit selection and puncturing. The output bits of the RM function are defined as $b_0, b_1, \ldots, b_{J-1}$, where J is the total number of transmitted bits, and the value depends on the desired code rate [31]. Afterward, the RM outputs are modulated using quadrature amplitude modulation (QAM) modulation with each QAM symbol on the n_tth transmit antenna, s^{n_t}, consisting of Q bits of $b_j^{n_t}$.

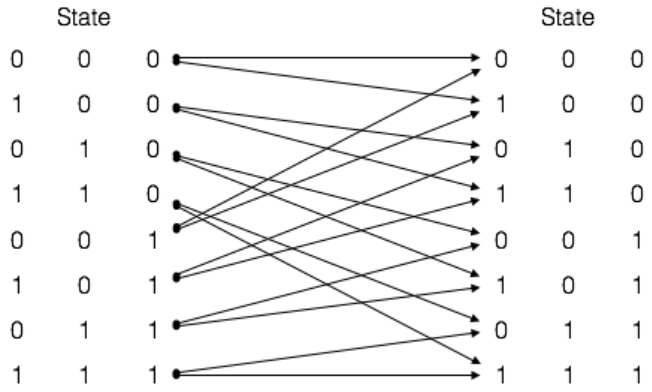

Fig. 2.2. Trellis diagram of turbo codes in LTE.

2.2.2 OFDM Transmission and Reception

The QAM symbols are then arranged from serial into parallel and assigned to F data subcarriers [48]. The OFDM symbol is then created by conducting inverse discrete Fourier transform (IDFT) to the OFDM subcarriers. A guard interval (GI) is then added by replicating the last part of the OFDM symbol. For the case of LTE, the standard of the GI length is described in [48].

Passing through a wireless channel, the transmitted signals are then received by N_{r} receive antennas. In each receive antennas, the GI is then removed and discrete Fourier transform (DFT) is conducted to demodulate the OFDM symbols. Denotes $\boldsymbol{y}[f] = [y_1[f], y_2[f], \ldots, y_{N_{\mathrm{r}}}[f]]^{\mathrm{T}}$ as the vector of received signals at fth subcarrier, $\boldsymbol{s}[f] = [s_1[f], s_2[f], \ldots, s_{N_{\mathrm{f}}}[l]]^{\mathrm{T}}$ as the vector of transmitted signals at fth subcarrier, and $\boldsymbol{n}[f] = [n_1[f], n_2[f], \ldots, n_{N_{\mathrm{r}}}[f]]^{\mathrm{T}}$ as the noise vector of fth subcarrier, respectively. In a matrix form, the vector of received signals for f subcarrier can be obtained by

$$\boldsymbol{y}[l] = \boldsymbol{H}[f]\boldsymbol{s}[f] + \boldsymbol{n}[f], \tag{2.1}$$

where

$$\boldsymbol{H}[f] = \begin{bmatrix} h_{1,1}[f] & h_{1,2}[f] & \cdots & h_{1,N_\mathrm{t}}[f] \\ h_{1,1}[f] & h_{1,2}[f] & \cdots & h_{1,N_\mathrm{t}}[f] \\ \vdots & \vdots & \vdots & \vdots \\ h_{N_\mathrm{r},1}[f] & h_{N_\mathrm{r},2}[f] & \cdots & h_{N_\mathrm{r},\mathrm{t}}[f] \end{bmatrix}. \tag{2.2}$$

In each receive antenna, the output of the DFT for all data subcarriers is then sent to the detection block to calculate a priori values.

2.2.3 Turbo decoding

The first step in the turbo decoding process is to obtain the a priori LLR value for each bit from the signal detection block. For MIMO-OFDM systems, the a priori LLR value for the fth subcarrier in the n_tth signal stream can be obtained by

$$L_\mathrm{a}(b_q^{n_\mathrm{t}}|\boldsymbol{y}[f]) = \log\left(\frac{\sum_{\mathbf{s}[f]:b_q^{n_\mathrm{t}}=1}\exp(-\frac{1}{\sigma^2}\|\boldsymbol{y}[f]-\boldsymbol{H}[f]\boldsymbol{s}[f]\|^2)}{\sum_{\mathbf{s}[f]:b_q^{n_\mathrm{t}}=0}\exp(-\frac{1}{\sigma^2}\|\boldsymbol{y}[f]-\boldsymbol{H}[f]\boldsymbol{s}[f]\|^2)}\right), \tag{2.3}$$

where $b_q^{n_\mathrm{t}}$ denotes the qth bit of symbol $s^{n_\mathrm{t}}[f]$ and σ^2 denotes the noise variance. In each stream, J a priori LLR values for $b_0^{n_\mathrm{t}}, b_1^{n_\mathrm{t}}, \ldots, b_{J-1}^{n_\mathrm{t}}$ are obtained from $\boldsymbol{y}[f]$. For bits that are not transmitted due to puncturing, the a priori LLR values are set to 0 in the rate recovery process, giving a total of $3L+12$ a priori LLR values.

After the rate recovery process, these a priori LLR values are rearranged back into three length-$L+4$ streams of soft input for the decoder that are denoted as $L_\mathrm{a}(d_l^{(0)})$, $L_\mathrm{a}(d_l^{(1)})$, and $L_\mathrm{a}(d_l^{(2)})$ which correspond to the a priori LLR values of the "Systematic", "Parity 1", and "Parity 2", respectively. Afterward, the turbo decoder uses these values to calculate the probabilities of the received bit, γ_l, the forward recursion, α_l, and the backward recursion, β_l, for the lth bit, which are required to obtain the extrinsic LLR values, L_e.

Using the log-BCJR algorithm [49], the value of γ_n from state ρ' to state ρ at step l in the first decoder can be obtained by

$$\gamma_l(\rho', \rho) = L_{\mathrm{a}}(d_l^{(0)}(\rho', \rho)) + L_{\mathrm{a}}(d_l^{(1)}(\rho', \rho)), \tag{2.4}$$

where $L_{\mathrm{a}}(d_l^{(0)}(\rho', \rho)) = L_{\mathrm{a}}(d_l^{(0)})$ if the bit associated with the transition from state ρ' to state ρ is 1, while $L_{\mathrm{a}}(d_l^{(0)}(\rho', \rho)) = 0$ if the bit associated with the transition from state ρ' to state ρ is 0. This condition also applies for $L_{\mathrm{a}}(d_l^{(1)}(\rho', \rho))$ or $L_{\mathrm{a}}(d_l^{(2)}(\rho', \rho))$ in the other decoder.

Afterward, the value of α_{l+1} for state ρ at step $l+1$ can be defined by

$$\alpha_{l+1}(\rho) = \max_{\rho' \in \{P'\}}^{*}(\gamma_l(\rho', \rho) + \alpha_l(\rho')), \tag{2.5}$$

where $\{P'\}$ is the aggregate of all the states ρ' in step l that end at state ρ in step $l+1$, while max* denotes the Jacobian logarithm function. Furthermore, the value of β_l for state ρ' at step l can be obtained from

$$\beta_l(\rho') = \max_{\rho \in \{P\}}^{*}(\gamma_l(\rho', \rho) + \beta_{l+1}(\rho)), \tag{2.6}$$

where $\{P\}$ is the aggregate of all the states ρ in step $l+1$ which are from state ρ' in step l.

After the values of γ_l, α_l, and β_l are obtained, the extrinsic LLR values can be calculated by

$$\begin{aligned} L_{\mathrm{e}}(d_l^{(0)}) = & \max_{(\rho', \rho) \in \{\tau_l^1\}}^{*}(\alpha_l(\rho') + \gamma_l(\rho', \rho) + \beta_{l+1}(\rho)) \\ & - \max_{(\rho', \rho) \in \{\tau_l^0\}}^{*}(\alpha_l(\rho') + \gamma_l(\rho', \rho) + \beta_{l+1}(\rho)), \end{aligned} \tag{2.7}$$

where $\{\tau_l^0\}$ and $\{\tau_l^1\}$ are the aggregates of all the transitions from state ρ' to state ρ at step l when the input bit is 0 and 1, respectively. The extrinsic LLR values are then used as the soft inputs of the other decoder or for the hard outputs after the desired number of iterations.

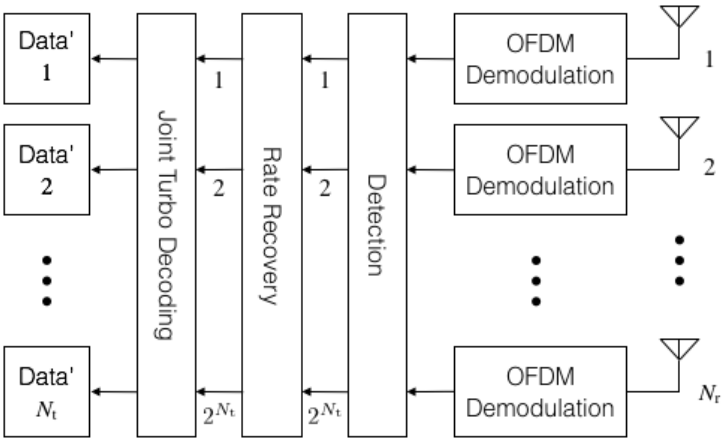

Fig. 2.3. Block diagram of joint turbo decoding.

2.3 Joint Turbo Decoding

2.3.1 Decoding Process

In the conventional technique, the MIMO detection block provides N_t soft information of each bit from all N_t transmitted streams. Each of this N_t soft information is then delivered to N_t separate turbo decoders. Joint turbo decoding, on the other hand, assigns the MIMO detection block to provide soft information for each combination of bits from all streams. Through this process, the reliability of soft information of the decoder input can be improved. This soft information is then processed by one joint-decoder instead of N_t separate decoders. As this one joint-decoder has to process soft information of 2^{N_t} combinations of bits, the trellis diagrams of the encoders from all streams should also be combined. For this purpose, a super-trellis diagram [50] is employed. The super-trellis diagram uses S^{N_t} states, where S is the number of states in each encoder.

Figure 2.3 shows a block diagram of the proposed joint decoding technique. As can be seen in the figure, joint turbo decoding uses 2^{N_t} soft information values as the decoder inputs, which represent the total number of possible bit combinations. The vector of each bit combination is denoted as $\mathbf{b}$. To calculate a priori LLR values, a certain bit

combination can be used as a reference point and denoted as $\tilde{\mathbf{b}}$. For each bit combination, the a priori LLR value for each corresponding subcarrier f can be defined as

$$L_{\mathrm{a}}(\boldsymbol{b}_q|\boldsymbol{y}[f]) = \log\left(\frac{\sum_{\boldsymbol{s}[f]:\boldsymbol{b}_q=\boldsymbol{b}} \exp(-\frac{1}{\sigma^2}\|\boldsymbol{y}[f]-\boldsymbol{H}[f]\boldsymbol{s}[l]\|^2)}{\sum_{\boldsymbol{s}[f]:\boldsymbol{b}_q=\tilde{\boldsymbol{b}}} \exp(-\frac{1}{\sigma^2}\|\boldsymbol{y}[f]-\boldsymbol{H}[f]\boldsymbol{s}[f]\|^2)}\right), \tag{2.8}$$

where $\boldsymbol{b}_q = [b_q^1, b_q^2, \ldots, b_q^{N_{\mathrm{t}}}]^{\mathrm{T}}$ is a combination of the qth bit of $\boldsymbol{s}[f]$.

For each bit combination, J a priori LLR values of $\boldsymbol{b}_0, \boldsymbol{b}_1, \ldots, \boldsymbol{b}_{J-1}$ are obtained from $\{\boldsymbol{y}[f]\}$. Similarly to the conventional technique, the a priori LLR values are set to 0 for bits that are not transmitted due to puncturing, giving a total of $3L+12$ a priori LLR values. After the rate recovery process, every $3L+12$ a priori LLR values of each bit combination of $\boldsymbol{b}_j$ are rearranged back into three length-$L+4$ streams of soft input for the decoder that are denoted as $L_{\mathrm{a}}(\boldsymbol{d}_l^{(0)})$, $L_{\mathrm{a}}(\boldsymbol{d}_l^{(1)})$, and $L_{\mathrm{a}}(\boldsymbol{d}_l^{(2)})$, which correspond to the a priori LLR values of "Systematic", "Parity 1", and "Parity 2", respectively. These inputs are used to calculate the values of γ_l, α_l, and β_l for obtaining the extrinsic LLR values, L_{e}.

In joint turbo decoding, the super-trellis diagram is implemented to combine the trellis diagrams from all streams in a MIMO system. The basic idea of this super-trellis implementation is similar with [50] which implements the super-trellis diagrams to trellis coded modulation for co-channel interference canceller. For the case of two transmit antennas, the super-trellis diagram in joint turbo decoding can be seen in Fig. 2.4. As can be seen in the figure, a super-trellis diagram which is constructed from two transmit antennas contains 8^2 states and 2^2 input combinations.

Defining ϕ as the state in the super-trellis diagram, the value of γ_l from state ϕ' to state ϕ in the first decoder is calculated as

$$\gamma_l(\phi', \phi) = L_{\mathrm{a}}(\boldsymbol{d}_l^{(0)}(\phi', \phi)) + L_{\mathrm{a}}(\boldsymbol{d}_l^{(1)}(\phi', \phi)), \tag{2.9}$$

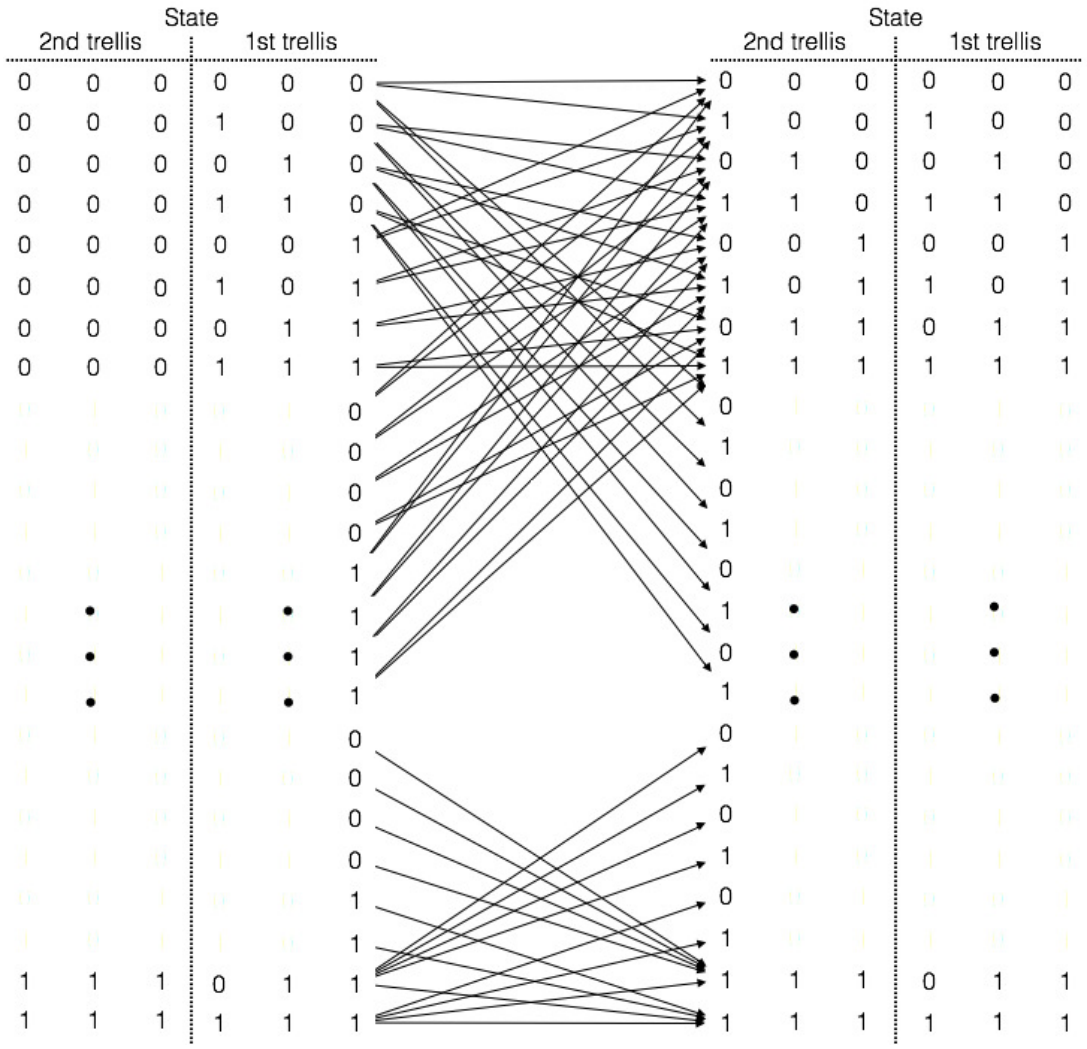

Fig. 2.4. Super-trellis diagram.

where $\boldsymbol{d}_l^{(0)}(\phi', \phi)$ and $\boldsymbol{d}_l^{(1)}(\phi', \phi)$ are the combinations of the encoder input bits and the combinations of the encoder output bits associated with the transition from state ϕ' to state ϕ, respectively.

Afterward, in the forward recursion, the values of α_{l+1} can be defined by

$$\alpha_{l+1}(\phi) = \max_{\phi' \in \{\Phi'\}}^{*}(\gamma_l(\phi', \phi) + \alpha_l(\phi')), \tag{2.10}$$

where $\{\Phi'\}$ is the aggregate of all the states ϕ' in step l which end at state ϕ in step $l+1$.

Meanwhile, the values of β_l in the backward recursion can be obtained from

$$\beta_l(\phi') = \max_{\phi \in \{\Phi\}}^{*} (\gamma_l(\phi', \phi) + \beta_{l+1}(\phi)), \tag{2.11}$$

where $\{\Phi\}$ is the aggregate of all the states ϕ in step $l+1$ which are from state ϕ' in step l.

After the values of γ_l, α_l, and β_l have been obtained, the extrinsic LLR values for the systematic bit combination $\boldsymbol{d}_l^{(0)}$ can be obtained by

$$\begin{aligned} L_{\mathrm{e}}(\boldsymbol{d}_l^{(0)}) = & \max_{(\phi', \phi) \in \{T_l^{\boldsymbol{d}_l^{(0)}}\}}^{*} (\alpha_l(\phi') + \gamma_l(\phi', \phi) + \beta_{l+1}(\phi)) \\ & - \max_{(\phi', \phi) \in \{T_l^{\tilde{\boldsymbol{d}}_l^{(0)}}\}}^{*} (\alpha_l(\phi') + \gamma_l(\phi', \phi) + \beta_{l+1}(\phi)), \end{aligned} \tag{2.12}$$

where $\tilde{\boldsymbol{d}}_l^{(0)}$ is the systematic bit combination chosen as the reference, while $\{T_l^{\boldsymbol{d}_l^{(0)}}\}$ and $\{T_l^{\tilde{\boldsymbol{d}}_l^{(0)}}\}$ are the aggregates of all transitions from state ϕ' to state ϕ in step l when the input bit combinations are $\boldsymbol{d}_l^{(0)}$ and $\tilde{\boldsymbol{d}}_l^{(0)}$, respectively. Similarly to in the conventional turbo decoding technique, the extrinsic LLR values can be used as the soft inputs for the next decoding process or used for the hard output decision. In joint turbo decoding, the bit combination with the highest extrinsic LLR value is selected as the output bits of the decoder.

2.3.2 EXIT charts

To obtain the characteristic of an iterative process in a decoder, an extrinsic information transfer (EXIT) chart can be drawn to show the exchange of mutual information (MI) between decoders [51], [52]. In joint turbo decoding, the maximum value of the average MI is equal to N_{t} as a result of cooperative decoding between N_{t} transmitted streams. Let $Pr(\boldsymbol{b}_l)$ denotes the probability of bit combination $\boldsymbol{b}$ in slot l. Then the MI can be obtained as

$$I = N_{\mathrm{t}} + \frac{1}{L}\sum_{l=1}^{L}\sum_{\boldsymbol{b}_l \in \mathcal{B}} Pr(\boldsymbol{b}_l)\log_2\left(Pr(\boldsymbol{b}_l)\right), \tag{2.13}$$

where $\mathcal{B}$ denotes all possible bit combinations.

To plot the EXIT chart, random Gaussian variables are required to approximate the LLR distribution of a priori information. For a MIMO system, the mean and variance of a priori information depend on the channel realization [53], [54]. Denoting $\boldsymbol{h}_{n_{\mathrm{t}}}$ as the channel response of the n_{t}th transmit antenna, the a priori LLR value, L_{a}, can be expressed as

$$L_{\mathrm{a}} = \frac{2}{\sigma^2}\left(\|\boldsymbol{h}_{n_{\mathrm{t}}}\|^2 u + \|\boldsymbol{h}_{n_{\mathrm{t}}}\| n\right), \tag{2.14}$$

where $u \in \{+1, -1\}$ is the modulated output bit of the turbo codes.

For the case of joint turbo decoding, a priori LLR values exist for each bit combination. Therefore, each bit combination has its own instantaneous values of the a priori LLR mean and variance. These a priori LLR values depend not only on the channel realization but also on the error vectors between the transmitted bit combination with each bit combination. Denoting $b_{n_{\mathrm{t}}}$ as the n_{t}th element of bit combination $\boldsymbol{b}$, and $\hat{b}_{n_{\mathrm{t}}}$ as the n_{t}th element of the transmitted bit combination $\hat{\boldsymbol{b}}$, the a priori LLR values in joint turbo decoding can be expressed as

$$L_{\mathrm{a}}(\boldsymbol{b}) = \frac{2}{\sigma^2}\sum_{n_{\mathrm{t}}=1}^{N_{\mathrm{t}}}\left(\|\boldsymbol{h}_{n_{\mathrm{t}}}\|^2 + \|\boldsymbol{h}_{n_{\mathrm{t}}}\| n\right)\left(b_{n_{\mathrm{t}}} - \hat{b}_{n_{\mathrm{t}}}\right). \tag{2.15}$$

2.3.3 Computational complexity

The implementation of the super-trellis diagram in joint turbo decoding results in greater computational complexity and a larger number of required memories. While the computational complexity of conventional turbo decoding increases linearly, that of joint turbo decoding increases exponentially with the number of transmit antennas. In terms of

Table 2.1. Comparison of computational complexity between conventional turbo decoding and joint turbo decoding

technique	**Add**	**Compare & Select**
Conventional turbo decoding	$5N_{\mathrm{t}}S + 1$	$6N_{\mathrm{t}}S$
Joint turbo decoding	$(4 \times 2^{N_{\mathrm{t}}} - 3)S^{N_{\mathrm{t}}} + 1$	$3 \times 2^{N_{\mathrm{t}}}S^{N_{\mathrm{t}}}$

the required memory, the joint turbo decoding technique requires a number of memories $\frac{1}{N_{\mathrm{t}}}2^{N_{\mathrm{t}}-1}S^{N_{\mathrm{t}}-1}$ times larger than that the conventional turbo decoding technique. Considering the exponential nature of its computational complexity, the maximum potential of the proposed technique can be obtained when the number of transmit antennas is relatively small (e.g. $1 < N_{\mathrm{t}} \leq 4$). An example of this scenario is when an MS located at the edge of the cell is jointly served by more than one BS. In this scenario, the proposed technique enables the multi-BS services through its superior performance enhancement. On the other hand, as the number of the serving BS is not significantly large, the addition in the computational complexity will not increase drastically.

Note, however, unlike in the IDD technique, the increase in the computational complexity in joint turbo decoding only occurs in the decoding block, which performs relatively simple add-compare-select operations. In addition, the calculation process for each step l in each iteration can be conducted in a parallel manner. Therefore, the advantage of joint turbo decoding can be preserved, especially for the case of an overloaded MIMO system. Furthermore, as shown later in the simulation results, joint turbo decoding requires only a small number of iterations to get beyond the waterfall area. In this regard, the processing time can be shorter than that of conventional turbo decoding, which requires many iterations.

Table 2.2. Simulation parameters

Channel code	Turbo Codes, Rates: 1/3, 1/2		
Interleaver Size	4800, 2432, 1600, 1216		
Modulation	QPSK, 16QAM, 64QAM, 256QAM		
Multiplexing	OFDM		
Channel Bandwidth	2.5 MHz		
Subcarrier Spacing	15 kHz		
DFT Size	256		
Occupied Subcarriers	151		
Sampling Frequency	3.84 MHz		
Cyclic Prefix	5.21 μs (first symbol) 4.69 μs (six following symbols)		
Transmit Antennas	2	3	4
Number of Iterations			
Conventional technique	64	171	8192
Proposed technique	8	8	8
Receive Antennas	2		
Channel Model	6-tap typical urban 18-tap Rayleigh fading		

2.4 Numerical Results

2.4.1 Simulation Parameters

In this simulations, 8-state memory turbo codes with interleaver sizes of 4800, 2432, 1600, and 1216 are employed [31]. The code rates of 1/3 and 1/2 are used with the RM function following the description in [31]. The coded symbols outputs by the turbo encoder are modulated using quadrature phase shift keying (QPSK) modulation and multiplexed by OFDM with a channel bandwidth of 2.5 MHz and a subcarrier spacing of 15 kHz. The DFT size in OFDM is 256 with 151 subcarriers are occupied for data transmissions. For

every seven OFDM symbols, the guard interval is set to 5.21 μs for the first symbol and 4.69 μs for the six following symbols [48].

The channel models for these simulations are 18-tap Rayleigh fading and 6-tap typical urban (TU) channels, both with perfect channel estimation. The TU channel characteristic follows the description in [55]. In addition, two receive antennas are used in the simulation with the number of transmit antennas varied from 2 to 4. To obtain equal complexity for each technique, the number of iterations for the conventional technique is set to $\frac{1}{N_t}2^{N_t-1}8^{N_t-1}$ times larger than the number of iterations for the joint turbo decoding technique. Furthermore, transmission using a single transmit antenna with higher-order modulation is also simulated for comparison.

2.4.2 BER performance

2.4.2.1 BER in a channel with low correlation

Fig. 2.5 shows the BER of an OFDM system with turbo codes in the 18-tap Rayleigh fading channel using code rates of 1/3 and 1/2 for both conventional turbo decoding and joint turbo decoding. The BER of the single-transmit-antenna technique using higher-order modulation is also plotted for comparison. From Fig. 2.5(a), it can be observed that the transmission using multiple antennas gives better performance than the single-antenna transmission. For the case of two transmit antennas, the multiple-antenna transmission with the conventional turbo decoding technique gives 0.8 dB performance gain compared with the single-antenna transmission with 16QAM. This performance can be further enhanced using the turbo joint decoding technique, which gives 0.4 dB better performance than the conventional turbo decoding technique.

Furthermore, the performance gain is even higher when the number of transmit antennas increases. For the case of four transmit antennas, the performance of joint turbo

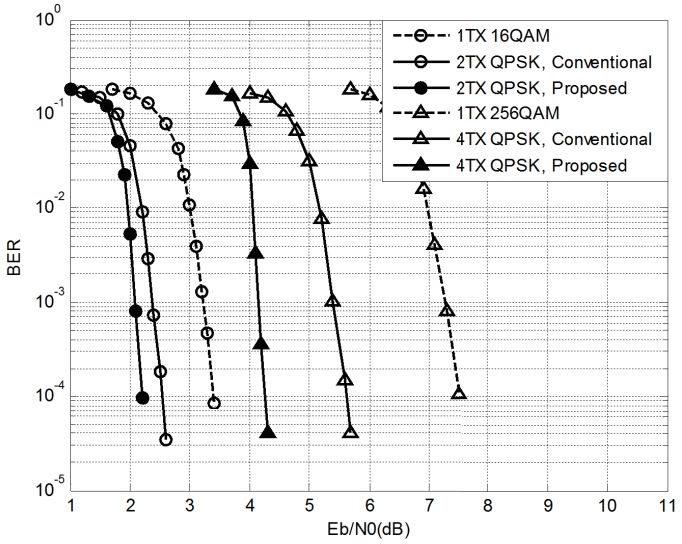

(a) Code rate of 1/3.

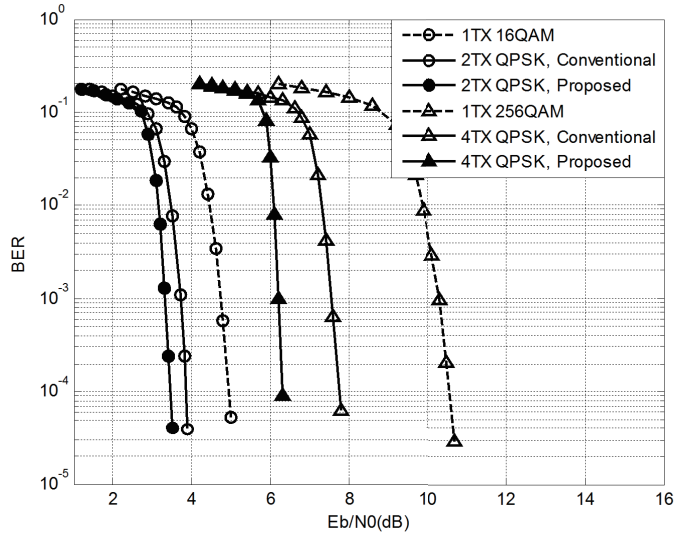

(b) Code rate of 1/2.

Fig. 2.5. BER performance of joint turbo decoding in the 18-tap Rayleigh fading channel (0018-9545 © 2016 IEEE).

decoding exceeds those of MIMO systems with the conventional turbo decoding technique and the single-transmit-antenna technique with 256QAM by about 1.5 dB and 3.4 dB, respectively.

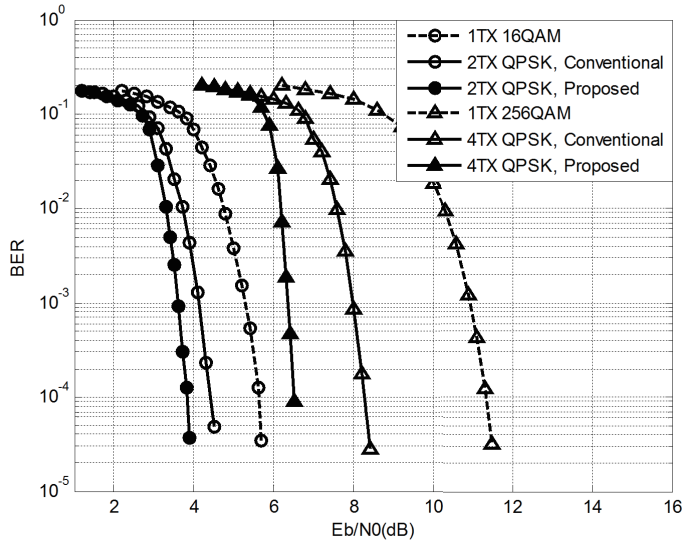

Fig. 2.6. BER performance of joint turbo decoding in the 6-tap TU channel with the code rate of 1/2 (0018-9545 © 2016 IEEE).

Transmission using multiple antennas has a greater advantage at a higher code rate. From Fig. 2.5(b), it can be seen that the performance of MIMO systems with two transmit antennas using the conventional turbo decoding technique exceeds the performance of the single-transmit-antenna technique with 16QAM by about 1.2 dB. Using four transmit antennas with the conventional turbo decoding technique, a 2.9 dB performance gain can be obtained as compared with the single-transmit-antenna technique with 256QAM.

Using the turbo joint decoding technique, this performance gain can be further enhanced. For the case of two transmit antennas, the performance can be increased by 1.6 dB, while the increase is about 4.4 dB for the case of four transmit antennas. In addition, it can be observed from both figures that the performance gain of the joint turbo decoding technique can be maintained regardless the code rate used by the turbo codes.

2.4.2.2 BER in a channel with high Correlation

One of the factors that could degrade the performance of an OFDM system is the channel correlation between subcarriers. A channel with higher correlation will have worse performance than a channel with lower correlation. Fig. 2.6 shows the performance of the MIMO-OFDM system using turbo codes with the code rate of 1/2 in a 6-tap TU channel. The performance curves of the joint turbo decoding technique and the conventional technique are plotted. For reference, the performance is also compared with that of a single-transmit-antenna technique with higher-order modulation.

From the figure, it can be seen that for all the techniques, performance degradation occurs compared with the case of a low correlation. However, it can also be observed that in the channel with the higher correlation, the proposed technique provides a larger performance gain. Compared with the conventional turbo decoding technique, the proposed technique has a superior performance by about 0.6 dB for the case of two transmit antennas and by about 2.0 dB for the case of four transmit antennas. Moreover, using four transmit antennas, the performance gain of the proposed technique compared with the single-antenna transmission technique with 256QAM increases from 4.4 dB for a low-correlation channel to 5.1 dB for a high correlation channel.

2.4.2.3 BER in the case of equal total number of information bits

In the previous simulation, an equal interleaver size was used for both single-antenna transmission and multiple-antenna transmission. In Fig. 2.7, the numerical results obtained through computer simulation are shown for the case of an equal total number of information bits. The turbo code with the code rate of 1/3 is used for the simulation in the 18-tap Rayleigh fading channel. In the figure, the single-antenna transmission with higher-order modulation uses an interleaver with a size of 4800 while the multiple-antenna transmission uses an interleaver with a size of $\approx 4800/N_{\mathrm{t}}$.

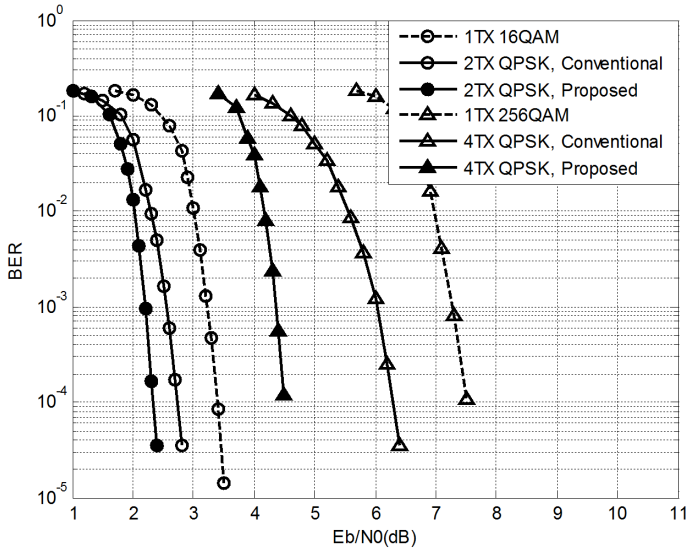

Fig. 2.7. BER performance of joint turbo decoding in the 18-tap Rayleigh fading channel with equal total number of information bits (0018-9545 © 2016 IEEE).

Comparing Fig. 2.5(a) and Fig. 2.7, it can be observed that the performance gain of the proposed technique compared with the single-antenna transmission with higher-order modulation is decreased due to the smaller interleaver size. For the case of two transmit antennas, the performance gain decreases from 1.2 dB to 1.0 dB while for the case of four transmit antennas, the performance gain decreases from 3.4 dB to 3.0 dB. However, compared with the results obtained for conventional turbo decoding, a larger performance gain can be observed when a smaller interleaver size is used. For the case of four transmit antennas, for example, the performance gain increases from 1.5 dB to 1.9 dB.

2.4.3 EXIT charts

Fig. 2.8 shows the EXIT charts of the joint turbo decoding technique with two transmit antennas and two receive antennas in an 18-tap Rayleigh fading channel. The turbo code with a coding rate of 1/3 is used. The EXIT charts are plotted together with the decoding

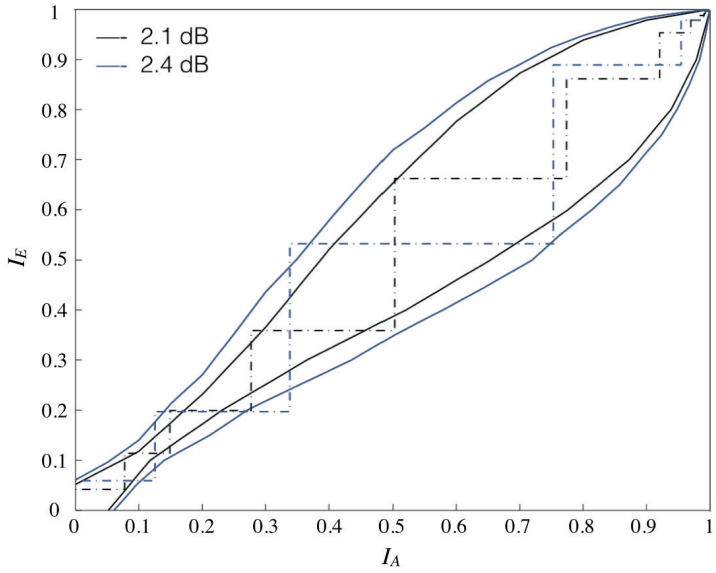

Fig. 2.8. EXIT chart of joint turbo decoding (0018-9545 © 2016 IEEE).

trajectories for $Eb/N0$ values of 2.1 dB and 2.4 dB. The values of a priori MI, I_{A}, and the values of extrinsic MI, I_{E}, are normalized to 1. From the figure, it can be observed that the EXIT charts are relatively consistent with the decoding trajectories. Therefore, the approximation of a priori LLR values in Eq. (2.15) is suitable for representing the actual LLR distribution in joint turbo decoding.

When $Eb/N0$ is 2.1 dB, the EXIT chart starts to converge. This $Eb/N0$ value corresponds to the waterfall region in Fig. 2.5(a). In addition, the 'gate' of the EXIT chart in joint turbo decoding is located at the value of MI is equal to 0.13. In other words, the critical point of joint turbo decoding appears at a relatively small value of MI. Using this characteristic, unreliable data transmissions can be easily detected after a small number of iterations in the decoding process. Furthermore, when the value of MI is sufficiently large, the decoding trajectories for this $Eb/N0$ value are smaller than those in the EXIT chart. This is due to the fact that the limited size of the interleaver has the greatest effect in the waterfall region. When $Eb/N0$ is 2.4 dB, both the decoding

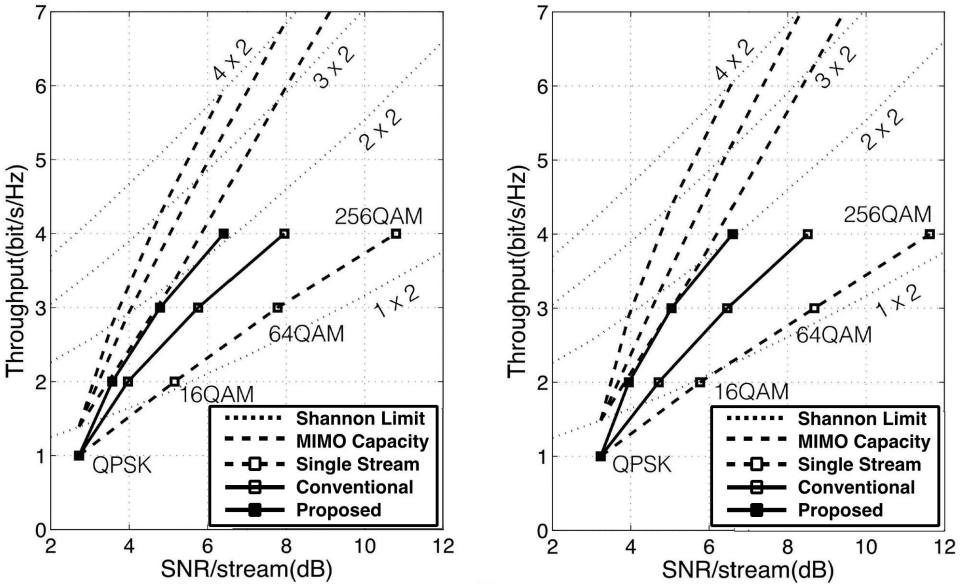

(a) 18-tap Rayleigh fading channel. (b) 6-tap TU channel.

Fig. 2.9. Throughput improvement of joint turbo decoding (0018-9545 © 2016 IEEE).

trajectory and the EXIT chart easily converge. In the BER chart, this $Eb/N0$ value corresponds to the error-floor region.

2.4.4 Throughput improvement

A comparison of the throughput between the conventional and proposed techniques is shown in Fig. 2.9. For both figures, the turbo code with a code rate of 1/2 is used. For the MIMO systems, QPSK modulation is employed. As QPSK contains two bits in each symbol, each transmit antenna will have a throughput of 1 bit/s/Hz when the BER threshold is fulfilled. In this figure, the BER threshold is set to 10^{-5}, which is generally acceptable for data transmissions. The value of SNR/stream required by the conventional and proposed technique to achieve this threshold is represented by the horizontal axis. For comparison, the throughput of the single-transmit-antenna technique with higher-order modulation is also plotted, where the horizontal axis represents the required SNR/2bits. In addition, the dashed lines are the Shannon limit curves for 1×2,

2×2, 3×2, and 4×2 MIMO systems. The MIMO capacities are then drawn by connecting the capacity limits for the corresponding values of the required SNR/stream using bold dashed lines.

From the figure, it can be seen that the proposed technique has a larger throughput than the conventional turbo decoding technique. In the 18-tap Rayleigh fading channel, it can be observed from Fig. 2.9(a) that the conventional technique supports a throughput of 3.34 bit/s/Hz at an SNR/stream of 6.4 dB. For the same SNR/stream, the proposed technique is able to support a throughput of 4 bit/s/Hz, which is an improvement of 20%. In addition, this throughput is also larger than that of the single-transmit-antenna transmission technique with higher-order modulation, which only provides 2.56 bit/s/Hz.

In the channel with a higher correlation between the subcarriers, the throughput enhancement of the proposed technique is greater. It can be observed from Fig. 2.9(b) that in the 6-tap TU channel, the conventional technique only achieves a throughput of 3.15 bit/s/Hz at an SNR/stream of 6.6 dB. For the same SNR/stream, the proposed technique is able to support a throughput of 4 bit/s/Hz, which is an improvement of 27%. Compared with the single-transmit-antenna transmission technique, this throughput is equal to an improvement of 71%.

Furthermore, it can be observed from the figure that the proposed technique has a throughput/(SNR/stream) ratio close to that of the theoretical MIMO capacity. Therefore, adding more transmit antennas will not significantly increase the gap between the achievable throughput and the maximum capacity.

2.5 Summary

In this thesis, a joint decoding technique for turbo codes, so-called joint turbo decoding, has been proposed. In joint turbo decoding, calculations of soft information are conducted for each combination of bits from all streams instead of separately between each

stream. In addition, the trellis diagrams of the encoders from all streams are combined using a super-trellis diagram.

The numerical results obtained through computer simulation show that the performance of the proposed technique surpasses that of the conventional technique especially for the case of an overloaded MIMO system. For the case of four transmit and two receive antennas, for example, the performance of the proposed technique using an interleaver size of 4800 in the 18-tap Rayleigh fading channel exceeds that of the conventional technique by about 1.5 dB at a BER of 10^{-5}. The performance gain increases in a highly correlated channel. In the 6-tap TU channel, the performance of the proposed technique exceeds the performance of the conventional technique by about 2.0 dB. The performance gain also increases for a smaller interleaver size. When the interleaver size is decreased from 4800 to 1216, the performance gain increases from 1.5 dB to 1.9 dB.

Furthermore, it has been shown that joint turbo decoding can increase the throughput of MIMO systems as compared with that of conventional turbo decoding. In the 18-tap Rayleigh fading channel, the throughput increases by about 23% compared with that of conventional turbo decoding and by about 57% compared with that of single-transmit-antenna transmission. In the channel with higher correlation, the throughput increases by about 30% compared with that of conventional turbo decoding and by about 70% compared with that of single-transmit-antenna transmission.

Chapter 3

MU-MIMO with Collaborative Interference Cancellation: User Selection Techniques and Field Experiments

3.1 Introduction

In MU-MIMO, the advantages of MIMO systems can be preserved even when the number of receive antennas in each user is limited. Considering this potential, therefore, MU-MIMO has been attracted many researchers in wireless communication areas [56, 57]. Owing to the distance between the MSs, MU-MIMO ensures that the channel correlation is relatively low and preserves the spatial multiplexing gain [58, 59].

In MU-MIMO scenario, one of the possible approaches to conduct interference cancellation is by CIC [5–8]. In this technique, the users share their received signals with other users to virtually increase the number of receive antennas. This technique does not require accurate CSI at the transmitter and thus, is suitable for high user density and high mobility environments such as when the users are on trains and buses. In addition, users in this scenario move together and their positional relationships are relatively constant. Therefore, it is not difficult to establish the cooperation between users and conduct CIC.

In CIC, the number of available users is most likely larger than the number of transmit antennas. To capture its most advantages, therefore, a user selection can be implemented to select K_{col} collaborating users out of K_{ava} available users [14–16]. By employing user selection, the wireless traffic and power consumption for CIC can be minimized, while its diversity can be maintained to be equal to the number of available users [14]. It should be noted, however, user selection process should be tailored based on its purposes and the receiver design. In [60–64], for example, the user selection is designed to maximize the channel capacity. On the other hand, [17–21] propose user selection techniques by considering the error rates performance. Research in [17–21], however, only consider the basic receiver design scenarios such as MLD, ZF, and MMSE detection algorithms. In this thesis, therefore, a user selection technique which maximizes the BER performance for the case of QRM-MLD [65–67] is used a the detection algorithm is proposed.

Except to the number of signal exchanges, the issue on the MU-MIMO with CIC lies on its applicability. This issue is important as the performance of CIC in an actual environment depends heavily on several factors. Unlike the theoretical scenario which commonly considers i.i.d. Rayleigh fading, actual environments experiencing channel shadowing and channel correlation between users. In the signal processing at the users, the differences at the user sampling time, frequency offset, and signal to noise ratio might also affect the CIC performance. In addition, the reliability of the interuser links in a mobile environment, also needs to be confirmed.

In this regards, therefore, field experiment is conducted to confirm the effectiveness of MU-MIMO with CIC in an actual environment. In this field experiment, a BS equipped with multiple transmit antennas is employed to serve several active users. These active users are located in a car that moves at a certain speed. In addition to these active users, other users are also available in the car and can be used in CIC. Therefore, the number of collaborating users is larger than or equal to that of the active users. These collaborating

users then conduct CIC by sharing their received signals through short range wireless communication links. Afterward, MLD and MMSE are used as the detection algorithms for obtaining the estimated transmitted data. Due to the time constraint, however, the field experiments did not consider any user selection technique yet.

3.2 System Model

3.2.1 MU-MIMO with CIC

In this thesis, an MU-MIMO where N_t transmit antennas serves K_act active users out of K_ava available users is considered. For simplicity, it is assumed that $N_\mathrm{t} = K_\mathrm{act}$. First, N_t transmit antennas in the BS transmit N_t independent streams. On the receiver side, K_col users conduct CIC by sharing their received signals and equivalently increase the number of their receive antennas. It is worth to note that $K_\mathrm{act} \leq K_\mathrm{col} \leq K_\mathrm{ava}$. Let $\boldsymbol{y} = [y_1, y_2, \ldots y_{K_\mathrm{col}}]^\mathrm{T}$, where y_k is the received signal for kth user. The received signals for K_col collaborating users can be written as

$$\boldsymbol{y} = \boldsymbol{H}\boldsymbol{s} + \boldsymbol{n}, \tag{3.1}$$

where $\boldsymbol{H} \in \mathbb{C}^{K_\mathrm{col} \times N_\mathrm{t}}$ is an $K_\mathrm{col} \times N_\mathrm{t}$ matrix of a wireless channel, $\boldsymbol{s}$ is an $N_\mathrm{t} \times 1$ vector of transmitted symbols, and $\boldsymbol{n}$ is an $K_\mathrm{col} \times 1$ vector of noise.

The signal-exchange process in CIC can be seen in Fig. 3.1. As can be seen in the figure, two steps are conducted on the receiver side, namely user selection, and signal detection. In this figure, K_QRM is a variable in QRM-MLD and will be introduced in Chapter 3.2.2. On the other hand, G_S is a variable in the proposed technique and will be described in Sect. 3.3. The optimum value of G_S depends on K_QRM.

In the first step of CIC, $K_\mathrm{ava} - 1$ users transmit their CSI to one of the active users that acts as a master user. Based on this CSI, the master user selects the best K_col users that will be used to conduct the detection process. In this thesis, a user selection

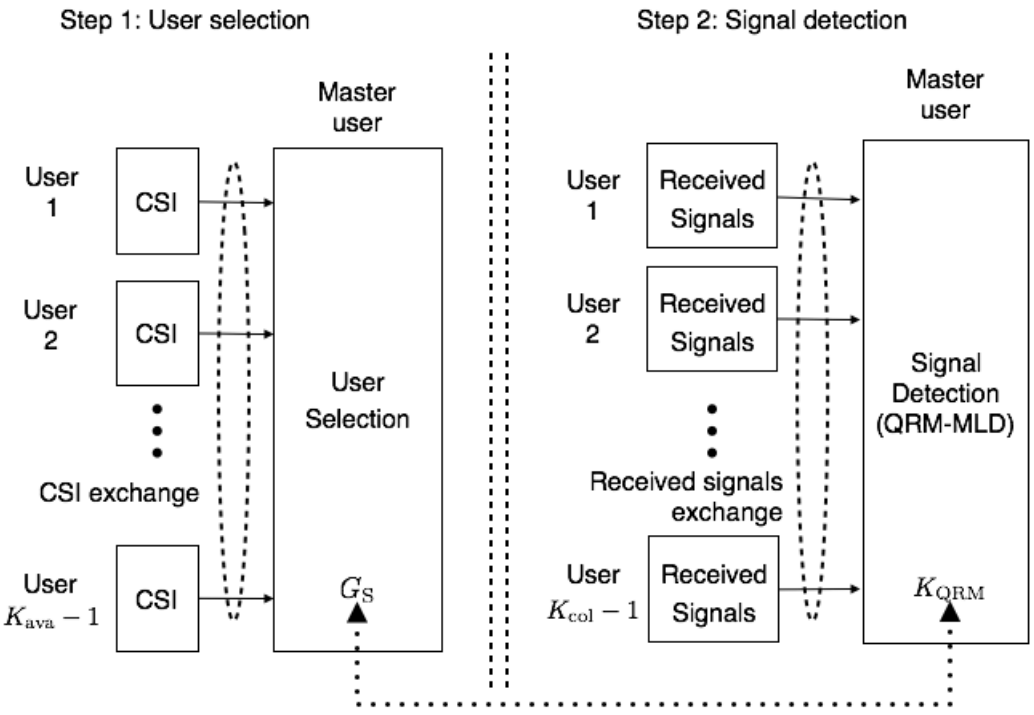

Fig. 3.1. Signal-exchange in CIC.

technique to optimize the BER performance when QRM-MLD [65–67] is used as the detection algorithm is proposed.

In the user selection process, the master user should consider $\binom{K_{\text{ava}}}{K_{\text{col}}}$ possible user subsets. After conducting user selection, the master user transmits signal-requests to those K_{col} selected-users. In the second step of CIC, the detection process is conducted. In this step, the K_{col} selected-users broadcast their received signals after receiving the signal-request. In CIC, two scenarios can be employed to conduct the signal detection process. In the first scenario, the broadcasted received signals from K_{col} selected users are received by K_{act} active users. Then, each of these active users conducts signal detection independently. Therefore, there will be K_{act} detection processes in the cluster. In this scenario, however, no user is required to broadcast the detection results. Therefore, this scenario is effective when a linear detection algorithm is applied with a relatively large

value of K_{col}.

In the second scenario, the broadcasted received signals from K_{col} selected users are received by one of K_{act} active users. Afterward, only this user conducts a signal detection. In this scenario, additional inter-user signal transmissions are required to distribute the results of the signal detection to the other $K_{\mathrm{act}} - 1$ active users. Therefore, this scenario is effective when a nonlinear detection algorithm is implemented with a relatively small value of K_{col}. As QRM-MLD is used as the detection algorithm in this thesis, the second scenario is employed.

3.2.2 QRM-MLD

QRM-MLD is well known as a detection algorithm which is able to achieve a BER performance near equal to MLD with a significant reduction in complexity [65–67]. Let $\hat{U}$ be the user subset which is selected to conduct the CIC process. The received signals from this user subset can be denoted as

$$\boldsymbol{y}_{\hat{U}} = \boldsymbol{H}_{\hat{U}}\boldsymbol{s} + \boldsymbol{n}_{\hat{U}}, \tag{3.2}$$

where $\boldsymbol{H}_{\hat{U}}$ is the $K_{\mathrm{col}} \times N_{\mathrm{t}}$ sub-matrix of $\boldsymbol{H}$ which corresponds to the user subset $\hat{U}$, while $\boldsymbol{n}_{\hat{U}}$ is the $K_{\mathrm{col}} \times 1$ sub-vector of $\boldsymbol{n}$ which corresponds to the user subset $\hat{U}$. In QRM-MLD, the first step of the detection process is to decompose $\boldsymbol{H}_{\hat{U}}$ into a unitary matrix, $\boldsymbol{Q}_{\hat{U}}$, and an upper triangular matrix, $\boldsymbol{R}_{\hat{U}}$. Therefore, Eq. (3.2) can be written as

$$\boldsymbol{y}_{\hat{U}} = \boldsymbol{Q}_{\hat{U}}\boldsymbol{R}_{\hat{U}}\boldsymbol{s} + \boldsymbol{n}_{\hat{U}}. \tag{3.3}$$

Multiplying both sides with $\boldsymbol{Q}_{\hat{U}}^{\mathrm{H}}$, Eq. (3.3) can be modified as

$$\tilde{\boldsymbol{y}}_{\hat{U}} = \boldsymbol{R}_{\hat{U}}\boldsymbol{s} + \tilde{\boldsymbol{n}}_{\hat{U}}, \tag{3.4}$$

where $\tilde{\boldsymbol{y}}_{\hat{U}} = \boldsymbol{Q}_{\hat{U}}^{\mathrm{H}} \boldsymbol{y}_{\hat{U}}$ and $\tilde{\boldsymbol{n}}_{\hat{U}} = \boldsymbol{Q}_{\hat{U}}^{\mathrm{H}} \boldsymbol{n}_{\hat{U}}$.

To obtain the vector of the transmitted symbols, the ML criterion is given by

$$\begin{aligned} \hat{\boldsymbol{s}} &= \underset{\boldsymbol{s} \in \mathcal{S}^{\mathcal{N}_\mathrm{t}}}{\operatorname{argmin}} \| \tilde{\boldsymbol{y}}_{\hat{U}} - \boldsymbol{R}_{\hat{U}} \boldsymbol{s} \|_{\mathrm{F}}^2 \\ &= \underset{\boldsymbol{s} \in \mathcal{S}^{N_\mathrm{t}}}{\operatorname{argmin}} \left(\sum_{j=1}^{N_\mathrm{t}} \left| \tilde{y}_j^{\hat{U}} - \sum_{i=j}^{N_\mathrm{t}} r_{j,i}^{\hat{U}} s_i \right|^2 \right), \end{aligned} \tag{3.5}$$

where $\mathcal{S}^{N_\mathrm{t}}$ is the set of all possible vectors of $N_\mathrm{t} \times 1$ transmitted symbols, $\tilde{y}_j^{\hat{U}}$ is the jth element of the vector $\tilde{\boldsymbol{y}}_{\hat{U}}$, and $r_{j,i}^{\hat{U}}$ is the j,ith element of matrix $\boldsymbol{R}_{\hat{U}}$.

In QRM-MLD, the detection process is conducted in a recursive manner [65]. Denotes $\mathcal{S}$ as the set of all possible symbols from one transmit antenna. At the first stage of QRM-MLD, the branch metric values are calculated for all values of $\mathcal{S}$. Afterward, K_{QRM} candidates with the smallest values of branch metric are selected as the surviving nodes while the nodes from the other candidates are discarded. In the n_{QRM}th ($1 < n_{\mathrm{QRM}} < N_\mathrm{t}$) stage, the branch metric values of $K_{\mathrm{QRM}} |\mathcal{S}|$ nodes are calculated. Again, K_{QRM} candidates with the smallest values of branch metric are selected as the surviving nodes and the nodes from the other candidates are discarded. Finally, in the N_tth stage, the node with the minimum accumulated branch metric is selected as the result of the QRM-MLD algorithm together with its ancestor nodes.

In a recursive-based detection algorithm such as QRM-MLD, channel ordering holds a significant role in optimizing the BER performance. Employing channel ordering, the probability of the signal with a high signal-to-noise ratio (SNR) is detected at the early stage of detection can be increased and minimizes the error propagation [68, 69]. In this thesis, a simple channel ordering technique based on the sum of Frobenius norm values of all elements in each column is used.

3.2.3 Conventional User Selection Technique

To achieve its optimum potential, the user selection should be tailored based on the purpose of the user selection. The user selection, for example, can be used to maximize the capacity or to optimize the BER performance. In addition, user selection should also consider the detection algorithm used in the receiver. User selection technique for MLD, for example, should be different with the user selection for ZF and MMSE.

3.2.3.1 User Selection for Capacity Maximization

Let U denotes the user subset where $U \in \mathcal{U}$ and $|\mathcal{U}| = \binom{K_{\text{ava}}}{K_{\text{col}}}$. The channel sub-matrix which corresponds to the user subset U is then denoted as $\boldsymbol{H}_U$. Using the capacity maximization (CM) technique, the selected user subset can be obtained by

$$\hat{U} = \underset{U \in \mathcal{U}}{\operatorname{argmax}} \prod_{r=1}^{R} \lambda_r^U, \tag{3.6}$$

where R is the rank of $\boldsymbol{H}_U$ and λ_r^U is the rth singular value of $\boldsymbol{H}_U$. For the case of $R = N_{\text{t}}$, the value of the product of λ_r^U in Eq. (3.6) can be equally obtained by

$$\hat{U} = \underset{U \in \mathcal{U}}{\operatorname{argmax}} \prod_{n_{\text{t}}=1}^{N_{\text{t}}} \left| r_{n_{\text{t}},n_{\text{t}}}^U \right|, \tag{3.7}$$

where $r_{n_{\text{t}},n_{\text{t}}}^U$ is the n_{t}th diagonal element of matrix $\boldsymbol{R}_U$ which is obtained from the QR decomposition of channel submatrix $\boldsymbol{H}_U$.

3.2.3.2 User Selection for BER Optimization

User selection for ZF detecion In the linear detection, an equalizer matrix is applied to the vector of received signals, $\boldsymbol{y}$, to obtain the estimate of the transmitted symbols, $\hat{\boldsymbol{s}}$. For the case of ZF precoder, the equalizer matrix is equal to the pseudo inverse of the channel matrix. This equalizer will affect the noise and causes the noise power to vary according to the function of the channel. In the ZF detection, therefore, the

post-processing SNR becomes the key parameter in the user selection. For each user subset, U, the post processing SNR value for the n_{t}th transmitted stream, $SNR'_{n_{\mathrm{t}}}$, can be obtained by

$$SNR'^{U}_{n_{\mathrm{t}}} = \frac{E_{\mathrm{s}}}{N_{\mathrm{t}}\sigma^2[\boldsymbol{H}_U^{\mathrm{H}}\boldsymbol{H}_U]^{-1}_{n_{\mathrm{t}},n_{\mathrm{t}}}}. \tag{3.8}$$

The selected user subset, $\hat{U}$, then can be obtained by

$$\hat{U} = \underset{U\in\mathcal{U}}{\operatorname{argmax}} \min_{n_{\mathrm{t}}} SNR'^{U}_{n_{\mathrm{t}}}. \tag{3.9}$$

User selection for MLD In a receiver implementing MLD algorithm, the probability of symbol errors can be upper-bounded by the minimum Euclidean distance between all possible transmitted symbols as

$$P_{\mathrm{e}} < \left(\left|\mathcal{S}^{N_{\mathrm{t}}}\right| - 1\right) \mathrm{Q}\left(\sqrt{\frac{E_{\mathrm{s}}}{2\sigma^2} d^2_{\min}}\right), \tag{3.10}$$

where Q(.) is the Q function, E_{s} is the average energy of the transmitted signals and $d^2_{\min}$ is the minimum Euclidean distance of all possible transmitted symbols [70]. In each signal subset, the value of $d^2_{\min}$ can be obtained by

$$d^2_{\min} = \min_{\boldsymbol{s}_p,\boldsymbol{s}_q\in\mathcal{S}^{N_{\mathrm{t}}},\boldsymbol{s}_p\neq\boldsymbol{s}_q} \|\boldsymbol{R}_U(\boldsymbol{s}_p - \boldsymbol{s}_q)\|^2_{\mathrm{F}}, \tag{3.11}$$

where $\boldsymbol{s}_p$ and $\boldsymbol{s}_q$ are two possible vectors of transmitted symbols.

By examining Eqs. (3.10) and (3.11), it can be concluded that in order to minimize the BER, the master user should select the signal subset having the largest minimum Euclidean distance as the collaborating users. In this thesis, this technique is labeled as the MMED technique. For the case of point-to-point MIMO, MMED is described in [17]. In MMED, the selected signal subset, $\hat{U}$, can be obtained by

$$\begin{aligned}\hat{U} &= \underset{U\in\mathcal{U}}{\operatorname{argmax}} \min_{\boldsymbol{s}_p,\boldsymbol{s}_q\in\mathcal{S}^{N_\mathrm{t}},\boldsymbol{s}_p\neq\boldsymbol{s}_q} \|\boldsymbol{R}_U(\boldsymbol{s}_p-\boldsymbol{s}_q)\|_\mathrm{F}^2 \\ &= \underset{U\in\mathcal{U}}{\operatorname{argmax}} \min_{\boldsymbol{e}\in\mathcal{E}^{N_\mathrm{t}},\boldsymbol{e}\neq 0} \|\boldsymbol{R}_U\boldsymbol{e}\|_\mathrm{F}^2 \\ &= \underset{U\in\mathcal{U}}{\operatorname{argmax}} \min_{\boldsymbol{e}\in\mathcal{E}^{N_\mathrm{t}},\boldsymbol{e}\neq 0} \left(\sum_{j=1}^{N_\mathrm{t}} \left|\sum_{i=j}^{N_\mathrm{t}} r_{j,i}^U e_i\right|^2\right),\end{aligned} \tag{3.12}$$

where e_i is the symbol error between two possible transmitted symbol of the ith user, $\boldsymbol{e} = [e_1, e_2, \ldots, e_{N_\mathrm{t}}]^\mathrm{T}$ is the vector of symbol error between two possible vector of transmitted symbols, and $\mathcal{E}^{N_\mathrm{t}}$ is the set of all possible vector of symbol error.

It should be noted, however, some of these symbol errors are actually identical. Thus, to minimize the complexity, the Euclidean distance calculations can be conducted only for all those unique symbol errors. Furthermore, the Euclidean distance for $\boldsymbol{e}$ is equal to the Euclidean distance for $-\boldsymbol{e}$, $\boldsymbol{e}$i, and $-\boldsymbol{e}$i. Therefore, the calculation of Euclidean distance for four vectors of symbol error that can be represented by $\boldsymbol{e}$, $-\boldsymbol{e}$, $\boldsymbol{e}$i, and $-\boldsymbol{e}$i, can be conducted once. As the Euclidean distance calculation for $\boldsymbol{e} = 0$ can be discarded, the number of required Euclidean distance calculations in MMED for each signal subset can be written as

$$N_\mathrm{ED} = \frac{1}{4}(|\mathcal{E}_1|^{N_\mathrm{t}} - 1), \tag{3.13}$$

where $\mathcal{E}_1$ is the set of all unique error vectors in each element of $\boldsymbol{e}$.

The value of $|\mathcal{E}_1|$ in Eq. (3.13) corresponds to the modulation technique which is used in the transmission. Denotes Q as the number of bits in each symbol of a square-shaped QAM. The value of $|\mathcal{E}_1|$ can be obtained by

$$|\mathcal{E}_1| = \left(2^{\frac{Q}{2}+1} - 1\right)^2. \tag{3.14}$$

In Fig. 3.2, all of the unique symbol error for QPSK modulation are shown. As can be seen in the figure, there are nine unique symbol errors in the QPSK modulation, which

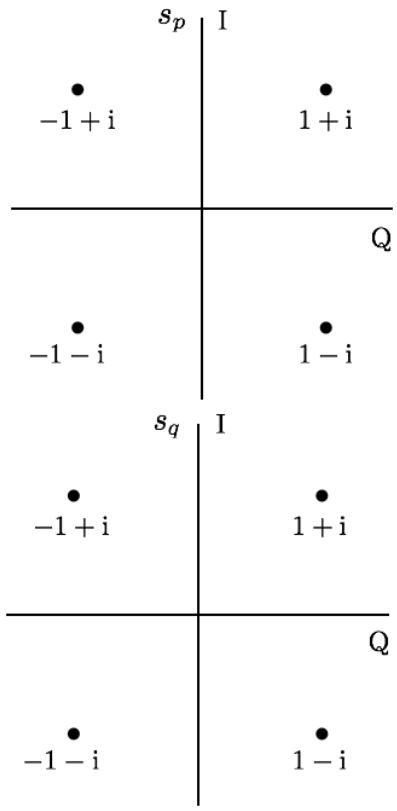

Group No.	$s_p - s_q$	Error vectors	Squared-distance
1	(–1 + i) – (–1 + i)	0	0
	(1 + i) – (1 + i)		
	(–1 – i) – (–1 – i)		
	(1 – i) – (–1 + i)		
2	(1 + i) – (–1 + i)	2	4
	(1 – i) – (–1 – i)		
	(–1 + i) – (1 + i)	–2	
	(–1 – i) – (1 – i)		
	(–1 + i) – (–1 – i)	2i	
	(1 + i) – (1 – i)		
	(–1 – i) – (–1 + i)	–2i	
	(1 – i) – (1 + i)		
3	(1 + i) – (–1 – i)	2 + 2i	8
	(1 – i) – (–1 + i)	2 – 2i	
	(–1 + i) – (1 + i)	–2 + 2i	
	(–1 – i) – (1 + i)	–2 – 2i	

Fig. 3.2. Error vectors in QPSK modulation.

are $\mathcal{E}_1 = \{0, 2, -2, 2i, -2i, 2+2i, 2-2i, -2+2i, -2-2i\}$. Each of this unique symbol error is denoted as E_1, where $E_1 \in \mathcal{E}_1$.

From Eq. (3.12), it can be seen that the selection process in MMED is conducted by directly multiplying matrix $\boldsymbol{R}$ with the vector of symbol error, $\boldsymbol{e}$. In other words, MMED considers only the total accumulative Euclidean distance in its selection process. This selection criterion, therefore, cannot minimize the error propagation in QRM-MLD. In addition, this direct multiplication incurs high computational complexity. As can be observed from Eq. (3.13), MMED requires a large number of Euclidean distance calculations, which makes implementation infeasible. In the case of four transmit antennas with 16QAM modulation, for example, selecting four out of eight users requires more than 100 million calculations of Euclidean distance.

3.3 Proposed User Selection Tecnhique for QRM-MLD

QRM-MLD is a detection algorithm which is based on the MLD algorithm. To optimize the BER performance, therefore, the user should be selected based on the user selection algorithm for MLD. It should be noted, however, the user selection process should accommodate the recursive nature of QRM-MLD. In the proposed technique, therefore, the calculation of the minimum accumulative Euclidean for each signal subset is conducted in a recursive manner using an M-algorithm. Hereafter, the proposed technique is labeled as MMED-M.

In each stage of the selection process, the calculation of Euclidean distance is conducted only for a certain number of symbol error and greatly reduce the computational complexity. In addition, MMED-M stores the minimum value of Euclidean distance in each stage of selection. This process is required as the detection error in QRM-MLD is possible to occur in the early stage of detection. By considering the minimum Euclidean distance in each selection stage, the error propagation in QRM-MLD can be minimized and better BER performance can be expected especially for the case of K_{QRM} is relatively small.

The pseudocode of the proposed technique, in general, can be seen in Algorithm 1. In the pseudocode, $\bar{d}_{\mathrm{min}}$ denotes the minimum accumulative Euclidean distance in a user subset. The largest value of $\bar{d}_{\mathrm{min}}$ from all possible user subsets is denoted as $\bar{d}_{\mathrm{max}}$. In addition, $\bar{\boldsymbol{d}}$ is a $(G_{\mathrm{S}}+1)\times 1$ vector of the stored accumulative Euclidean distances where G_{S} is the number of surviving nodes at each selection stage. The elements in $\bar{\boldsymbol{d}}$ are arranged in increasing order so that $\bar{d}_1 < \bar{d}_2 < \cdots < \bar{d}_{G_{\mathrm{S}}+1}$. Next, the surviving nodes at each selection stage are stored in a matrix and denoted as $\boldsymbol{E}$. The number of columns in matrix $\boldsymbol{E}$ is equal to G_{S} while the number of its rows at the n_{QRM}th stage of selection is equal to m. To support the selection process, a temporary variable, vector, and matrix, which are d, $\boldsymbol{d}'$, and $\boldsymbol{E}'$ are also required in the algorithm.

Algorithm 1 MMED-M algorithm.

$\bar{d}_{\max} = 0$ % initiate the value of $\bar{d}_{\max}$
Define the number of surviving nodes, G_{S}
for $U \in \mathcal{U}$ **do**
  $\bar{d}_{\min} = \infty$ % initiate the value of $\bar{d}_{\min}$
  Obtain $\boldsymbol{R}_U$ from $\boldsymbol{H}_U$
  $\bar{\boldsymbol{d}} = \boldsymbol{\infty}_{(G_{\mathrm{S}}+1)\times 1}$ % initiate vector $\bar{\boldsymbol{d}}$
  $\boldsymbol{E} = \boldsymbol{0}_{1\times G_{\mathrm{S}}}$ % initiate matrix $\boldsymbol{E}$
  for $E_1 \in \mathcal{E}_1$ **do**
    $d = r^U_{N_{\mathrm{t}},N_{\mathrm{t}}} E_1$
    if $d < \bar{d}_{G_{\mathrm{S}}+1}$ **then**
      Stores d to $\bar{\boldsymbol{d}}$
      if $d < \bar{d}_{G_{\mathrm{S}}}$ **then**
        Stores E_1 to $\boldsymbol{E}$
  for $n_{\mathrm{t}} = 2 : N_{\mathrm{t}}$ **do**
    $\boldsymbol{E}' = \boldsymbol{E}$
    $\boldsymbol{d}' = \bar{\boldsymbol{d}}$
    $\boldsymbol{E} = \boldsymbol{0}_{m\times G_{\mathrm{S}}}$ % expand matrix $\boldsymbol{E}$
    $\bar{\boldsymbol{d}} = \boldsymbol{\infty}_{(G_{\mathrm{S}}+1)\times 1}$ % reset vector $\bar{\boldsymbol{d}}$
    for $g = 1 : G_{\mathrm{S}}$ **do**
      for $E_1 \in \mathcal{E}_1$ **do**
        $d = d'_g + \left| r^U_{N_{\mathrm{t}}-n_{\mathrm{t}}+1,N_{\mathrm{t}}-n_{\mathrm{t}}+1:N_{\mathrm{t}}} \begin{bmatrix} E_1 \\ \boldsymbol{E}'_{(:,g)} \end{bmatrix} \right|^2$
        if $d < \bar{d}_{G_{\mathrm{S}}+1}$ **then**
          Stores d to $\bar{\boldsymbol{d}}$
          if $d < \bar{d}_{G_{\mathrm{S}}}$ **then**
            Stores $\begin{bmatrix} E_1 \\ \boldsymbol{E}'_{(:,g)} \end{bmatrix}$ to $\boldsymbol{E}$
    if $n_{\mathrm{t}} = N_{\mathrm{t}}$ **then**
      if $\bar{d}_2 < \bar{d}_{\min}$ **then**
        $\bar{d}_{\min} = \bar{d}_2$
    else
      if $\bar{d}_{G_{\mathrm{S}}+1} < \bar{d}_{\min}$ **then**
        $\bar{d}_{\min} = \bar{d}_{G_{\mathrm{S}}+1}$
  if $\bar{d}_{\min} > \bar{d}_{\max}$ **then**
    $\bar{d}_{\max} = \bar{d}_{\min}$
    $\hat{U} = U$

3.3.1 M-algorithm Implementation

Fig. 3.3 shows a tree diagram of the MMED-M user selection technique for the case of QPSK transmission with $N_{\mathrm{t}} = 3$. In the figure, $d_{n_{\mathrm{t}},q}$ denotes the qth largest accumulative

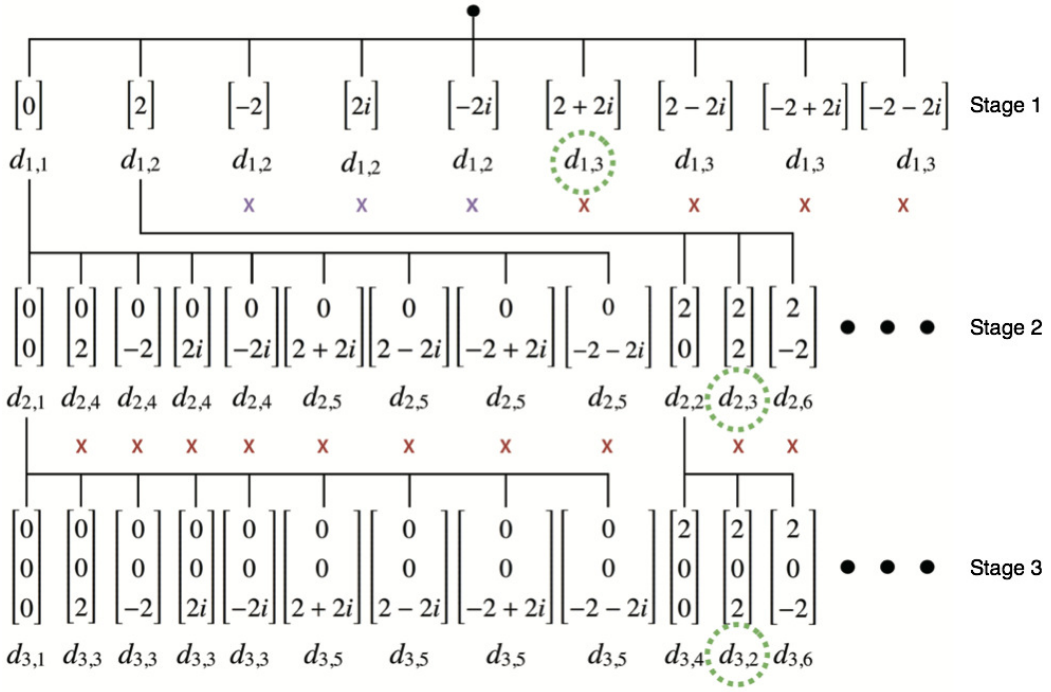

Fig. 3.3. Tree diagram representation of MMED-M.

Euclidean distance at the stage of n_{t}. At the first stage of selection, Euclidean distances are calculated by multiplying $r^{U}_{N_{\mathrm{t}},N_{\mathrm{t}}}$ with all unique error vectors, $\mathcal{E}_1$. The Euclidean distance obtained from the multiplication of the error vector of $\left[2\right]$, $\left[-2\right]$, $\left[2i\right]$, and $\left[-2i\right]$ with any values of $r^{U}_{N_{\mathrm{t}},N_{\mathrm{t}}}$, however, will produce the equal result. In Fig. 3.3, the result is written as $d_{1,2}$. The equal result will also be obtained from the multiplication to the error vector of $\left[2+2i\right]$, $\left[2-2i\right]$, $\left[-2+2i\right]$, and $\left[-2-2i\right]$. In Fig. 3.3, the result is written as $d_{1,3}$, where $d_{1,3} > d_{1,2}$.

To significantly reduce the computational complexity, the nodes having large Euclidean distances are discarded. As an example, the nodes having the Euclidean distance of $d_{1,3}$ in Fig. 3.3 are discarded. Furthermore, MMED-M considers the nodes having the equal Euclidean distance as one node. Therefore, in Fig. 3.3, only one from four nodes which have the Euclidean distance of $d_{1,2}$, survived, while the other three nodes are discarded.

Table 3.1. Symmetry properties of the error vectors in MMED-M.

Vector of symbol error						
Stage 1	Stage 2					
	$\boldsymbol{e}_1$	$\boldsymbol{e}_2$	$\boldsymbol{e}_3$	$\boldsymbol{e}_4$		$\boldsymbol{e}_9$
$[2]$	$\begin{bmatrix}2\\0\end{bmatrix}$	$\begin{bmatrix}2\\2\end{bmatrix}$	$\begin{bmatrix}2\\-2\end{bmatrix}$	$\begin{bmatrix}2\\2\mathrm{i}\end{bmatrix}$	$\cdots$	$\begin{bmatrix}2\\-2-2\mathrm{i}\end{bmatrix}$
	$-\boldsymbol{e}_1$	$-\boldsymbol{e}_3$	$-\boldsymbol{e}_2$	$-\boldsymbol{e}_5$		$-\boldsymbol{e}_6$
$[-2]$	$\begin{bmatrix}-2\\0\end{bmatrix}$	$\begin{bmatrix}-2\\2\end{bmatrix}$	$\begin{bmatrix}-2\\-2\end{bmatrix}$	$\begin{bmatrix}-2\\2\mathrm{i}\end{bmatrix}$	$\cdots$	$\begin{bmatrix}-2\\-2-2\mathrm{i}\end{bmatrix}$
	$\boldsymbol{e}_1\mathrm{i}$	$\boldsymbol{e}_5\mathrm{i}$	$\boldsymbol{e}_4\mathrm{i}$	$\boldsymbol{e}_2\mathrm{i}$		$\boldsymbol{e}_8\mathrm{i}$
$[2\mathrm{i}]$	$\begin{bmatrix}2\mathrm{i}\\0\end{bmatrix}$	$\begin{bmatrix}2\mathrm{i}\\2\end{bmatrix}$	$\begin{bmatrix}2\mathrm{i}\\-2\end{bmatrix}$	$\begin{bmatrix}2\mathrm{i}\\2\mathrm{i}\end{bmatrix}$	$\cdots$	$\begin{bmatrix}2\mathrm{i}\\-2-2\mathrm{i}\end{bmatrix}$
	$-\boldsymbol{e}_1\mathrm{i}$	$-\boldsymbol{e}_4\mathrm{i}$	$-\boldsymbol{e}_5\mathrm{i}$	$-\boldsymbol{e}_3\mathrm{i}$		$-\boldsymbol{e}_7\mathrm{i}$
$[-2\mathrm{i}]$	$\begin{bmatrix}-2\mathrm{i}\\0\end{bmatrix}$	$\begin{bmatrix}-2\mathrm{i}\\2\end{bmatrix}$	$\begin{bmatrix}-2\mathrm{i}\\-2\end{bmatrix}$	$\begin{bmatrix}-2\mathrm{i}\\2\mathrm{i}\end{bmatrix}$	$\cdots$	$\begin{bmatrix}-2\mathrm{i}\\-2-2\mathrm{i}\end{bmatrix}$

This discarding process is possible owing to the symmetry property of the vectors of symbol error. In Table 3.1, the second column shows all possible vectors of symbol error at the second stage of selection which are from the nodes with the symbol error of $[2]$, $[-2]$, $[2\mathrm{i}]$, and $[-2\mathrm{i}]$. In the table, $\boldsymbol{e}_v$ denotes the vth possible vector of symbol error at the second stage of selection, originated from the symbol error of $[2]$ from the first selection stage. Herein, $v = \{1, 2, ..., |\mathcal{E}_1|\}$. As can be seen in the table, all of the nodes in the second stage of selection originated from the nodes with the error vector of $[-2]$, $[2\mathrm{i}]$, and $[-2i]$ can be represented as $-\boldsymbol{e}_v$, $\boldsymbol{e}_v\mathrm{i}$, and $-\boldsymbol{e}_v\mathrm{i}$, and will produce the equal Euclidean distance. This representation is also applicable for the third stage onwards. Therefore, for each signal subset, the number of required Euclidean distance calculations using the MMED-M technique with G_S surviving nodes can be written as

$$N'_\mathrm{ED} = |\mathcal{E}_1| + (N_\mathrm{t} - 1)\, G_\mathrm{S}\, |\mathcal{E}_1|. \tag{3.15}$$

Similar to the case of QPSK modulation, symbol-error-grouping can also be held for the case of 16QAM modulation and can be seen in Table 3.2. In the table, the vectors

Table 3.2. Vector of symbol error grouping at the first stage of MMED-M for 16QAM.

Group No.	Squared-distance	Error Vectors
1	0	$\{0\}$
2	4	$\{2, -2, 2\mathrm{i}, -2\mathrm{i}\}$
3	8	$\{2+2\mathrm{i}, 2-2\mathrm{i}, -2+2\mathrm{i}, -2-2\mathrm{i}\}$
4	16	$\{4, -4, 4\mathrm{i}, -4\mathrm{i}\}$
5	20	$\{2+4\mathrm{i}, -4+2\mathrm{i}, 4-2\mathrm{i}, -2-4\mathrm{i}\}$
6	20	$\{4+2\mathrm{i}, -2+4\mathrm{i}, 2-4\mathrm{i}, -4-2\mathrm{i}\}$
7	32	$\{4+4\mathrm{i}, 4-4\mathrm{i}, -4+4\mathrm{i}, -4-4\mathrm{i}\}$
⋮	⋮	⋮
13	72	$\{6+6\mathrm{i}, 6-6\mathrm{i}, -6+6\mathrm{i}, -6-6\mathrm{i}\}$

of error symbol that can be represented by $\boldsymbol{e}$, $\boldsymbol{e}\mathrm{i}$, $-\boldsymbol{e}$, and $-\boldsymbol{e}\mathrm{i}$ are unified into one group. For the case of 16QAM modulation, however, the equal Euclidean distances can be produced by the vectors of symbol error from different groups. In Table 3.2, it can be observed that both groups 5 and 6 have an equal Frobenius norm of 20. Fortunately, this case only occurs when a large number of surviving nodes is used. Since a small number of surviving nodes is sufficient, this phenomenon will not give any effect in the MMED-M technique.

3.3.2 Determining the Optimum Value of surviving nodes

In MMED-M, the number of surviving nodes, G_{S}, can affect the performance of QRM-MLD at the detection process. The optimum value of G_{S} depends on the value of K_{QRM}, and vice versa. At the first stage of user selection, determining the optimum number of surviving nodes is relatively easy, but yet, critical.

At the first detection stage of QPSK transmission, QRM-MLD with $K_{\mathrm{QRM}} = 2$ could only select a symbol with its vertical or horizontal neighbors in constellation mapping as its candidates. Using QPSK with Gray mapping, for example, QRM-MLD could not select symbol {0, 3} or {1, 2} as its candidates. In the user selection process, therefore,

besides consider the symbol error of 0, only the symbol errors which have the vertical or horizontal direction should be considered. In the conventional MMED, all of the symbol errors are considered in the selection process even when two candidates in QRM-MLD could not have those symbol errors. The conventional MMED, therefore, is not suitable for the QRM-MLD detection algorithm.

In Fig. 3.2, the symbol error of 0 and the symbol errors which have the vertical or horizontal direction are grouped in group one and group two. Therefore, only the symbol error in these groups should be considered in the selection process while the symbol errors in group three should be discarded. Next, at the first stage of selection, the symbol errors in group two produce the equal Euclidean distance and can be considered as one node. Therefore, for the case of QRM-MLD with $K_{\mathrm{QRM}} = 2$, the optimum value of G_{S} in the MMED-M is 2. As can be seen later in the simulation results, selecting $G_{\mathrm{S}} > 2$ causes an error floor on the BER performance.

For the case of $K_{\mathrm{QRM}} = 4$, QRM-MLD selects all of the QPSK symbols as its candidates at the first stage of detection. In the user selection process, therefore, all possible symbol errors should be considered. As the vertical and horizontal symbol errors will produce an equal Euclidean distance at the first stage of selection, they can be considered as one node. The same consideration can be applied to the diagonal symbol errors. Therefore, for the case of $K_{\mathrm{QRM}} = 4$, the optimum value of G_{S} is 3.

At the stage of 2 to $N_{\mathrm{t}} - 1$, determining the optimum number of the surviving nodes is relatively hard, owing to the random nature of the channel matrix and the noise vector. However, as it will be shown later in the simulation results, excellent BER performance can be obtained by keeping the number of surviving nodes at the stage of 2 to $N_{\mathrm{t}} - 1$ to be equal to the number of surviving nodes at the first stage of selection.

3.3.3 Determining the Stored-Accumulative-Euclidean distance

In Eq. (3.12), it can be seen that in MMED, the minimum Euclidean distance in each user subset is obtained by directly multiplying $\boldsymbol{R}_U$ with all possible vectors of symbol error. Therefore, only the total accumulative Euclidean distances are considered in MMED. On the other hand, one of the problems of QRM-MLD lays in the error events which are possible to occur at each stage of detection. As a result, for the QRM-MLD implementation, conventional MMED is only able to provide optimum BER performance if the value of K_{QRM} is sufficiently large or if an optimum channel ordering technique is employed. For the case of the value of K_{QRM} is relatively small and a sub-optimum channel ordering technique is used, the error propagation will occur at the QRM-MLD detection process.

To avoid the error-events in the early stage of QRM-MLD, MMED-M user selection considers the accumulative Euclidean distance at each stage of the selection. At the stage of 1 to $N_{\mathrm{t}} - 1$, the performance of QRM-MLD will be affected by the minimum value of the accumulative Euclidean distance of the discarded nodes. Therefore, at these stages, MMED-M stores the value of $d_{n_{\mathrm{t}},G_{\mathrm{S}}+1}$. At the stage of N_{t}, however, QRM-MLD selects the smallest branch metric instead of selects K_{QRM} candidates. Therefore, at this stage, MMED-M stores the value of $d_{n_{\mathrm{t}},2}$.

In Fig. 3.3, the stored value at each stage of selection is shown by the dashed circle. The minimum value of all of these stored-values is then selected as the minimum accumulative Euclidean distance for the corresponding signal subset, $\bar{d}_{\mathrm{min}}$. In Table 3.3, an example of Euclidean distance information obtained through MMED-M user selection is shown.

In the conventional MMED, only the total accumulative Euclidean distances are considered in the selection process. In MMED-M representation, this total Euclidean

Table 3.3. Example of Euclidean distance values obtained through MMED-M.

Stage	Euclidean distance at each stage of selection		
	U_1	U_2	U_3
1	1.5	1.3	1.1
2	1.2	1.4	1.7
3	1.8	1.7	1.9

distance is equal to the Euclidean distance at the N_tth stage of user selection process. In Table 3, therefore, the minimum Euclidean distances for U_1, U_2, and U_3 using the conventional MMED, are 1.8, 1.7, and 1.9, respectively. As signal subset U_3 has the largest Euclidean distance at that stage, this signal subset is selected by MMED to conduct detection process.

This signal subset is, indeed, suitable for MLD algorithm. As MLD calculates the branch metric for all possible transmitted symbols, only the total Euclidean distance will determine the MLD performance. It should be noted, however, the detection process in QRM-MLD is conducted in a recursive manner. Therefore, the BER performance of QRM-MLD is determined by the Euclidean distance at each stage of selection. When signal subset U_1 is used for detection process, for example, the error event of QRM-MLD will most likely occurs at the second stage of detection process. On the other hand, When signal subset U_2 or U_3 is used for detection process, the error event of QRM-MLD will most likely occur at the first stage of the detection process. Therefore, in MMED-M, the minimum Euclidean distances for U_1, U_2, and U_3 are 1.2, 1.3, and 1.1, respectively. Thus, rather than selects signal subset U_3, MMED-M selects signal subset U_2 to conduct the detection process.

3.3.4 Computational Complexity

Table 3.4 shows the comparison of the computational complexities between CM, MMED, and MMED-M. In this table, the comparison is made based on the number of complex multiplications. In Eq. (3.7), it can be seen that in CM, the computation for each user subset depends only on the QR decomposition process. Therefore, in CM, the number of complex multiplications in one loop of user selection process is equal to the number of complex multiplications in the QR decomposition multiplied by $\binom{K_{\text{ava}}}{K_{\text{col}}}$.

In MMED, besides the QR decomposition process, the Euclidean distance calculations are also required. However, for some user subsets, these QR decompositions and Euclidean distance calculations can be omitted. In MMED, $|r_{1,1}^{U}|^2 \geq \bar{d}_{\text{min}}^2$. The value of $|r_{1,1}^{U}|^2$ itself is equal to $||\boldsymbol{h}_1^U||^2$, where $\boldsymbol{h}_1^U$ is the first column vector of $\boldsymbol{H}_U$. Therefore, for the user subsets which have the value of $||\boldsymbol{h}_1^U||^2$ less than the value of $\bar{d}_{\text{min}}^2$ from the previous user subset, the QR decomposition and Euclidean distance calculations can be omitted. In Table 3.4, δ denotes the average number of QR decompositions and Euclidean distance calculations in one user selection loop.

In MMED-M, $N_{\text{t}}K_{\text{ava}}$ additional complex multiplications are required for channel ordering. Similar to MMED, not all of QR decompositions and Euclidean distance calculations have to be calculated. In addition, the calculations of Euclidean distances in MMED-M are not required for all stage of selection. When the stored value of Euclidean distance at the stage of n_{t} is less than the value of $\bar{d}_{\text{min}}^2$ from the previous user subset, the Euclidean calculations from the stage of $n_{\text{t}}+1$ to the stage of N_{t} can be skipped. In Table 3.4, $\mu_{n_{\text{t}}}$ denotes the average number of Euclidean distance calculation processes at the stage of n_{t}. For the case of $N_{\text{t}} = 4$, the value of δ and $\mu_{n_{\text{t}}}$ can be seen in Table 3.5.

Table 3.4. Number of complex multiplications in CM, MMED, and MMED-M.

Technique	Number of complex multiplications
CM	$\binom{K_{\text{ava}}}{K_{\text{col}}} \sum_{n_{\text{t}}=1}^{N_{\text{t}}} (2N_{\text{t}}(N_{\text{t}} - n_{\text{t}} + 1))$
MMED	$\delta \binom{K_{\text{ava}}}{K_{\text{col}}} \sum_{n_{\text{t}}=1}^{N_{\text{t}}} (2N_{\text{t}}(N_{\text{t}} - n_{\text{t}} + 1))$
	$+\delta \binom{K_{\text{ava}}}{K_{\text{col}}} \sum_{n_{\text{t}}=1}^{N_{\text{t}}} (n_{\text{t}} + 1)(\lvert\mathcal{E}_1\rvert^{n_{\text{t}}} - 1)/4$
MMED-M	$N_{\text{t}}K_{\text{ava}} + \delta \binom{K_{\text{ava}}}{K_{\text{col}}} \sum_{n_{\text{t}}=1}^{N_{\text{t}}} (2N_{\text{t}}(N_{\text{t}} - n_{\text{t}} + 1))$
	$+\delta \binom{K_{\text{ava}}}{K_{\text{col}}} \left(2\mu_1\lvert\mathcal{E}_1\rvert + \sum_{n_{\text{t}}=2}^{N_{\text{t}}} \mu_{n_{\text{t}}}(n_{\text{t}} + 1)G_{\text{S}}\lvert\mathcal{E}_1\rvert\right)$

Table 3.5. Values of δ and $\mu_{n_{\text{t}}}$ in MMED and MMED-M for $N_{\text{t}} = 4$.

Technique	Item	K_{ava}				
		6	7	8	9	10
MMED	δ	0.92	0.87	0.82	0.77	0.72
MMED-M	δ	0.52	0.38	0.28	0.21	0.16
	μ_1	0.36	0.43	0.48	0.51	0.53
	μ_2	0.13	0.16	0.17	0.18	0.19
	μ_3	0.03	0.04	0.04	0.04	0.05
	μ_4	0.47	0.37	0.31	0.27	0.24

3.4 Simulation Results

3.4.1 BER Performance

Figure 3.4 shows the BER performance of an MU-MIMO system with CIC for the case of four transmit antennas at the BS serve four active users. A user selection is conducted to select four collaborating users out of six available users. At the detection process,

QRM-MLD is used with the number of candidates, K_{QRM}, is set to 2 or 4. The BER performances of QRM-MLD when using MMED, and MMED-M user selection techniques are compared. For the case of $K_{\mathrm{QRM}} = 2$, the value of G_{S} of MMED-M is set to 2, while for the case of $K_{\mathrm{QRM}} = 4$, the value of G_{S} of MMED-M is set to 3. In addition, the BER performance when the capacity maximization (CM) is used as the user selection technique is also plotted.

From the figures, it can be observed that in the case of the number of candidates in QRM-MLD, K_{QRM}, is sufficiently large (i.e: 4), both MMED and MMED-M is able to achieve a performance with the diversity close to 6 at the BER of 10^{-5}. At this BER value, this performance surpasses the performance of CM by about 0.9dB. The performance degradation which occurs in CM comes from the fact the BER performance of a MIMO system at the high SNR value is determined by the minimum Euclidean distance from all possible vector of the transmitted symbols. On the other hand, CM considers only the channel sub-matrix in its selection process.

For the case of the value of K_{QRM} is relatively small (i.e: 2), an error floor occurs when conventional MMED is used as the selection technique. This error floor occurs due to the fact that MMED considers only the accumulative Euclidean distance from all of the possible error vectors at the stage of N_{t}. On the other hand, QRM-MLD conducts its detection process in a recursive manner and have a potential to suffer from error propagation. The conventional MMED, therefore, is suitable for QRM-MLD implementations only when the number of candidates in QRM-MLD is sufficiently large. Using CM user selection technique, this error floor does not occur as CM user selection technique considers all of the diagonal values of matrix $\boldsymbol{R}_U$. In MMED-M, the accumulative Euclidean distance at each stage of selection is considered in the selection process and minimize the error events in the early stage of QRM-MLD detection. Using the proposed technique, the performance degradation compared with the case of $K_{\mathrm{QRM}} = 4$ is relatively small.

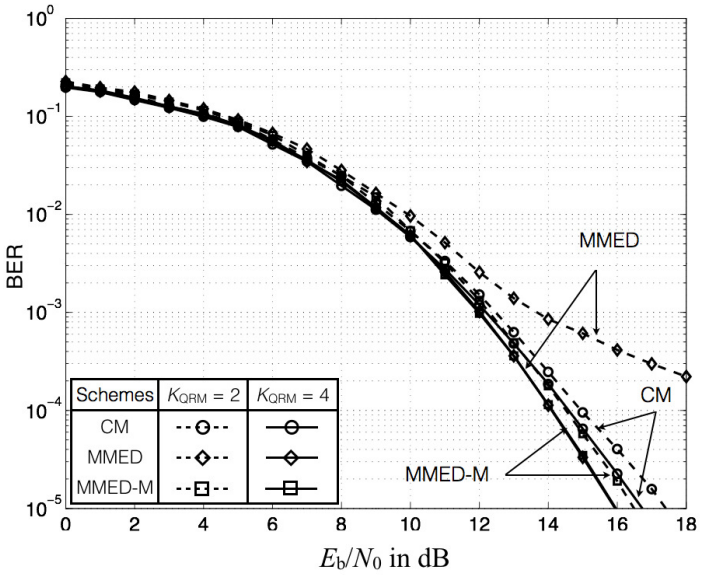

Fig. 3.4. BER performance of MMED-M user selection for a transmission of four QPSK signals, $K_{\mathrm{ava}} = 6$ (Copyright(©) 2016 IEICE, [71] Fig. 5).

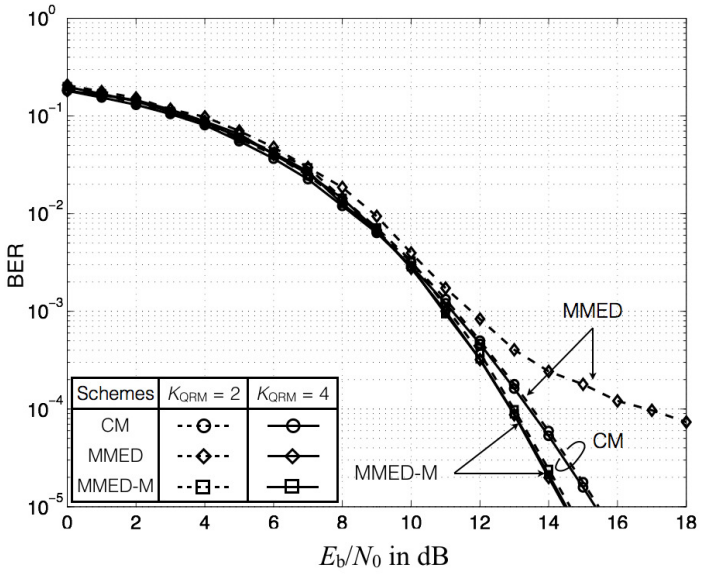

Fig. 3.5. BER performance of MMED-M user selection for a transmission of four QPSK signals, $K_{\mathrm{ava}} = 8$ (Copyright(©) 2016 IEICE, [71] Fig. 6).

This performance degradation is even smaller when a larger number of users is available. As can be seen in Fig. 3.5, the performance degradation is negligible when eight users are available.

3.4.2 Effect of the number of surviving nodes

In Fig. 3.6, the effect of the number of surviving nodes, G_{S}, is shown. For this simulation, a transmission of four QPSK signals is employed with $K_{\mathrm{ava}} = 8$ and $K_{\mathrm{act}} = 4$. MMED-M is employed to select four out of eight users to conduct CIC. From the figure, it can be seen that for the case of $K_{\mathrm{QRM}} = 4$, the BER performance of MMED-M with $G_{\mathrm{S}} = 3$ is slightly better than the BER performance of MMED-M with $G_{\mathrm{S}} = 2$. For the case of $K_{\mathrm{QRM}} = 2$, however, an error floor occurs when $G_{\mathrm{S}} = 3$, while a better performance is obtained when $G_{\mathrm{S}} = 2$. As mentioned in the Sect. 3.3.2, the error floors when $G_{\mathrm{S}} = 3$ occurs as several symbol errors which have the zero probability to become a symbol error between two candidates at the QRM-MLD are still considered in the user selection process.

Observing Fig. 3.6, it can be concluded that there is an optimum value for G_{S} for each K_{QRM}. In addition, it can also be seen from the figure that for the case of $G_{\mathrm{S}} = 2$ is used on MMED-M, the performance of QRM-MLD with $K_{\mathrm{QRM}} = 2$ and $K_{\mathrm{QRM}} = 4$ is relatively equal. Therefore, for the case of four QPSK signals, the value of $G_{\mathrm{S}} = 2$ can be selected for a stable performance.

3.4.3 Computational Complexity

Figure 3.7 shows the comparison of the computational complexities of CM, MMED, and MMED-M user selection techniques. The comparison is conducted by comparing the number of complex multiplications on those techniques with the increasing number of K_{ava}. In this comparison, QPSK modulation is employed for the transmissions. For MMED-M, the number of surviving nodes, G_{S}, is set to 2.

As can be seen in the figure, the number of complex multiplications in MMED is larger than the other two techniques for all values of N_{t} and K_{ava}. In addition, it can also be observed from the figure that for a relatively small number of available users, CM

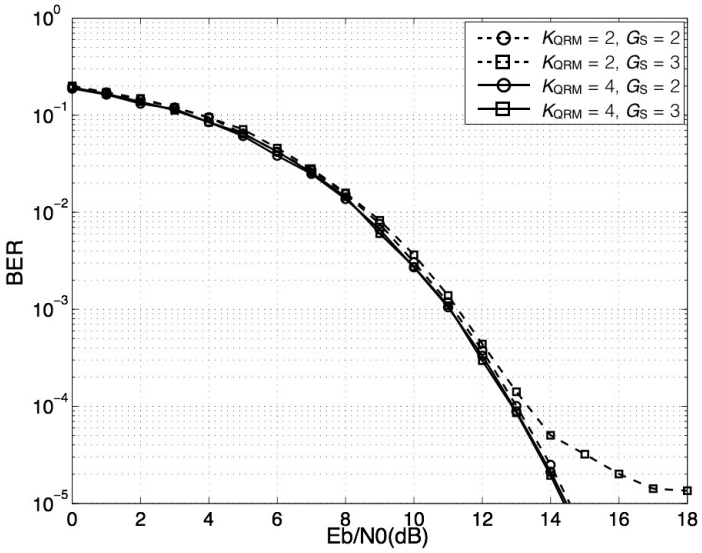

Fig. 3.6. Effect of the number of surviving nodes in MMED-M (Copyright(©) 2016 IEICE, [71] Fig. 8).

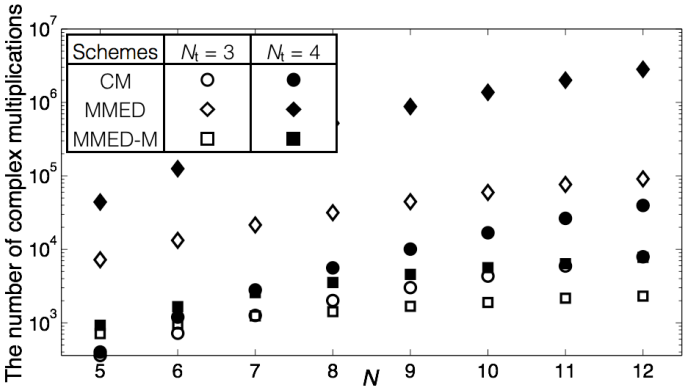

Fig. 3.7. Number of complex multiplications in CM, MMED, and MMED-M for QPSK transmissions (Copyright(©) 2016 IEICE, [71] Fig. 10).

requires a smaller number of complex multiplications compared to that of MMED-M. In a relatively large value of K_{ava}, however, the number of complex multiplications in the CM technique is larger than that of MMED-M technique.

This circumstance occurs as in the large number of K_{ava}, the value of $\binom{K_{\text{ava}}}{K_{\text{col}}}$ grows rapidly and directly increases the number of complex multiplications in the CM technique. On the other hand, as the early breaking process can be employed in MMED-M,

not all of the QR decomposition processes have to be conducted. Therefore, the number of complex multiplications can be significantly reduced, especially for a large number of K_{ava}. As an example, for the case of $N_{\text{t}} = 4$ and $K_{\text{ava}} = 8$, MMED-M is able to reduce the number of complex multiplications by about 37% and 99% compared to CM and MMED, respectively. In addition, the number of complex multiplications in MMED-M increases relatively linear and makes implementation feasible.

3.5 Field Experiments

3.5.1 Experiment Setup

In order to verify the effectiveness of MU-MIMO with CIC, field experiments with the parameters shown in Table 3.6 are conducted. It should be noted, however, due to the time limitation, no user selection is applied in the field experiments. Figure 3.8(a) shows signal generators that generates four QPSK signals at a symbol rate of 312.5 k symbols/s. These QPSK signals are then sent to four antennas in the BS. The height of the BS is 25.5m. In the BS, the antennas are installed in perpendicular positions, as shown in Fig. 3.8(b). From the BS, packet signals are broadcasted to the users. Each of these packets contains 15 BPSK symbols of synchronization word, 16 BPSK symbols of training sequences, 15 QPSK symbols for control, and 80 QPSK symbols of data, including the cyclic redundancy check (CRC). In this field experiment, the performance of MU-MIMO with CIC is observed for both MLD and MMSE algorithms.

The BS in this experiment is located at a building in Kyoto University. The MSs are installed inside a car that moves along the route shown in Fig. 3.9. The route can be divided into two parts. In part A, the speed of the car is about 15 km/hour, and in part B, the speed of the car is about 45 km/hour. Inside the car, seven universal software radio peripherals (USRPs) are used to represent the MSs. Each USRP in Fig. 3.10(a) uses 3 dBi antenna gains. Inside the USRP, an analog to digital converter (ADC)

Table 3.6. Experiment parameters of MU-MIMO with CIC

System Parameters	Values
Number of antennas of BS	4
Number of antennas of MS	1
Number of active MSs	4
Number of collaborating MSs	4, 7
Frame length	50 ms
Carrier frequency	5.11 GHz
Symbol rate	312.5 k symbols/s
Modulation	QPSK
BS Parameters	**Values**
Transmit filter	Square Root Nyquist (roll-off factor=0.4)
Antenna hight	25.5 m
Antenna gain	5 dBi
MS Parameters	**Values**
Antenna gain	3 dBi
ADC resolution	14 bits
Packet Configuration	**Values**
Synchronization word	15 BPSK symbols
Training sequence	16 BPSK symbols
Control	15 QPSK symbols
Data + CRC	80 QPSK symbols

with 14 bit resolution is used. The position of each MS can be seen in Fig. 3.10(b). To conduct a signal exchange, WiFi connections with IEEE 802.11n in the 5 GHz band are used as inter-MS communications. Each MS broadcasts its quantized-received-signal to the other MSs in a dedicated time slot by using User Datagram Protocol (UDP). For each real and imaginary part, 8 bits quantization is used.

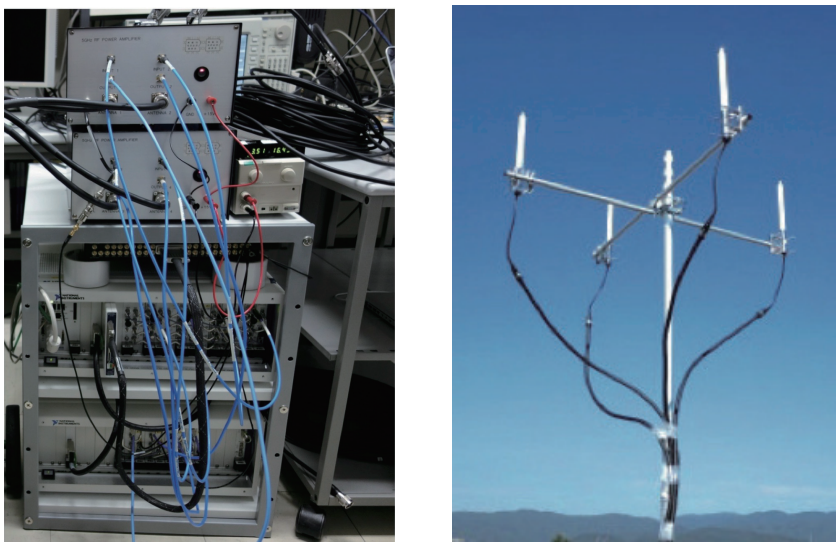

(a) Signal generators. (b) Antennas.

Fig. 3.8. Transmitter setup on the field experiment of MU-MIMO with CIC (Copyright(©) 2017 IEICE, [72] Fig. 2).

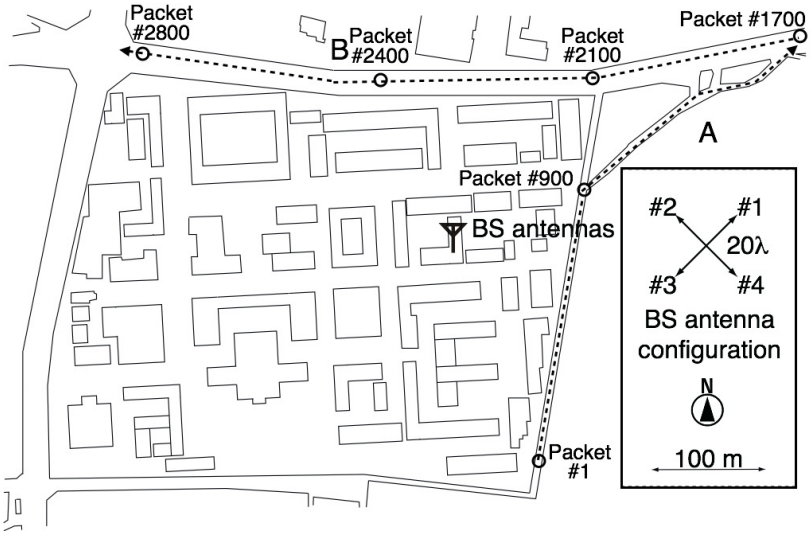

Fig. 3.9. Experiment route of MU-MIMO with CIC (Copyright(©) 2017 IEICE, [72] Fig. 3).

3.5.2 Experiment Results

The results obtained through the field experiment can be seen in Figs. 3.11-3.14. In Figs 3.11-3.13, packet index from 1 to 1700 corresponds to the part A of the route, while

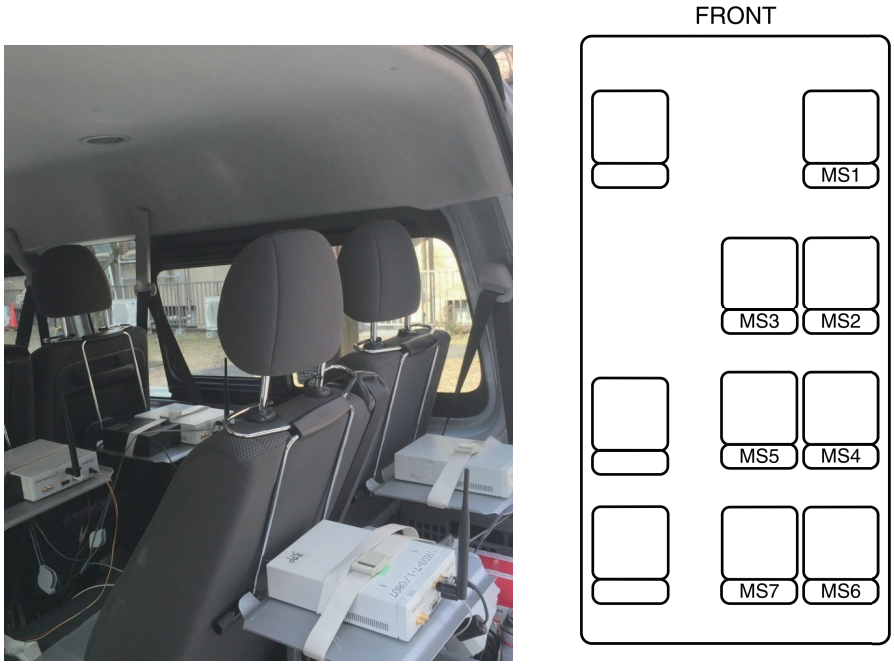

(a) USRP + PC. (b) MS positions.

Fig. 3.10. MS setup (Copyright(©) 2017 IEICE, [72] Fig. 4).

packet index from 1701 to 2800 corresponds to the part B of the route. Figure 3.11 shows the number of signals successfully shared to MS1 for each packet of transmitted data. The average numbers of signals successfully shared to MS2, MS3, and MS4 are also shown. From this figure, it can be observed that the interuser links for signal information exchange are generally successful and very reliable.

In Fig. 3.12, the received power of the transmitted signals of the BS at MS1 is shown. The average power at MS1 is -95 dBm. The median of the received power at all active MSs is also shown. From the figure, it can be seen that all of the MSs have similar received powers. This similar received power, together with an equal number of received signals from the other MSs, results in a similar BER performance of all MSs for all packets, as shown in Fig. 3.13. In this figure, the black-dashed line is the BER for the case of 4×4 MLD, while the red line is the BER for the case of 4×7 MMSE.

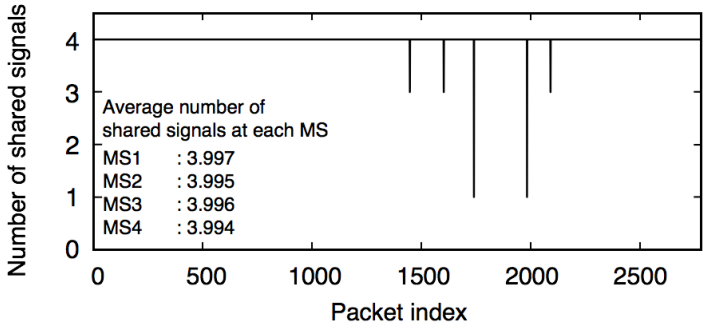

(a) Four collaborating MSs.

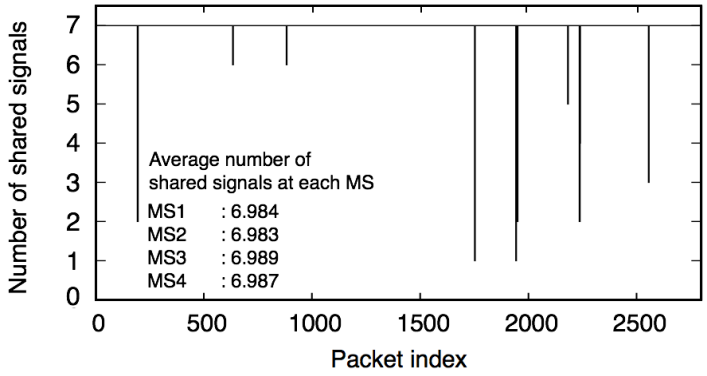

(b) Seven collaborating MSs.

Fig. 3.11. Number of shared signals at MS1 (Copyright(©) 2017 IEICE, [72] Fig. 5).

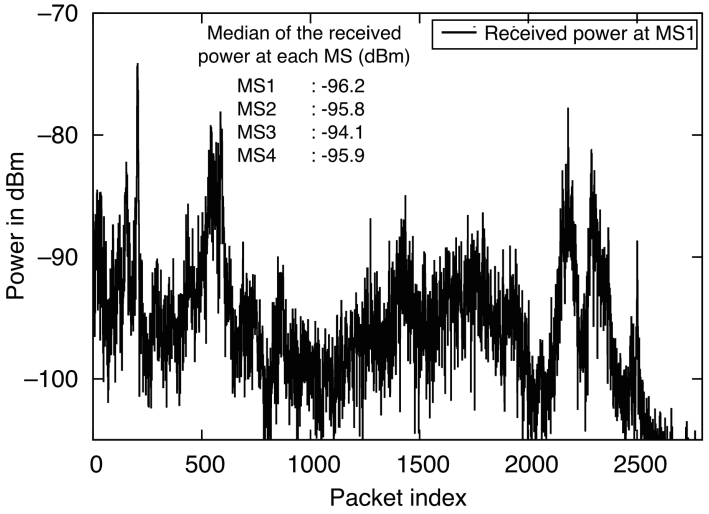

Fig. 3.12. Received power measured at MS1 (Copyright(©) 2017 IEICE, [72] Fig. 6).

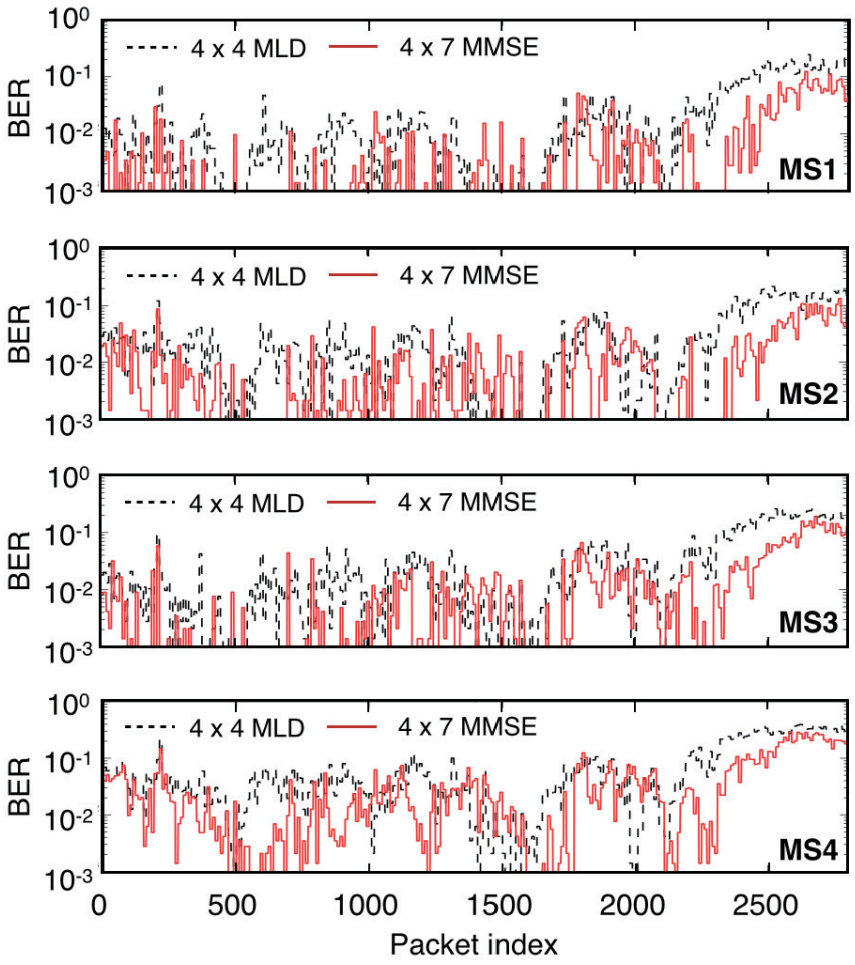

Fig. 3.13. BER in each packet transmission (Copyright(©) 2017 IEICE, [72] Fig. 7).

Next, the CDF of the BER of MU-MIMO with CIC is shown in Fig. 3.14 for the case of $K_{\text{col}} = 4$ using MLD and for the case of $K_{\text{col}} = 7$ using both MLD and MMSE. In the CDF graph, the instantaneous BER is calculated for every 10 packets of data. As shown in the figure, the BER performance at part A is better than the BER performance at part B. This circumstance occurs as the received power in part A is larger than that of part B due to the difference on the geographical topology. In addition, the average speed in part B is higher, causing the channel response fluctuates faster. Furthermore, it can be seen from the figure that at the cost of higher complexity, MLD obtains better performance compared to that of MMSE when an equal value of K_{col} is used. However,

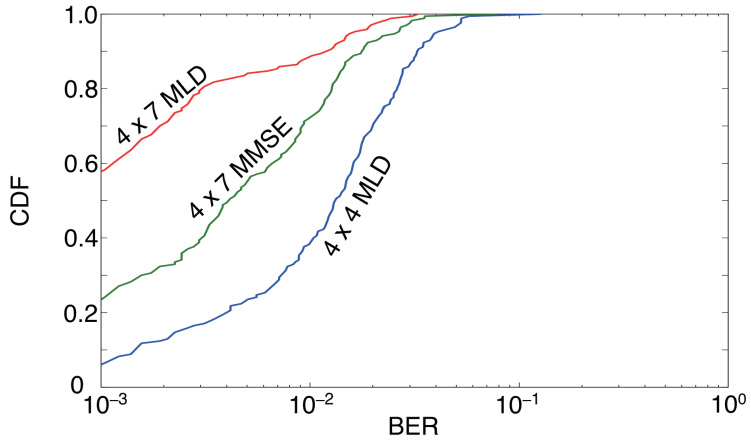

(a) Part A of the route (15 km/hour).

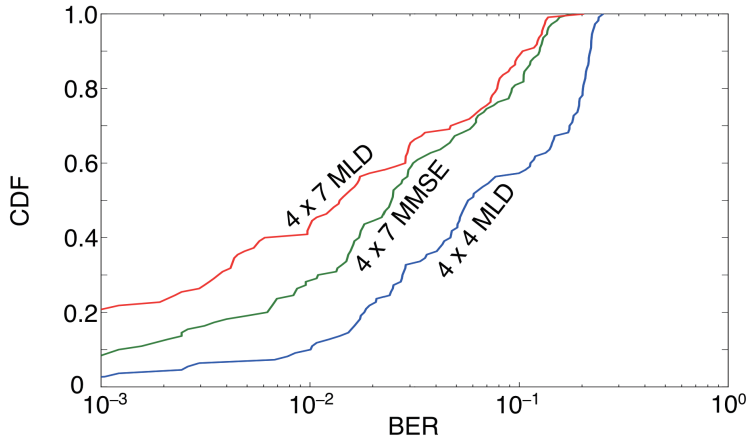

(b) Part B of the route (45 km/hour).

Fig. 3.14. CDF of BER of MU-MIMO with CIC (Copyright(©) 2017 IEICE, [72] Fig. 8).

it can also be seen that by having more array gain, 4×7 MMSE performs better than 4×4 MLD although these scenarios have a similar theoretical diversity. This better performance is obtained for both cases of average speed.

3.6 Summary

In this chapter, MU-MIMO transmission employing CIC is described. Afterward, it is shown that user selection will hold a key role in the implementation of MU-MIMO with CIC due the fact that MU-MIMO with CIC has to be able to exploit a large number of

available users while maintaining the number of signal exchanges relatively low. On the other hand, user selection technique for a contemporary signal detection technique, i.e., QRM-MLD has not been available yet. In this chapter, therefore, a novel user selection technique is proposed with the goal of optimizing the BER performance for the case of QRM-MLD is used as the detection algorithm.

Differ with the conventional user selection technique, the proposed technique stores the minimum Euclidean distance in each stage of selection and considers it for the user selection process. This feature is important, mainly to accommodate the recursive manner of QRM-MLD. In addition, an M-algorithm is also employed in the proposed technique. Through the M-algorithm implementation, the computational complexity of MMED-M only grows linearly with the number of transmit antennas and makes implementation feasible. In addition, the M-algorithm in MMED-M can be used to discard the symbol error which has a zero probability to become a symbol error between two candidates of QRM-MLD. By maximizing the accumulative Euclidean distance in each stage of selection and selecting the appropriate number of surviving nodes, MMED-M is able to provide excellent BER performance even when the number of candidates in QRM-MLD is relatively small.

In addition to user selection, this chapter also presents the field experiment which is conducted to verify the effectiveness of MU-MIMO with CIC. Through the results of the field experiments, it can be concluded that in the actual environment, MU-MIMO with CIC is applicable, despite the moving nature of the group mobility and the unideal condition occurred in the interuser links. As accurate CSI at the transmitter is not required, CIC could become a potential approach for MU-MIMO communications in group mobility scenarios. In addition, through the field experiment, it is also worth to note that a higher number of collaborating users with MMSE has better performance compared to that of a smaller number of collaborating users with MLD even when the theoretical

diversity order is equal. On the other words, the large number of collaborating users has better potential to combat unideal condition which occurs in the actual environment, e.g. the channel correlation among users.

Chapter 4

Interference Driven Power Allocation for MU-MIMO with Precoding Under Time-Varying Channel

4.1 Introduction

The most common approach for interference cancellation in MU-MIMO systems is by using precoding technique [9–11]. When perfect CSI is available, this technique can be used to greatly reduce the interuser interference or to significantly increase the power of the received symbols. In its implementation, hundreds of transmit antenna elements can be used at the BS to serve tenths of users. Such scenario is called massive MIMO [73–75], which currently becomes one of the hottest topics in wireless communications.

4.1.1 Review of Previous Works

4.1.1.1 Power Allocation

To exploit its full potential, power allocation technique can be applied to MU-MIMO. The design of the power allocator itself will depend heavily on its main purpose. In [76], power allocation is used to improve the security of the transmission from the eavesdropper. In [77–86], power allocation was implemented to improve the sum-rate capacity. Specifically,

research in [77] proposed power allocation techniques in a single cell downlink MU-MIMO for several linear precoding techniques. Research in [78], on the other hand, proposed a power allocation technique designed to maximize the capacity of multicell massive MIMO. A more specific scenario, i.e. where the beam division multiple access is employed in multicell massive MIMO, is considered in [79]. Power allocation for capacity maximization is also presented in [80], where power allocation is used jointly with the user scheduling for the case of distributed massive MIMO with backhaul capacity constraint. Meanwhile, a joint optimization of power allocation and antenna selection is suggested in [81–83]. For the case of massive MIMO with joint spatial division and multiplexing, a designated power allocation technique can be found in [84]. The extended version of [84], where the user scheduling is also jointly considered with the power allocation, is then proposed in [85]. Taking the quality of service as consideration, research in [86] employs a game theory approach to design a power allocation technique to maximize the sum-rate capacity.

Besides to the capacity, power allocation can also be used to improve the energy efficiency (EE) of MU-MIMO transmission. In [87], the number of users and transmit power were jointly optimized. The idea is then extended in [88], where the number of antennas, users, and transmit power were jointly optimized for the case of single cell massive MIMO system with zero forcing (ZF) precoding. For the case of maximum ratio transmission (MRT) precoding, a power allocation technique to increase the EE can be found in [89]. In [90], a power control algorithm for multicell massive MIMO where channel estimation error, pilot contamination, and channel correlation are taken into account was presented. Research in [91], on the other hand, presented a power allocation algorithm which could maximize the EE when the power amplifier efficiency is taken into account.

Considering the channel characteristic, research in [92] designed a power allocation technique to optimize the EE of massive MIMO in the Ricean fading environment. Meanwhile, the power allocation technique is designed in [93] by taking the quality of service as the main consideration. In [94], power allocation is jointly used with the resource, antenna, and sub-carrier allocation to optimize the EE of an orthogonal frequency division multiple access massive MIMO systems. Taking the sum user transmit power and user data rate constraint into consideration, research in [95] has designed a power allocation technique which could optimize the EE of the systems. To improve the EE even further, research in [96] uses power allocation jointly with the user scheduling, in particular, for the case of multi-cell massive MIMO. Meanwhile, research in [97] proposed a power allocation which jointly considers both spectral efficiency and EE and discussed its trade-off. It should be noted, however, all of these schemes consider a convenient block fading channel on the transmission. In this thesis, therefore, power allocation is investigated for the case of time-varying MU-MIMO.

4.1.2 Effect of Channel Aging

The full benefit of MU-MIMO relies heavily on the congruity between the CSI used in the precoder and the actual channel. Unfortunately, this condition is hard to be fulfilled, in particular, due to the time varying nature of the channel caused by the relative movement between the users and BS. In the near future, this challenge will be even harder as the forthcoming wireless communication system will most likely implement the higher-frequency bands [26]. In addition, the system should also be able to serve users with high mobility. In this condition, the channel will fluctuate faster and the effect of channel aging will be more severe [98].

Channel aging refers to the mismatch between the CSI used in the precoder calculation and the actual channel when the data are transmitted. This discrepancy causes the

intended signal to be phase shifted and interuser interference arises. The effect of channel aging on the achievable rates of large MIMO systems has been analyzed in [99, 100]. Closed form bounds for the achievable sum rate and deterministic equivalents of the signal-to-interference-plus-noise ratio for maximal ratio combining and regularized linear receivers in the presence of channel aging are derived in [101,102]. A tighter lower bound on the achievable sum rate has been presented in [103] for an arbitrary number of users and antennas at the BS. In [104, 105], the combined effects of phase noise and channel aging for massive MIMO are observed by means of an autoregressive model. Research in [106], on the other hand, investigates the effect of increasing the number of transmit antenna on the outage capacity performance on massive MIMO in time varying channel. A difference aspect has been investigated in [107], where the effect of channel aging to the energy efficiency of massive MIMO has been derived.

To combat the channel aging effect, several techniques have been proposed in previous literature. In [108], the channel aging effect is reduced by using a narrow beam receiver at the MS. Meanwhile, [109] proposed a combination of beamforming, followed by Doppler compensation to minimize the channel aging in a single-input multiple-ouput system. This technique is then generalized in [110] for the case of MIMO system. Similar techniques are also used in [111] to reduce the effect of channel aging, mainly in an OFDM system. All of these techniques, however, compensate the Doppler spread effect at the MS side. Implementing these techniques to the MU-MIMO scenario would be difficult as the MS will receive signals from tenths to hundreds transmit antennas.

4.1.3 Our Study

One straight forward approach to mitigate the channel aging effects on MU-MIMO is by frequently update the precoder matrix. To minimize the required uplink transmission,

the CSI for updating the precoder can be obtained by using channel prediction techniques such in [99, 101–103, 112]. Those works, however, only discuss the effect of the channel prediction to the sum-rate capacity of time-varying MU-MIMO. A method of how to intelligently exploit those channel prediction to improve the system performance, therefore, still become an open task. This issue is important, as exploiting the channel prediction by directly use it for frequently updating the precoder matrix will drastically increase the computational complexity.

To reduce the effect of channel fluctuation, a novel power allocation technique for time-varying MU- MIMO is proposed in this research. First, by using pilots from the users, the BS extracts Doppler shift information experienced by the user to create a predicted channel matrix. This matrix is then used to calculate the predicted interference level for each user. Based on this information, the BS then allocates the power for each user in a recursive manner. As the precoder matrix is not necessarily updated frequently, this technique could minimize the interuser interference with a low addition in the computational complexity.

4.2 Time-Varying MU-MIMO

In a moving environment, all rays arrived at the MSs are experiencing Doppler shift. As each ray arrives at a different angle, the values of the Doppler shift will vary. The variation on the Doppler shift values, i.e. Doppler *spread*, causes each element in the channel matrix $\boldsymbol{H}$ to fluctuate. The channel matrix, $\boldsymbol{H}$, therefore, becomes time-dependent and is denoted as $\boldsymbol{H}(t)$. Denotes $a_{k,n_\mathrm{t}}[\bar{n}]$ and $\bar{f}_{k,n_\mathrm{t}}[\bar{n}]$ as the amplitude and the Doppler shift of the $\bar{n}$ ray at $t = 0$ occurs between n_tth transmit antenna and kth user. The value of (k, n_t)th element of $\boldsymbol{H}(t)$ can be written as

$$h_{k,n_\mathrm{t}}(t) = \sum_{\bar{n}=1}^{\bar{N}_{k,n_\mathrm{t}}} a_{k,n_\mathrm{t}}[\bar{n}] e^{\mathrm{j}2\pi t \bar{f}_{k,n_\mathrm{t}}[\bar{n}]}. \tag{4.1}$$

While the actual channel, $\boldsymbol{H}(t)$, fluctuates, the precoder matrix, $\boldsymbol{W}$, is constant inside one precoder update period. This circumstance causes a mismatch between $\boldsymbol{H}(t)$ and $\boldsymbol{W}$. The mismatch causes the original signal for each MS is phase-shifted, and the interference from the other MSs arises. The channel-equivalent matrix, as the result of the multiplication between $\boldsymbol{H}(t)$ and $\boldsymbol{W}$, therefore, will be no longer an identity matrix, $\boldsymbol{I}_{K\times K}$. This problem can be diminished by frequently update the precoder matrix $\boldsymbol{W}$. However, although the CSI required for recalculating $\boldsymbol{W}$ can be obtained by channel prediction such in [99, 101–103, 112], frequently updating $\boldsymbol{W}$ significantly increases the computational complexity.

4.3 Interference Minimization through Power Allocation

In this thesis, a novel power allocation technique to minimize the channel aging effect on the MU-MIMO system is proposed. First, the BS will extract the Doppler shift information from the pilot symbols sent by the MS to create a predicted channel. Next, based on the predicted channel, the BS calculates the predicted interference level at all MSs to allocate the power for each MS. The predicted channel is also used to determine the phase-shift compensation for each MS. Using this technique, the BS did not have to update the precoder matrix frequently, and thus, enable the MU-MIMO transmission without significantly increasing the computational complexity.

4.3.1 Channel prediction

In the proposed technique, the channel prediction is conducted based on the Doppler shift information of the signals. Using this approach, perfect channel prediction can be obtained when the BS has information of the amplitude and the Doppler shift of each ray in Eq. (4.1). This ideal condition, however, is hard to be fulfilled. In this research, therefore, the channel prediction is conducted by firstly represent the predicted channel

as the addition of $\tilde{N}$ virtual rays. Each of these rays has a fixed value of Doppler shift which lays linearly between $-f_{\mathrm{D}}$ and $+f_{\mathrm{D}}$, and can be obtained by

$$\tilde{f}_{k,n_{\mathrm{t}}}[\tilde{n}] = -f_{\mathrm{D}} + 2f_{\mathrm{D}}\frac{\tilde{n}-1}{\tilde{N}-1}, \tag{4.2}$$

where $\tilde{n} = 1, 2, \ldots, \tilde{N}$. Denotes $\tilde{a}_{k,n_{\mathrm{t}}}[\tilde{n}]$ as the amplitude of the signal with the estimated Doppler shift of $\tilde{f}_{k,n_{\mathrm{t}}}[\tilde{n}]$, the predicted signal can be written as

$$\tilde{h}_{k,n_{\mathrm{t}}}(t) = \sum_{\tilde{n}=1}^{\tilde{N}} \tilde{a}_{k,n_{\mathrm{t}}}[\tilde{n}] e^{\mathrm{j}2\pi t \tilde{f}_{k,n_{\mathrm{t}}}[\tilde{n}]}. \tag{4.3}$$

The larger value of $\tilde{N}$ in Eq. (4.2) produces a smaller gap between $\tilde{f}_{k,n_{\mathrm{t}}}[\tilde{n}]$ and the actual Doppler shift value. When an appropriate value of $\tilde{N}$ is used, the difference between $h_{k,n_{\mathrm{t}}}$ and $\tilde{h}_{k,n_{\mathrm{t}}}$ will be small.

In Eq. (4.3), the values of $\tilde{a}_{k,n_{\mathrm{t}}}[\tilde{n}]$ can be obtained by transmitting X training symbols at the uplink transmission. Here, $X \geq \tilde{N}$. Denotes, $\ddot{\boldsymbol{y}}_{k,n_{\mathrm{t}}} = [\ddot{y}_{k,n_{\mathrm{t}}}[1], \ddot{y}_{k,n_{\mathrm{t}}}[2], \ldots, \ddot{y}_{k,n_{\mathrm{t}}}[X]]^{\mathrm{T}}$ as the vector of the received signal of X training symbols from kth MS to n_{t}th antenna arrays and $\tilde{\boldsymbol{a}}_{k,n_{\mathrm{t}}} = [\tilde{a}_{k,n_{\mathrm{t}}}[1], \tilde{a}_{k,n_{\mathrm{t}}}[2], \ldots, \tilde{a}_{k,n_{\mathrm{t}}}[\tilde{N}]]^{\mathrm{T}}$. The amplitude of each estimated Doppler shift can be obtained by

$$\tilde{\boldsymbol{a}}_{k,n_{\mathrm{t}}} = \tilde{\boldsymbol{F}}^{-1}\ddot{\boldsymbol{y}}_{k,n_{\mathrm{t}}}, \tag{4.4}$$

where

$$\boldsymbol{F} = \begin{bmatrix} e^{\mathrm{j}2\pi t_1 \tilde{f}_{k,n_{\mathrm{t}}}[1]} & e^{\mathrm{j}2\pi t_1 \tilde{f}_{k,n_{\mathrm{t}}}[2]} & \cdots & e^{\mathrm{j}2\pi t_1 \tilde{f}_{k,n_{\mathrm{t}}}[\tilde{N}]} \\ e^{\mathrm{j}2\pi t_2 \tilde{f}_{k,n_{\mathrm{t}}}[1]} & e^{\mathrm{j}2\pi t_2 \tilde{f}_{k,n_{\mathrm{t}}}[2]} & \cdots & e^{\mathrm{j}2\pi t_2 \tilde{f}_{k,n_{\mathrm{t}}}[\tilde{N}]} \\ \vdots & \vdots & \ddots & \vdots \\ e^{\mathrm{j}2\pi t_X \tilde{f}_{k,n_{\mathrm{t}}}[1]} & e^{\mathrm{j}2\pi t_X \tilde{f}_{k,n_{\mathrm{t}}}[2]} & \cdots & e^{\mathrm{j}2\pi t_X \tilde{f}_{k,n_{\mathrm{t}}}[\tilde{N}]} \end{bmatrix}, \tag{4.5}$$

where $t_x = t_1, t_2, \ldots, t_X$ is the time index of the training symbols. The value of $\tilde{\boldsymbol{a}}_{k,n_{\mathrm{t}}}$ obtained from Eq. (4.4) is then inserted to Eq. (4.3) to create the predicted channel.

4.3.2 Power Allocation

In this thesis, a novel power allocation technique to reduce the interuser interference at time-varying MU-MIMO is proposed. This technique exploits the fact that even a mismatch between $\boldsymbol{H}(t)$ and $\boldsymbol{W}$ occurs, the interference level varies between the MSs. In particular, low interference levels could occur at several MSs either because the MSs have low mobility, the signals arrived at the MSs in a near orthogonal direction relative to the MSs movement, and or the interference from the other MSs added destructively at the designated MS.

To determine the power allocation for each MS, the interference level of all MSs at the end of each precoder update period, T_{P}, has to be calculated. Denotes $g_{k,j}(t)$ as the (k,j)th element of $\boldsymbol{G}(t)$. The interference level for kth MS at time T_{P} can be obtained by

$$R_k(T_{\mathrm{P}}) = \sum_{j \neq k} ||g_{k,j}(T_{\mathrm{P}})||^2 \, p_j \tag{4.6}$$

where p_j is the allocated power for jth MS. In the matrix form, Eq. (4.6) can be written as

$$\begin{aligned} \begin{bmatrix} R_1(T_{\mathrm{P}}) \\ R_2(T_{\mathrm{P}}) \\ \vdots \\ R_K(T_{\mathrm{P}}) \end{bmatrix} &= \begin{bmatrix} 0 & ||g_{1,2}(T_{\mathrm{P}})||^2 & \dots & ||g_{1,K}(T_{\mathrm{P}})||^2 \\ ||g_{2,1}(T_{\mathrm{P}})||^2 & 0 & \dots & ||g_{2,K}(T_{\mathrm{P}})||^2 \\ \vdots & \vdots & 0 & \vdots \\ ||g_{K,1}(T_{\mathrm{P}})||^2 & ||g_{K,2}(T_{\mathrm{P}})||^2 & \dots & 0 \end{bmatrix} \begin{bmatrix} p_1 \\ p_2 \\ \vdots \\ p_K \end{bmatrix} \\ &= \boldsymbol{V}\,\boldsymbol{p}. \end{aligned} \tag{4.7}$$

The proposed power allocation algorithm can be seen in Algorithm 1. In the algorithm, $\bar{p}$ is the power for each MS when an equal power allocation is used for all MSs, $\tilde{p}_k$ is the minimum power for kth MS to achieve its target BER, and $\hat{p}$ is the excess power of the MS in obtaining its target BER, which could be transferred to the next MS.

First, the BS will calculate the interference level for all MSs, and arrange the MS in an ascending order based on its interference level. The BS then allocates the power

Algorithm 2 Proposed power allocation technique

$\hat{p} = 0$
for $i = 1 : K$ **do**
  $\tilde{k} = \underset{k}{\operatorname{argmin}} \sum_{j=1}^{K} v_{k,j}$
  if $\hat{p} + \bar{p} > \tilde{p}_{\tilde{k}} + (K - i)(\hat{p} + \bar{p} - \tilde{p}_{\tilde{k}}) \max_j v_{\tilde{k},j}$ **then**
    $p_{\tilde{k}} = \tilde{p}_{\tilde{k}} + (K - i)(\hat{p} + \bar{p} - \tilde{p}_{\tilde{k}}) \max_j v_{\tilde{k},j}$
    $\hat{p} \leftarrow \hat{p} + \bar{p} - \tilde{p}_{\tilde{k}}$
  else
    $p_{\tilde{k}} = \hat{p} + p_{\tilde{k}}$
  $v_{\tilde{k},*} = []$
  $v_{*,\tilde{k}} \leftarrow \frac{p_{\tilde{k}}}{\bar{p}} v_{*,\tilde{k}}$

firstly to the MS having the smallest interference level. In the allocating process, if the available power is larger than the power to achieve the target BER, the power should be reduced. The excess power is then kept and transferred to the next MS in the recursion process. Before goes to the next recursion, the $\tilde{k}$th column of matrix $\boldsymbol{V}$ should be updated according to the value of $p_{\tilde{k}}$. In addition, the $\tilde{k}$th row of $\boldsymbol{V}$ should be removed so that it will no longer be calculated in the next recursion. Similar processes are then repeated until the power for the last MS, p_K, has been allocated.

In addition to the power allocation purpose, the predicted channel is also used to calculate the phase shift of the signals. The value of the phase shift at time T_{P} can be represented by the diagonal values of $\boldsymbol{G}(T_{\mathrm{P}})$. Using this value, the value of the phase shift of kth MS at time t can be obtained by simple interpolation. Denotes $\theta_k = \angle g_{k,k}(T_{\mathrm{P}})$ as the phase shift occurs on kth MS at the end of each precoder update period. Using the proposed technique, the modulated symbol for kth MS should be updated before the precoding process as

$$\tilde{s}_k(t) = \frac{p_k t}{T_{\mathrm{P}}} s_k(t) e^{-\frac{\mathrm{j}t\theta_k}{T_{\mathrm{P}}}}. \tag{4.8}$$

Table 4.1. Parameters of Time-Varying MU-MIMO Simulation

Parameters	Values
Number of antenna arrays	36
Beam width of −3dB AF	10°
Side lobe gain	−23 dB
Precoding	ZF
Carrier frequency	6 GHz
Precoder updating period	every 200 μs
Number of MSs	6
MS velocity	0, 0, 40, 40, 80 and 80 m/s
Symbol period	1 μs
Modulation	QPSK

In Algorithm 1, it is probable that the power allocating process stops at a certain MS. This circumstance could take place when severe channel aging occurs in a large number of MSs, causing the total interference power for all MSs becomes significantly large. In this condition, the following MS will endure a significant performance degradation. This problem can be tackled by updating the precoder more than once in every downlink period. The number of precoder updating processes, however, should be minimized by intelligently utilizing the predicted channel. In addition, this problem can also be solved by using a proper user selection or user scheduling techniques. In this thesis, however, a method to tackle this issue is left as a potential future research.

4.4 Simulation Parameters and Results

4.4.1 Simulation Parameters

Table 4.1 shows the parameters used in the computer simulation. In this simulation, an MU-MIMO scenario where the BS is equipped with a large number of antenna arrays, i.e. massive MIMO, with hybrid beamforming technique [113] is considered. The BS

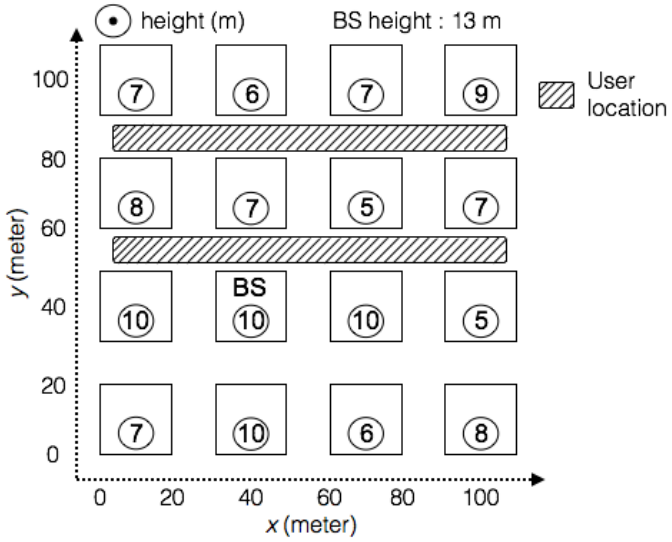

Fig. 4.1. Height and locations of the buildings, BS, and MSs in a virtual building database.

is assumed to have 36 antenna arrays. Each antenna array consists of several antenna elements which are arranged in a cosine distribution function to forms a 10° beam width of −3 dB array factor (AF) and −23 dB of side lobe [114]. The precoder matrix is updated in every 200 μs. Six MSs with the velocity of 0, 0, 40, 40, 80, and 80 m/s are assumed in this simulation. To obtain a near realistic channel characteristic, a ray launching method is used to generate the channel [115]. The locations of the MSs are randomly selected in the virtual building database which can be seen in Fig. 4.1. The symbols are modulated using QPSK modulator, with a symbol period of 1 μs.

4.4.2 Channel-Equivalent Characteristic

Fig. 4.2 shows the comparison of the fluctuation on the channel-equivalent matrix with and without the proposed technique when the MSs are located at the coordinate of (51, 86), (134, 88), (387, 88), (24, 83), (447, 88), and (354, 54) on the virtual building database. A target signal to noise ratio (SNR) of 16 dB is assumed. In the figure, the

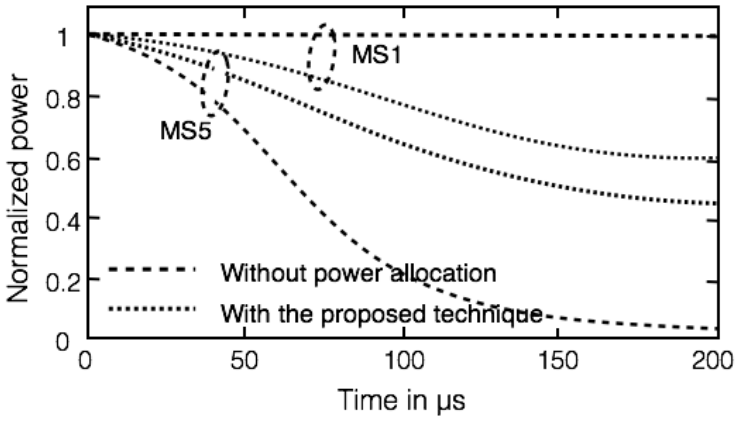

Fig. 4.2. Normalized power of channel-equivalent matrix.

normalized power is defined as the ratio between the intended signal and the total power of intended signal plus interference and is plotted for MS1 and MS5. As can be seen in the figure, the normalized power of MS5 without Doppler compensation at $t = 200\,\mu$s is very low. Using the proposed technique, on the other hand, the normalized power of MS5 can be significantly improved. Although the normalized power for MS1 is reduced, the proposed technique could maintain the normalized power above the acceptable power limit.

4.4.3 BER Performance

In Fig. 4.3 comparison on the BER performance of MS1, MS3, and MS5 with and without the proposed technique are plotted. In the simulation, a target BER of 10^{-3} is assumed, which in general, is acceptable for the case of no channel code is applied. For the case of MS1, an optimum performance can be obtained for both with and without the proposed power allocation technique. This circumstance occurs as MS1 has zero velocity, and thus, there is no mismatch between the precoder matrix and the actual channel. Without the proposed technique, however, an error floor above a BER of 10^{-2} occurs at MS3 and MS5 due to the fluctuation on their channel. Using the proposed technique, the performance degradation at MS3 and MS5 can be significantly reduced while maintaining

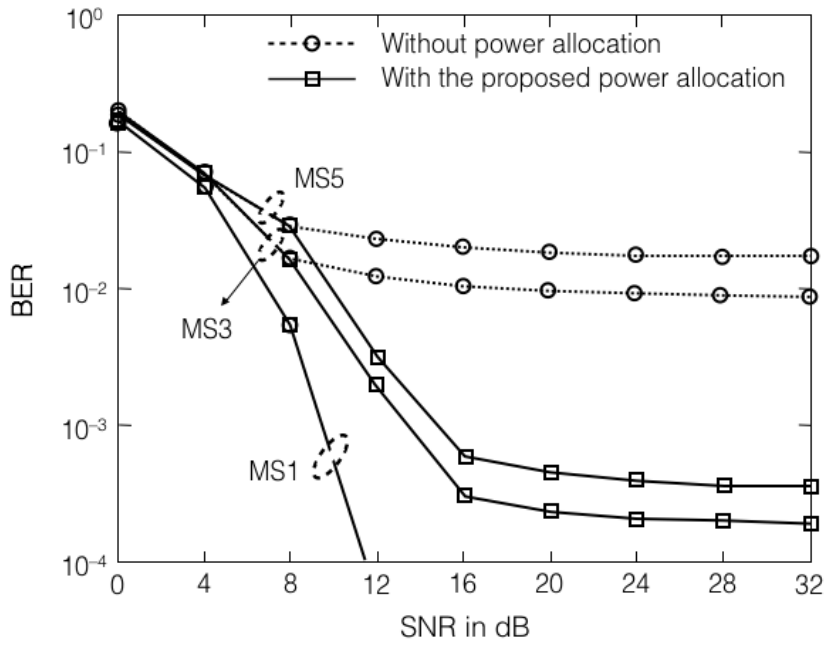

Fig. 4.3. BER performance of the proposed technique.

the performance of MS1. This improvement can be obtained as the proposed power allocation technique could minimize the interuser interference at the MS. In addition, the phase shift of the signal is also reduced by the phase compensator. Using the proposed technique, error floors below 10^{-3} can be obtained after a target SNR of 16 dB for both MS3 and MS5.

4.5 Summary

In this chapter, a novel technique to minimize the performance degradation on time varying MU-MIMO is proposed. The proposed technique improves the BER performance by exploiting power allocation to minimize the interuser interference. First, the BS extracts the Doppler shift information from the pilots sent by the MSs to create the predicted channel. Using the predicted channel, the interuser interference at the MS can be predicted. Recursive power allocation is then conducted so that the interuser

interference at the MSs can be minimized. Computer simulation shows that by using the proposed technique, the performance of MSs having large Doppler spread can be significantly improved while maintaining the performance of MSs experiencing small Doppler spread.

Chapter 5

Concluding Remarks

This thesis has focused on offering solution for performance enhancement of MIMO transmission technique, in particular, for the case of the number of receive antennas is limited. In such case, three approaches can be taken, which are overloaded MIMO, MU-MIMO with CIC, and MU-MIMO with precoding. Throughout this thesis, the challenges which arising for each approach has been derived, and solutions have been proposed.

For the case of overloaded MIMO approach, the challenge lies on performance degradation in the detection process. In a system with channel coding, this degradation leads to a significant reduction in the LLR quality as the decoder input. In Chapter 2, therefore, a joint decoding technique which could significantly improve the decoding capabilities of the system in the overloaded MIMO scenario is proposed. In this technique, rather than for each bit, the LLR is calculated for each combination bits. The decoding process is then conducted jointly between streams instead of separately. Using the proposed technique, the BER performance can be improved, throughput can be increased, and the mutual information on the EXIT function could converge faster.

For the case of MU-MIMO with CIC, the challenges lie in the number of signal exchanges required to obtain an excellent performance. To counter this issue, the user selection can be applied to select only several users from the available users to conduct CIC. It should be noted, however, user selection should be tailored to the detection

algorithm design. In this regard, user selection technique for the contemporary signal detection such as QRM-MLD is not yet available. In Chapter 3, therefore, a user selection technique suitable for QRM-MLD detection algorithm is proposed. In the proposed technique, the user selection is conducted in a recursive manner to adapt with the recursive property of QRM-MLD. Using computer simulation, it has been shown that the proposed technique gives significant performance improvement especially when the number of candidates in QRM-MLD is relatively small.

In addition to the signal exchange issue, MU-MIMO with CIC also faces challenges for the real environment implementations such as channel shadowing, channel correlation between users, and the difference on user sampling time and frequency offset. This thesis, therefore, also shows field experiment results of MU-MIMO with CIC. Through the field experiment, it has been shown that regardless the above issues, MU-MIMO with CIC still applicable and has a solid potency to be implemented in the future wireless communication systems.

In Chapter 4, the common form of MU-MIMO, i.e. MU-MIMO with precoding have been described. As described in this thesis, the challenge of using this approach is its sensitivity to the precoder accuracy. The mismatch between the precoder and the actual channel causes the interuser interference arises in the users. This circumstance especially occurs when the user experiencing channel aging phenomena caused by the Doppler spread effect. In this thesis, channel prediction is exploited to minimize the interuser interference. Specifically, the information contained in the channel prediction is used to conduct power allocation. In the proposed power allocation technique, the power is allocated in such a way that the interference level in the users can be minimized. Using the proposed technique, the BER performance of users having large Doppler spread can be significantly improved while maintaining the performance of the users having small Doppler spread.

Certainly, in order to extend the current investigation towards much more complicated real wireless communication systems, further extensive research is required. As a future research direction, below extension might be appealing.

- For the case of joint turbo decoding, it is worth to note that even the joint turbo decoding can be conducted in a parallel manner and saves the processing time, the computational complexity remains relatively high. A lower complexity joint turbo decoding can be an attractive research. This can be done for example, by reducing the number of super-trellis state in the LLR calculation. It can also be done by using a hybrid technique between the conventional and joint turbo decoding. For example, joint turbo decoding can be conducted first in only for several iterations. Once the critical point at EXIT function is passed, the decoding process can be continued by the conventional decoding technique.

- For the case of MU-MIMO with CIC, the field experiment is still conducted for the basic signal detection techniques, i.e. MLD and MMSE. It can be interesting to observe the performance of the system when the contemporary signal detection technique such as QRM-MLD is used. In this regard, the user selection technique can also be employed to observe its performance in the real environment.

- For the case of MU-MIMO with precoding, it will be interesting to investigate the usefulness of the channel prediction even further. Except for power allocation which is proposed in this thesis, channel prediction might also be useful for user scheduling. Taking channel prediction into consideration might improve the performance of user scheduling, in particular when the served-users have a broad Doppler spread variation between users.

By extending the research to those directions, a better showcase of the potency of the proposed technique towards more complex real wireless communication systems can be obtained.

Bibliography

[1] J. H. Winters, "On the capacity of radio communications systems with diversity in Rayleigh fading environments," *IEEE J. Sel. Areas Commun.*, vol. 5, no. 6, pp. 871–878, June 1987.

[2] G. J. Foschini and M. J. Gans, "On the limits of wireless communications in a fading environment when using multiple antennas," *Wireless Pers. Commun.*, vol. 6, no. 3, pp. 311–335, Mar. 1998.

[3] E. Telatar, "Capacity of multi-antenna Gaussian channels," *Eur. Trans. Telecommun.*, vol. 10, no. 6, pp. 585–596, Nov. 1999.

[4] D. Tse and P. Viswanath, "MIMO IV: Multiuser Communications," in *Fundamentals of Wireless Communication*, 1st ed. Cambridge, United Kingdom: Cambridge Univ. Press, 2005, ch. 10, pp. 497–563.

[5] I. H. Wang and D. Tse, "Interference mitigation through limited receiver cooperation," *IEEE Trans. Inf. Theory*, vol. 57, no. 5, pp. 2913–2940, May 2011.

[6] H. Kwon and J. Cioffi, "MISO broadcast channel with user-cooperation and limited feedback," in *Proc. IEEE Int. Symp. Inform. Theory*, Seoul, 2009, pp. 1694–1698.

[7] J. Jiang, J. Thompson, H. Sun, and P. Grant, "Performance assessment of virtual multiple-input multiple-output systems with compress-and-forward cooperation," *IET Commun.*, vol. 6, no. 11, pp. 1456–1465, Nov. 2012.

[8] H. Mao, W. Feng, and N. Ge, "MIMO broadcast channels with cooperation among densely clustered receivers," in *Proc. IEEE Int. Conf. Commun. Syst*, Macau, 2014, pp. 288–292.

[9] Q. Spencer, A. Swindlehurst, and M. Haardt, "Zero-forcing methods for downlink spatial multiplexing in multi-user MIMO channels," *IEEE Trans. Signal Proc.*, vol. 52, no. 2, pp. 461–471, Feb. 2004.

[10] M. Joham, W. Utschick, and J. Nossek, "Linear transmit processing in MIMO communications systems," *IEEE Trans. Signal Process.*, vol. 53. no. 8, pp. 2700–2712, Aug. 2005.

[11] X. Gao, O. Edfors, F. Rusek, and F. Tufvesson, "Linear precoding performance in measured very-large MIMO channels," in *Proc. IEEE Veh. Technol. Conf. Fall*, San Fransisco, 2011, pp. 1–5.

[12] K. Zu, R. C. de Lamare, and M. Haardt, "Multi-branch Tomlinson-Harashima precoding design for MU-MIMO systems: Theory and algorithms," *IEEE Trans. Commun.*, vol. 62, no. 3, pp. 939–951, Mar. 2014.

[13] S. Grant and J. Cavers, "Performance enhancement through joint detection of co-channel signals using diversity arrays," *IEEE Trans. Commun.*, vol. 46, no. 8, pp. 1038–1049, Aug. 1998.

[14] A. Gorokhov, D. A. Gore, and A. J. Paulraj, "Receive antenna selection for MIMO spatial multiplexing: Theory and algorithms," *IEEE Trans. Signal Process.*, vol. 51, no. 11, pp. 2796–2807, Nov. 2003.

[15] S. Sanayei and A. Nosratinia, "Antenna selection in MIMO systems," *IEEE Commun. Mag.*, vol. 42, no. 10, pp. 68–73, Oct. 2004.

[16] A. F. Molisch and M. Z. Win, "MIMO systems with antenna selection," *IEEE Microwave Mag.*, vol. 5, no. 1, pp. 46–56, Mar. 2004.

[17] R. W. Heath Jr. and A. Paulraj, "Antenna selection for spatial multiplexing systems based on minimum error rate," in *Proc. IEEE Int. Conf. Commun.*, Helsinki, 2001, pp. 2276–2280.

[18] R. W. Heath Jr., S. Sandhu, and A. J. Paulraj, "Antenna selection for spatial multiplexing systems with linear receivers," *IEEE Commun. Lett.*, vol. 5, no. 4, pp. 142–144, Apr. 2001.

[19] D. A. Gore, R. W. Heath, and A. J. Paulraj, "Transmit selection in spatial multiplexing systems," *IEEE Commun. Lett.*, vol. 6, no. 11, pp. 491–493, Nov. 2002.

[20] X. Zhibin, W. Jinkuan, W. Yun, and M. Yan, "Fast algorithm for antenna selection in MIMO systems based on minimum error rate," in *Proc. Int. Symp. Intelligent Signal Process. Commun. Syst.*, Xiamen, 2007, pp 510–513.

[21] D. Lu and D. K. C. So, "Performance based receive antenna selection for V-BLAST systems," *IEEE Trans. Wireless Commun.*, vol. 3, no. 1, pp. 214–225, Jan. 2009.

[22] Y. Inoue, K. Saito, T. Kawamura, and H. Andoh, "Field experiments on antenna configuration associated with fading correlation for downlink multi-user MIMO in LTE-Advanced," in *Proc. IEEE Veh. Technol. Conf. Spring*, Dresden, 2013, pp. 1–5.

[23] Y. Hatakawa, T. Matsumoto, K. Kitagawa, and S. Konishi, "Indoor experiment of 8-by-2 multiuser MIMO transmission using Tomlinson-Harashima precoding subject to limited CSI feedback," in *Proc. IEEE Radio Wireless Symp.*, Newport Beach, 2014, pp. 49–51.

[24] D. Takeda, Y. Inoue, K. Saito, T. Kawamura, and H. Andoh, "Field experiments on antenna element grouping for smart vertical MIMO in LTE-advanced downlink," in *Proc. IEEE Veh. Technol. Conf. Fall*, Vancouver, 2014, pp. 1–5.

[25] G. Dahman, J. Flordelis, and F. Tufvesson, "Experimental evaluation of the effect of BS antenna inter-element spacing on MU-MIMO separation," in *Proc. IEEE Int. Conf. Commun.*, London, 2015, pp. 1685–1690.

[26] P. Morgensen *et al*, "Centimeter-wave concept for 5G ultradense small cells," in *Proc. IEEE Veh. Technol. Conf. Spring*, Seoul, 2014, pp. 1–5.

[27] C. Berrou, A. Glavieux, and P. Thitimajshima, "Near Shannon limit error-correcting coding and decoding: Turbo-codes," in *Proc. IEEE Int. Conf. Commun.*, Geneva, 1993, pp. 1064–1070.

[28] C. Berrou and A. Glavieux, "Near optimum error correcting coding and decoding: Turbo-codes," *IEEE Trans. Commun.*, vol. 44, no. 10, pp. 1261–1271, Oct. 1996.

[29] M. Sellathurai and S. Haykin, "Turbo-BLAST for wireless communications: Theory and experiments," *IEEE Trans. Signal Process.*, vol. 50, no. 10, pp. 2538–2546, Nov. 2002.

[30] S. Haykin, M. Sellathurai, Y. de Jong, and T. Willink, "Turbo-MIMO for wireless communications," *IEEE Commun. Mag.*, vol. 42, no. 10, pp. 48–53, Oct. 2004.

[31] *Multiplexing and channel coding*, 3GPP TS 36.212 V11.4.0, Jan. 2014.

[32] K. K. Wong, A. Paulraj, and R. D. Murch, "Efficient high-performance decoding for overloaded MIMO antenna systems," *IEEE Trans. Wireless Commun.*, vol. 6, no. 5, pp. 1833–1842, May 2007.

[33] N. Prasad, K. Y. Kalbat, and X. Wang, "Optimally efficient max-log APP demodulation in MIMO systems," *IEEE J. Sel. Topics Signal Process.*, vol. 5, no. 8, pp. 1400–1414, Sept. 2011.

[34] Y. Sanada and Q. Wang, "A co-channel interference cancellation technique using orthogonal convolutional codes," *IEEE Trans. Commun.*, vol. 44, no. 5, pp. 549–556, May 1996.

[35] J. Zhang, S. Chen, X. Mu, and L. Hanzo, "Turbo multi-user detection for OFDM/SDMA systems relying on differential evolution aided iterative channel estimation," *IEEE Trans. Commun.*, vol. 60, no. 6, pp. 1621–1633, June 2012.

[36] J. Zhang, S. Chen, X. Mu, and L. Hanzo, "Evolutionary-algorithm-assisted joint channel estimation and turbo multiuser detection/decoding for OFDM/SDMA," *IEEE Trans. Veh. Technol.*, vol. 63, no. 3, pp. 1204–1222, Mar. 2014.

[37] H. V. Poor, "Iterative multiuser detection," *IEEE Signal Process. Mag.*, vol. 21, no. 1, pp. 81–88, Jan. 2004.

[38] B. M. Hochwald and S. ten Brink, "Achieving near-capacity on a multiple-antenna channel," *IEEE Trans. Commun.*, vol. 50, no. 10, pp. 2538–2546, Nov. 2002.

[39] S. Ahmed and S. Y. Kim "Evaluation of reduced search iterative MIMO detection schemes," in *Proc. Int. Conf. ICT Convergence*, Jeju, 2013, pp. 112–116.

[40] S. Ahmed and S. Y. Kim, "Efficient soft bit estimation for joint iterative multiple-input multiple-output detection," *IET Commun.*, vol. 9, no. 17, pp. 2107–2113, Nov. 2015.

[41] Y. Yang, J. Hu, and H. Zhang, "Iterative group MAP detection in MIMO wireless systems," in *Proc. IEEE Veh. Technol. Conf. Fall*, Baltimore, 2007, pp. 680–684.

[42] X. Wang and H. V. Poor, "Iterative (turbo) soft interference cancellation and decoding for coded CDMA," *IEEE Trans. Commun.*, vol. 47, no. 7, pp. 1046–1061, July 1999.

[43] K. Li and X. Wang, "EXIT chart analysis of turbo multiuser detection," *IEEE Trans. Wireless Commun.*, vol. 4, no. 1, pp. 300–311, Jan. 2005.

[44] B. Lu and X. Wang, "Iterative receivers for multiuser space-time coding systems," *IEEE J. Sel. Areas Commun.*, vol. 18, no. 11, pp. 2322–2335, Nov. 2000.

[45] T. Ito, X. Wang, Y. Kakura, M. Mahidian, and A. Ushirokawa, "Performance comparison of MF and MMSE combined iterative soft interference canceller and V-BLAST technique in MIMO/OFDM systems," in *Proc. IEEE Veh. Technol. Conf. Fall*, Orlando, 2003, pp. 488–492.

[46] H. Lee, B. Lee and I. Lee, "Iterative detection and decoding with an improved V-BLAST for MIMO-OFDM systems," *IEEE J. Sel. Areas Commun.*, vol. 24, no. 3, pp. 504–513, Mar. 2006.

[47] B. Han, T. Ebihara, H. Taoka, T. Kawamura, and M. Sawahashi, "Effect of joint modulation and coding scheme selection on turbo SIC for OFDM-MIMO multiplexing," in *Proc. Int. Conf. Wireless Commun. Signal Process.*, Hangzhou, 2013, pp. 1–6.

[48] *Physical channels and modulation*, 3GPP TS 36.211 V11.5.0, Jan. 2014.

[49] P. Robertson, E. Villebrun, and P. Hoeher, "A comparison of optimal and sub-optimal MAP decoding algorithms operating in the log domain," in *Proc. IEEE Int. Conf. Commun.*, Seattle, 1995, pp. 1009–1013.

[50] H. Murata and S. Yoshida, "Trellis-coded co-channel interference canceler for micro-cellular radio," *IEEE Trans. Commun.*, vol. 45, no. 9, pp. 1088–1094, Sept. 1997.

[51] S. ten Brink, "Convergence behaviour of iteratively decoded parallel concatenated codes," *IEEE Trans. Commun.*, vol. 49, no. 10, pp. 1727–1737, Oct. 2001.

[52] A. Ashikhmin, G. Kramer, and S. ten Brink, "Extrinsic information transfer functions: Model and erasure channel properties," *IEEE Trans. Inf. Theory*, vol. 50, no. 11, pp. 2657–2673, Nov. 2004.

[53] W. Li and H. Dai, "EXIT chart analysis of turbo-BLAST receivers in Rayleigh fading channels," in *Proc. IEEE Veh. Technol. Conf. Fall*, Los Angeles, 2014, pp. 1396–1400.

[54] R. Sapra and A. K. Jagannatham, "EXIT chart based BER expressions for turbo decoding in fading MIMO wireless systems," *IEEE Commun. Lett.*, vol. 19, no. 1, pp. 10–13, Jan. 2015.

[55] *Radio transmission and reception*, 3GPP TS 45.005 V11.4.0, Jan. 2014.

[56] F. Boccardi *et al*, "Multiple-antenna techniques in LTE-advanced," *IEEE Commun. Mag.*, vol. 50, no. 3, pp. 114–121, Mar. 2012.

[57] C. Lim, T. Yoo, B. Clerckx, B. Lee, and B. Shim, "Recent trend of multiuser MIMO in LTE-advanced," *IEEE Commun. Mag.*, vol. 51. no. 3, pp. 127–135, Mar. 2013.

[58] Q. H. Spencer, C. B. Peel, A. L. Swindlehurst, and M. Haardt, "An introduction to the multi-user MIMO downlink," *IEEE Commun. Mag.*, vol. 42. no. 10, pp. 60–67, Oct. 2004.

[59] D. Gesbert, M. Kountouris, R. W. Heath Jr., C. Chae, and T. Salzer, "Shifting the MIMO paradigm," *IEEE Signal Process. Mag.*, vol. 24, no. 5, pp. 36–46, Oct. 2007.

[60] A. F. Molisch, M. Z. Win, and J. H. Winters, "Capacity of MIMO systems with antenna selection," in *Proc. IEEE Int. Conf. Commun.*, Helsinki, 2001, pp. 570–574.

[61] A. Gorokhov, D. Gore, and A. Paulraj, "Receive antenna selection for MIMO-flat fading channels: Theory and algorithms," *IEEE Trans. Inf. Theory*, vol. 49, no. 10, pp. 2687–2696, Oct. 2003.

[62] M. G. Alkhansari and A. B. Gershman, "Fast antenna subset selection in MIMO systems," *IEEE Trans. Signal Process.*, vol. 52, no. 2, pp. 339–346, Feb. 2004.

[63] M. A. Jensen and M. L. Morris, "Efficient capacity-based antenna selection for MIMO systems," *IEEE Trans. Veh. Technol.*, vol. 54, no. 1, pp. 110–116, Jan. 2005.

[64] B. H. Wang, H. T. Hui, and M. S. Leong, "Global and fast antenna selection for MIMO systems," *IEEE Trans. Commun.*, vol. 53, no. 9, pp. 2505–2510, Sept. 2010.

[65] K. J. Kim and R. A. Iltis, "Joint detection and channel estimation algorithms for QS-CDMA signals over time-varying channels," *IEEE Trans. Commun.*, vol. 50, no. 5, pp. 845–855, May 2002.

[66] B. Kim and K. Choi, "A very low complexity QRM-MLD algorithm based on limited tree search for MIMO systems," in *Proc. 2008 IEEE Veh. Technol. Conf. Spring*, Singapore, 2008, pp. 1246–1250.

[67] K. C. Lai and L. W. Lin, "Low-complexity adaptive tree search algorithm for MIMO detection," *IEEE Trans. Wireless Commun.*, vol. 8, no. 7, pp. 3716–3726, July 2009.

[68] P. W. Wolniansky, G. J. Foschini, G. D. Golden, and R. A. Valenzuela, "V-BLAST: An architecture for realizing very high data rate over the rich-scattering wireless channel," in *Proc. URSI Int. Symp. Signal, Syst., Electron.*, Pisa, 1998, pp. 295–300.

[69] D. Wubben, R. Bohnke, V. Kuhn, and K. D. Kammeyer, "MMSE extension of V-BLAST based on sorted QR decomposition," in *Proc. IEEE Veh. Technol. Conf. Fall*, Orlando, 2003, pp 508–512.

[70] R. W. Heath and A. J. Paulraj, "Switching between diversity and multiplexing in MIMO systems," *IEEE Trans. Commun.*, vol. 53, no. 6, pp. 962–968, June 2005.

[71] I. Shubhi and H. Murata, "An error-propagation minimization based signal selection scheme for QRM-MLD," *IEICE Trans. Commun.*, vol. E99-B, no. 7, pp. 1566–1576, July 2016.

[72] I. Shubhi, Y. Hayashi, and H. Murata, "User collaborated reception of spatially multiplexed signals: an experimental study in group mobility," *IEICE Trans. Fundam. Electron. Commun. Comput. Sci.*, vol. E100-A, no. 1, pp. 227–231, Jan. 2017.

[73] T. L. Marzetta, "Noncooperative cellular wireless with unlimited numbers of base station antennas," *IEEE Trans. Wireless Commun.*, vol. 9, no. 11, pp. 3590–3600, Nov. 2010.

[74] H. Q. Ngo, E. G. Larsson, and T. L. Marzetta, "Energy and spectral efficiency of very large multiuser MIMO systems," *IEEE Trans. Commun.*, vol. 61, no. 4, pp. 1436–1449, Apr. 2013.

[75] E. G. Larsson, O. Edfors, F. Tufvesson, and T. L. Marzetta, "Massive MIMO for next generation wireless systems," *IEEE Commun. Mag.*, vol. 52, no. 2, pp. 186–195, Feb. 2014.

[76] K. Guo, Y. Guo, and G. Ascheid, "Security-constrained power allocation in MU-massive-MIMO with distributed antennas," *IEEE Trans. Wireless Commun.*, vol. 15, no. 12, pp. 8139–8153, Dec. 2016.

[77] S. Zarei, W. Gerstacker, and R. Schober, "A low-complexity linear precoding and power allocation scheme for downlink massive MIMO systems," in *Proc. Asilomar Conf. Signals, Syst, Comput.*, Pacific Grove, 2013, pp. 285–290.

[78] Q. Zhang, S. Jin, M. McKay, D. M. Jimenez, and H. Zhu, "Power allocation schemes for multicell massive MIMO systems," *IEEE Trans. Wireless Commun.*, vol. 14, no. 11, pp. 5941–5955, June 2015.

[79] C. Sun, X. Gao, and Z. Ding, "BDMA in multicell massive MIMO communications: Power allocation algorithms," *IEEE Trans. Signal Process.*, vol. 65, no. 11, pp. 2962–2974, Mar. 2017.

[80] X. Guozhen, L. An, J. Wei, X. Haige, and L. Wu, "Joint user scheduling and antenna selection in distributed massive MIMO systems with limited backhaul capacity," *China Commun.*, vol. 11, no. 5, pp. 17–30, May 2014.

[81] A. Liu and V. K. N. Lau, "Joint power and antenna selection optimization for energy-efficient large distributed MIMO networks," in *Proc. IEEE Int. Conf. Commun. Syst.*, Singapore, 2012, pp. 230–234.

[82] M. Benmimoune, E. Driouch, W. Ajib, and D. Massicotte, "Joint transmit antenna selection and user scheduling for massive MIMO systems," in *Proc. IEEE Wireless Commun. Networking Conf.*, New Orleans, 2015, pp. 381–386.

[83] R. Hamdi and W. Ajib, "Joint optimal number of RF chains and power allocation for downlink massive MIMO systems," in *Proc. IEEE Veh. Technol. Conf. Fall*, Boston,. 2015, pp. 1–5.

[84] X. Wang, Z. Zhang, K. Long, and X. Zhang, "Joint group power allocation and prebeamforming for joint spatial-division multiplexing in multiuser massive MIMO systems," in *Proc. IEEE Int. Conf. Acoust., Speech, Signal Process.*, Brisbane, 2015, pp. 2934–2938.

[85] Y. Sun, S. Lv, S. Liu, and Y. H. Zhang, "Joint user scheduling and power allocation for massive MIMO downlink with two-stage precoding," in *Proc. IEEE Int. Conf. Comput. Commun.*, Chengdu, 2016, pp. 2917–2921.

[86] X. Xie, H. Yang, W. Lei, and B. Ma, "Robust power allocation based on game theory for multi-user MIMO system with SLNR precoding," in *Proc. IEEE Veh. Technol. Conf. Spring*, Seoul, 2014, pp. 1–5.

[87] H. Yang and T. L. Marzetta, "Total energy efficiency of cellular large scale antenna system multiple access mobile networks," in *Proc. IEEE Online Conf. Green Commun.*, Piscataway, 2013, pp. 27–32.

[88] E. Björnson, L. Sanguinetti, J. Hoydis, and Merouane Debbah, "Optimal design of energy-efficient multi-user MIMO systems: Is massive MIMO the answer?," *IEEE Trans. Wireless Commun.*, vol. 14, no. 6, pp. 3059–3075, June 2015.

[89] L. Zhao, H. Zhao, F. Hu, K. Zheng, and J. Zhang, "Energy efficient power allocation algorithm for downlink massive MIMO with MRT precoding," in *Proc. IEEE Veh. Technol. Conf. Fall*, Las Vegas, 2013, pp. 1–5,.

[90] W. Liu, A. Zappone, C. Yang, and E. Jorswieck, "Global EE optimization of massive MIMO systems," in *Proc. IEEE Int. Workshops Signal Process. Advances Wireless Commun.*, Stockholm, 2015, pp. 221–225.

[91] Y. Guo, J. Tang, G. Wu, and S. Li, "Power allocation for massive MIMO: Impact of power amplifier efficiency," in *Proc. IEEE/CIC Int. Conf. Commun. China*, Shenzhen, 2015, pp. 1–6.

[92] C. Kong, C. Zhong, M. Matthaiou, and Z. Zhang, "Performance of downlink massive MIMO in Ricean fading channels with ZF precoder," in *Proc. IEEE Int. Conf. Commun.*, London, 2015, pp. 1776–1782.

[93] Y. Zhou, D. Li, H. Wang, A. Yang, and S. Guo, "QoS-aware energy-efficient optimization for massive MIMO systems in 5G," in *Proc. Int. Conf. Wireless Commun. Signal Process.*, Hefei, 2014, pp. 1–5.

[94] D. W. K. Ng, E. S. Lo, and R. Schober, "Energy-efficient resource allocation in OFDMA systems with large numbers of base station antennas," *IEEE Trans. Wireless Commun.*, vol. 11, no. 6, pp. 3292–3304, Sept. 2012.

[95] J. Zhang, Y. Jiang, P. Li, F. Zheng, and X. You, "Energy efficient power allocation in massive MIMO systems based on standard interference function," in *Proc. IEEE Veh. Technol. Conf. Spring*, Nanjing, 2016, pp. 1–5.

[96] T. V. Chien, E. Björnson, and E. G. Larsson, "Joint power allocation and user association optimization for massive MIMO systems," *IEEE Trans. Wireless Commun.*, vol. 15, no. 9, pp. 6384–6399, Sept. 2016.

[97] Y. Hao, Z. Song, S. Hou, and H. Li, "Energy and spectral-efficiency tradeoff in massive MIMO systems with inter-user interference," in *Proc. IEEE Annu. Int. Symp. Personal, Indoor, Mobile Radio Commun.*, Hong Kong, 2015, pp. 553–557.

[98] F. Rusek *et al*, "Scaling up MIMO: Opportunities and challenges with very large arrays," *IEEE Signal Process. Mag.*, vol. 30, no. 1, pp. 40–60, Jan. 2013.

[99] K. Truong and R. Heath, "Effects of channel aging in massive MIMO systems," *J. Commun. Netw.*, vol. 15, no. 4, pp. 338–351, Sept. 2013.

[100] T. Kim, K. Min, and S. Choi, "Study on effect of training for downlink massive MIMO systems with outdated channel," in *Proc. IEEE Int. Conf. Commun.*, London, 2015, pp. 2369–2374.

[101] A. K. Papazafeiropoulos and T. Ratnarajah, "Deterministic equivalent performance analysis of time-varying massive MIMO systems," *IEEE Trans. Wireless Commun.*, vol. 14, no. 10, pp. 5795–5809, Oct. 2015.

[102] A. K. Papazafeiropoulos and T. Ratnarajah, "Linear precoding for downlink massive MIMO with delayed CSIT and channel prediction," in *Proc. IEEE Wireless Commun. Networking Conf.*, Istanbul, 2014, pp. 819–914.

[103] C. Kong, C. Zhong, A. K. Papazafeiropoulos, M. Matthaiou, and Z. Zhang, "Sum-rate and power scaling of massive MIMO systems with channel aging," *IEEE Trans. Commun.*, vol. 63, no. 12, pp. 4879–4893, Dec. 2015.

[104] A. K. Papazafeiropoulos, "Downlink performance of massive MIMO under general channel aging conditions," in *Proc. IEEE Global Commun. Conf.*, San Diego, 2015, pp. 1–6.

[105] A. K. Papazafeiropoulos, "Impact of general channel aging conditions on the downlink performance of massive MIMO," IEEE Trans. Veh. Technol., vol. 66, no. 2, pp. 1428–1442, Feb. 2017.

[106] R. Chopra, C. R. Murthy, and H. A. Suraweera, "On the throughput of large MIMO beamforming systems with channel aging," *IEEE Signal Process. Lett.*, vol. 23, no. 11, pp. 1523–1527, Nov. 2016.

[107] Q. Bao, H. Wang, Y. Chen, and C. Liu, "Downlink sum-rate and energy efficiency of massive MIMO systems with channel aging," in *Proc. Int. Conf. Wireless Commun. Signal Process.*, Yangzhou, 2016, pp. 1–5.

[108] R. H. Clarke, "A statistical theory of mobile radio reception," *Bell. Syst. Tech. J.*, vol. 47, no. 6, pp. 957–1000, July/Aug. 1968.

[109] O. Norklit and R. G. Vaughan, "Angular partitioning to yield equal Doppler contributions," *IEEE Trans. Veh. Technol.*, vol. 48, no. 5, pp. 1437–1442, Sept. 1999.

[110] D. Chizhik, "Slowing the time-fluctuating MIMO channel by beam forming," *IEEE Trans. Wireless Commun.*, vol. 3, no. 9, pp. 1554–1565, Sept. 2004.

[111] S. Serbetli and S. Baggen, "Doppler compensation by using dual antenna for mobile OFDM systems," in *Proc. IEEE Veh. Technol. Conf. Spring*, Singapore, 2008, pp. 1–4.

[112] R. Nagashima, T. Ohtsuki, W. Jiang, Y. Takatori, and T. Nakagawa, "Channel prediction for massive MIMO with channel compression based on principal component analysis," in *Proc. IEEE Annu. Int. Symp. Personal, Indoor, Mobile Radio Commun.*, Valencia, 2016, pp. 1–6.

[113] S. Han, I. Chih-Lin, Z. Xu, and C. Rowell, "Large-scale antenna systems with hybrid analog and digital beamforming for millimeter wave 5G," *IEEE Commun. Mag.*, vol. 53, no. 1, pp. 186–194, Jan. 2015.

[114] R. L. Haupt, "Array factors analysis," in *Antenna Arrays: A Computational Approach*, 1st ed. New Jersey,: Wiley-IEEE Press, 2010, ch. 2, sec. 7, pp. 83.

[115] H. Tanaka, H. Murata, K. Yamamoto, and S. Yoshida, "Performance evaluation of cooperative relaying networks using 3D ray launching method for wireless propagation prediction," in *Proc. IEEE Veh. Technol. Conf. Fall*, Calgary, 2008, pp. 1–4.

Author's Publication List

Journal Papers

1. I. Shubhi and Y. Sanada, "Joint turbo decoding for overloaded MIMO-OFDM systems," *IEEE Trans. Veh. Technol.*, vol. 66, no. 1, pp. 433–442, Jan. 2017.

2. I. Shubhi, Y. Hayashi, and H. Murata, "User collaborated reception of spatially multiplexed signals: an experimental study in group mobility," *IEICE Trans. Fundam. Electron. Commun. Comput. Sci.*, vol. E100-A, no. 1, pp. 227–231, Jan. 2017.

3. I. Shubhi and H. Murata, "An error-propagation minimization based signal selection scheme for QRM-MLD," *IEICE Trans. Commun.*, vol. E99-B, no. 7, pp. 1566–1576, July 2016.

4. I. Shubhi and Y. Sanada, "Pseudo distance for trellis coded modulation in overloaded MIMO OFDM with sphere decoding," *IEICE Trans. Commun.*, vol. E99-B, no. 3, pp. 723–731, Mar. 2016.

International Conference Papers

1. I. Shubhi and H. Murata, "Recursive Power Allocation with Interference Minimization for Time Varying Massive MIMO," in *Proc. IEEE Veh. Technol. Conf. Fall*, Toronto, 2017, pp. 1–5.

2. I. Shubhi and H. Murata, "Dynamic precoder for massive MIMO in the presence of large Doppler spread," in *Proc. IEEE Veh. Technol. Conf. Spring Workshops*, Sydney, 2017, pp. 1–5.

3. Y. Hayashi, I. Shubhi, and H. Murata, "User collaboration for interference cancellation on multi-user MIMO communication systems," in *Proc. IEEE Veh. Technol. Conf. Fall*, Boston, 2015, pp. 1–5.

4. I. Shubhi and H. Murata, "A signal selection scheme for QRM-MLD on MU-MIMO with user collaboration," in *Proc. Int. Symp. Wireless Commun. Syst.*, Brussels, 2015, pp. 596–600.

5. I. Shubhi and Y. Sanada, "Performance of turbo codes in overloaded MIMO-OFDM systems using joint decoding," in *Proc. IEEE Annu. Int. Symp. Personal, Indoor, Mobile Radio Commun.*, Washington, 2014, pp. 386–390.

6. I. Shubhi and Y. Sanada, "Trellis coded modulation with pseudo distance in overloaded MIMO-OFDM systems with sphere decoding," in *Proc. Int. Symp. Intelligent Signal Process. Commun. Syst.*, Okinawa, 2013, pp. 579–584.

Local Conference Papers

1. I. Shubhi and H. Murata, "Performance of beam forming with Doppler spread awareness for high frequency communications," in *Proc. IEICE Soc. Conf.*, Sapporo, 2016, B-5-30, pp. 300.

2. I. Shubhi and H. Murata, "Performance evaluation of beamforming technique for MU-MIMO transmission using 3D ray launching," in *Proc. IEICE General Conf.*, Fukuoka, 2016, B-5-114, pp. 507.

3. I. Shubhi and H. Murata, "A modified minimum euclidean distance based signal selection scheme suitable for QRM-MLD," in *Proc. IEICE Symp. Inform. Theory Applicat.*, Okayama, 2015, 8.2.1, pp. 560–564.

4. I. Shubhi and Y. Sanada, "Trellis coded modulation with pseudo distance in overloaded MIMO-OFDM with sphere decoding," in *Proc. IEICE Soc. Conf.*, Fukuoka, 2013, B-5-10, pp. 280.

Technical Report

1. I. Shubhi and H. Murata, "Performance of Linear Precoding with Doppler Compensation for Massive MIMO in Higher Frequency Bands," IEICE RCS Tech. Rep., RCS2016–322, Vol. 116, no. 479, pp. 181–185, Mar. 2017.

2. I. Shubhi and H. Murata, "3D ray launching evaluation of high frequency transmission with beamforming technique," IEICE RCS Tech. Rep., RCS2016–16, vol. 116, no. 11, pp. 89–92, Apr. 2016.

3. I. Shubhi and H. Murata, "An antenna selection scheme for QRM-MLD receivers based on error rate minimization," ITE Tech. Rep., BCT2016–21, vol. 40, no. 4, pp. 17–20, Feb. 2016.

4. I. Shubhi and H. Murata, "Collaborative interference cancellation on MU-MIMO transmission with QRM-MLD," IEICE RCS Tech. Rep., RCS2015–14, vol. 115, no. 2, pp. 71–76, Apr. 2015.

5. I. Shubhi and Y. Sanada, "A joint decoding scheme for turbo codes in overloaded MIMO OFDM systems," IEICE RCS Tech. Rep., RCS2014–130, vol. 114, no. 164, pp. 221–226, July 2014.

6. I. Shubhi and Y. Sanada, "Joint decoding scheme with sphere decoding and pseudo distance for trellis coded signal in overloaded MIMO-OFDM," IEICE RCS Tech. Rep., RCS2013–243, vol. 113, no. 361, pp. 213–218, Dec. 2013.

Awards

- IEEE VTS Japan Young Researcher's Encouragement Award
  Presented by Institute of Electrical and Electronic Engineers (IEEE) Vehicular Technology Society Japan Chapter, Sept. 2015.

Scholarships and Financial Support

- Indonesia Endowment for Education (LPDP) of the Ministry of Finance, Indonesia, October 2014–September 2017.

- Telecommunications Advancement Foundation Grants for Researchers Attending International Conferences, Sept. 2015.

- Asian Development Bank Scholarship, September 2012–September 2014.